

THESIS



This is to certify that the

dissertation entitled

The Effect of Composition on Charge Exchange,
Lattice Expansion, and Staging in
Potassium-Ammonia Graphite Intercalation Compounds

presented by

Brian R. York

has been accepted towards fulfillment
of the requirements for

Ph.D. degree in Physics

A handwritten signature in cursive script that reads "Stuart A. Solin".

Major professor

Stuart A. Solin

Date March 22, 1985



RETURNING MATERIALS:
Place in book drop to
remove this checkout from
your record. FINES will
be charged if book is
returned after the date
stamped below.

MAGIC 2
JAN 24 1999

THE EFFECT OF COMPOSITION ON CHARGE EXCHANGE, LATTICE EXPANSION, AND
STAGING IN POTASSIUM-AMMONIA GRAPHITE INTERCALATION COMPOUNDS

By

Brian R. York

A DISSERTATION

Submitted to
Michigan State University
in partial fulfillment of the requirements
for the degree of

DOCTOR OF PHILOSOPHY

Department of Physics and Astronomy

1984

ABSTRACT

THE EFFECT OF COMPOSITION ON CHARGE EXCHANGE, LATTICE EXPANSION, AND STAGING IN POTASSIUM-AMMONIA GRAPHITE INTERCALATION COMPOUNDS

By

Brian R. York

We have studied the charge exchange and compositional dependence of the sandwich thickness of stage-1 alkali-ammonia ternary graphite intercalation compounds $K(NH_3)_x C_y$, $0 \leq x \leq 4.33$, $12 \leq y \leq 24$. A model of the sandwich energy is presented which explicitly accounts for x -dependent charge exchange and size or stiffness effects and is in excellent agreement with experimental measurements of the dependence of the (00 l) x-ray diffraction patterns on ammonia vapor pressure. From this model we find that for the stage-1 compound $K(NH_3)_{4.33} C_{24}$, $f = 0.95$ and that the NH_3 molecules solvate some of the electron charge which was originally donated to the carbon layers in the KC_{24} starting material. In addition, the NH_3 molecules form planar 4-fold coordinated $K(NH_3)_4$ clusters and hence also solvate the K^+ ions in graphite galleries. We suggest that the $K(NH_3)_4$ clusters together with "spacer" NH_3 molecules constitute the two-dimensional analogue of the well-studied bulk, three-dimensional metal-ammonia solutions.

DEDICATION

This work is dedicated to my loving and understanding wife, Linda, for her support and friendship, to my adorable son, Bryan, for giving me such wonderful memories of parenthood, and to my father, mother, and family for their continued support for so many years.

ACKNOWLEDGEMENTS

It is a pleasure to acknowledge Professor Stuart A. Solin for his helpful criticism and invaluable support at all stages of this work and for introducing this author to James Joyce. I have also benefited from numerous fruitful discussions with Professors J.L. Dye, S.D. Mahanti, T.J. Pinnavaia, and Drs. S.K. Hark and P. Vora. I gratefully thank Professors R.D. Spence, J.A. Cowen, and G.L. Pollack for their help and useful advice which was sought at many stages of this study.

Thanks are also due to Y.B. Fan and X.W. Qian for their assistance and for useful discussions. There are many others, too numerous to mention, to whom I owe thanks, but in particular, M. Langer who has provided the technical glassblowing support that was essential to the success of this project and for remaining remarkably tolerant of demands for items to be finished "yesterday." I am appreciative of the support of this work by the NSF under grant #DMR 82-11554. Finally, I sincerely thank my typists, L. York and S. Lindsay, for their good nature and uncompromising quality of work, with special thanks going to L. York, who also devoted a large portion of her time and artistic talents to the many figures contained in the body of this thesis.

FORWARD

Our interest has been, and continues to be, the study of the structural phase transitions and related phenomena of layered solids. The term layered solids, as used here, refers to materials for which the interatomic forces within layers of atoms are stronger than the forces between layers. These materials inherently exhibit a high degree of anisotropy in their electronic and/or chemical and physical properties. The theoretical and experimental interest in layered solids stems from the fact that they provide a means of exploring quasi-two-dimensional phenomena.

This general class of layered solids can be broken down, based on the atomic thickness of the layer making up the solid, into the following three subclasses. Class I layered materials are formed by layers one atom thick; a typical example of this class would be graphite. Class II layered substances are formed by layers which are a few atoms thick; a common example of this class would be the dichalcogenide TaS_2 . Finally, class III layered solids are formed by layers many atoms thick. A representative example of this class would be the sheet silicate clays.

While my recent research activities have included investigations of class III materials, the bulk of my activity has been related to the class I materials, in particular, graphite intercalation compounds (GIC's) which are the focus of this dissertation. I present here a collection of studies on the structural characterization and phase

transition phenomena of several recently-developed, novel alkali-alkali and alkali-ammonia GIC's. The studies of the potassium-ammonia GIC's represents the main body of the dissertation with other investigations described in the appendices.

TABLE OF CONTENTS

	<u>Page</u>
List of Figures	vi
I. Introduction	1
II. Experimental Details and Results	5
III. Discussion and Analysis	17
A. Comparison with Rudorff's Results on K-NH ₃ GIC's	17
B. The Absorption Isotherm	20
C. The Residue Compound K(NH ₃) _{1.49} C ₂₄	23
D. The Generalized Reaction of KC ₂₄ with NH ₃	26
E. x ₁ vs. P _{NH₃} and the Fowler-Guggenheim Form	33
F. The Model	37
G. Comparison with Experiment	47
IV. Summary and Concluding Remarks	53
List of References	56
Appendices	59

LIST OF FIGURES

<u>Figure</u>		<u>Page</u>
1	Mole Fraction x vs. P_{NH_3} - McBain Balance Method	8
2	Mole Fraction x vs. P_{NH_3} - "Gas-Handling" Method	10
3	P_{NH_3} Evolution of (00 l) X-ray Diffraction Patterns of $\text{K}(\text{NH}_3)_x\text{C}_{24}$	12
4	d_1 vs. P_{NH_3}	14
5	d_2 vs. P_{NH_3}	15
6	Intensities of the (001) Reflection of Stage 1 and the (002) Reflection of Stage 2 vs. P_{NH_3}	16
7	(a) (00 l) X-ray Diffraction Pattern of $\text{KC}_8 + \text{NH}_3$ (b) (00 l) X-ray Diffraction Pattern of $\text{HOPG} + \text{K-NH}_3$	19
8	The Carbon/Potassium Mole Ratio y_n for Stage n vs. P_{NH_3}	29
9	The Fraction of Stage n P_n vs. P_{NH_3}	31
10	(00 l) X-ray Diffraction Pattern of $\text{KC}_{36} + \text{NH}_3$	32
11	Mole Fraction x_1 of Stage 1 vs. P_{NH_3}	34
12	The NH_3 Molecule in Graphite Gallery	36
13	The Daumas-Hèrold Model of a Mixed Stage 1 and 2 GIC	50
14	The (00 l) X-ray Diffraction Pattern of $\text{KC}_{48} + \text{NH}_3$	52

I. Introduction

Graphite is a prototypical layered solid in which the intralayer forces binding carbon atoms in a triangular planar lattice structure are much greater than the interplanar forces. This anisotropy in the interatomic forces makes it possible to intercalate graphite with many different chemical species. Intercalation is a process by which guest atoms, molecules, and/or ions are inserted into the interlayer spaces in the host graphite structure. The resulting graphite intercalation compound (GIC) shows a macroscopic expansion along the c-axis direction perpendicular to the carbon layer planes which themselves remain essentially undistorted.

The most fundamental and intrinsically interesting characteristic of graphite intercalation compounds is their ability to form pure stages. Pure staging is characterized by the long-range periodic placement of intercalant layers between host graphite layers. For example, pure stage n designates the periodic insertion or intercalation of layers of atoms and/or molecules (intercalants) between n carbon layers with this stacking arrangement repeating over extended (>500Å) distances. There is a charge transfer, in the intercalation process, between the intercalant layer and the graphite layers. Thus, in addition to characterization according to stage number, the intercalants in GIC's are also classified as donors or acceptors according to whether electron charge is transferred to or from the graphite sheets, respectively.

Detailed theoretical models outlining the physics of the staging phenomena have only recently been presented.^{1,2,3} An important ingredient of those models is the contribution of the carbon-intercalant-carbon sandwich energy to the free energy, which establishes the equilibrium stage. The sandwich thickness d_s (which is the perpendicular distance between carbon layers that flank an intercalant layer) can be determined by minimizing the free energy with respect to d_s .

Safran and Hamann^{4,5} considered both elastic and electrostatic contributions to the sandwich energy. They concluded that the elastic contribution to the sandwich energy was the dominant mechanism for the kinetics of intercalation while the electrostatic interactions were important in determining the equilibrium state or stage of the GIC. The recent model of Hawrylak and Subbaswamy³ is somewhat similar to that of Safran (for modifications see reference 3 and references therein), but takes into account volume and inplane intercalant density variations, and is capable of explaining experimentally observed effects^{6,7} in binary alkali GIC's which had not been addressed in earlier models. A binary GIC is one in which a single chemical species has been intercalated into the galleries between the layers of the graphite host.

While a theoretical description of binary GIC's based on elastic and electrostatic energies can explain many experimentally observed phenomena, other effects which couple those energies are also significant. The coupling of elastic and electrostatic forces would be experimentally visible in a variation of d_s with composition and/or charge exchange (the amount of charge per intercalant exchanged between the intercalated species and the carbon sheets). Thus, any acceptable

model of staging must adequately account for the variation in the sandwich thickness d_s with composition and charge exchange. To date, the experimental data necessary to test theoretical predictions for the variation of d_s with those parameters has been at best, sparse. Furthermore, the composition of the binary alkali GIC's, which are the most widely-studied and well-understood GIC's, cannot be conveniently varied at constant stage. The variation in the composition at a fixed stage allows a more detailed study of the role of charge exchange in determining the sandwich energy. For example, Woo and coworkers⁸ reported a small (.3%) composition dependent change in d_s for stage 2 LiC_{12} in comparison with stage 2 LiC_{18} , which they attribute to a competition between electrostatic and elastic effects. Similarly, Metrot et al.⁹ noted a weak dependence of d_s on the amount of chemical overcharging of stage-1 H_2SO_4 GIC's, but chose to focus on the chemical aspects of their measurements rather than to explore in detail the coupling of d_s to the charge exchange f . It should also be mentioned that large variations (-10%) in d_s with composition x have been reported for the ternary GIC's $\text{M}_x\text{M}'_{1-x}\text{C}_8$ ^{10,11} where M and M' are alkali metals, but such variations are predominantly elastic in origin¹⁰ and preclude a study of d_s vs. f . A ternary GIC is one in which two distinct guest species simultaneously occupy the carbon interlayer space.

We have shown¹² that the K-NH_3 ternary GIC's permit an indepth study of the variation of sandwich thickness d_s with composition and charge exchange f , at constant stage. The K-NH_3 intercalants form a two-dimensional (2D) liquid in the graphite galleries,¹³ which represents a natural 2D counterpart of the well-studied^{14,15,16} 3D K-NH_3 solution. In particular, the M-NH_3 (M = alkali metal) GIC's offer the

possibility of exploring the nonmetal-metal transition¹⁷ in 2D. In view of this, it is interesting to note that several decades ago Rudorff et al.¹⁸ prepared limited compositional forms of those compounds at low pressure, but they have only recently been investigated in detail.^{13,19,20}

In this paper we will discuss and extend the coupled elastic energy-charge exchange model which has to date only been addressed in a preliminary report.¹² We will provide here new experimental details and additional physical insight into the K-NH₃ ternary GIC's. Finally, the approach taken here includes modifications that we feel provide a more global understanding of the K-NH₃ GIC's.

II. Experimental Details and Results

All $K(NH_3)_x C_{24}$ samples were prepared by using a well characterized stage-2 KC_{24} sample made in the usual manner²¹ from the host material highly-oriented pyrolytic graphite (HOPG). The KC_{24} samples were rapidly transferred from their preparation vessel to another container, which was ultimately exposed to previously cleaned NH_3 gas. The transfer process was carried out in a Vacuum Atmospheres model MO-40-1 glove box maintained at $<.5\text{ppm } O_2/H_2O$ levels.

Many KC_{24} samples were prepared during the course of this work and their stoichiometry was carefully determined by accurately weighing the starting HOPG and the resultant intercalation compound. We found that the actual composition of the pure stage-2 compound was $KC_{24+\delta}$, where $-2.20 \pm .05 < \delta \leq 0$. Nevertheless, we will follow custom and hereinafter often designate specimens by their nominal compositions, e.g. $K(NH_3)_x C_{24}$, but the actual composition will be used in any relevant analysis.

Commercial grade NH_3 (main impurities are: 40ppm O_2 , 5ppm H_2O) was purified by condensing it onto Na metal with liquid nitrogen. The NH_3 was then warmed to $-70^\circ C$ with a dry ice/alcohol mixture. The solution was again frozen and any residual H_2 gas was pumped away. Hydrogen may be formed from the decomposition of NH_3 to the amide NH_2 by the reaction of NH_3 with impurities. This "freeze-pump-thaw" procedure²² was repeated until there was no evidence of the evolution of H_2 , determined by monitoring the pressure with a standard vacuum-thermocouple gauge.

Absorption isotherms or weight uptake measurements of KC_{24} for NH_3 gas were determined by two techniques: The first technique employed an archaic but quite useful device now referred to as a McBain balance.²³ This balance consisted of a very sensitive Hook's law quartz spring (force constant $k = 1mg/mm$, equilibrium length $l_0 = 30cm$), that was calibrated with premeasured wire weights. The spring was vertically suspended from a specially-designed flange in a glove box with the low H_2O/O_2 levels indicated above. Extreme care was used in attaching the KC_{24} specimen (mass ~ 100 mg) to the base of the spring. A thick-walled glass tube designed to withstand >10 atms pressure was used to enclose the specimen-spring assembly and was connected to the flange through an O-ring teflon coupling. The entire apparatus was removed from the glove box, connected to a vacuum system, and then exposed to clean NH_3 gas from a reservoir containing excess NH_3 liquid.

Vertical displacements from the KC_{24} equilibrium position which resulted from the intercalation of NH_3 vapor were monitored as a function of NH_3 pressure with a Wild KM-326 cathometer with an accuracy of $<.05mm$ or equivalently $<50\mu g$. By controlling the temperature of the excess liquid in the NH_3 reservoir, the ammonia gas pressure, P_{NH_3} , could be determined from the equation of state for the saturated vapor pressure of NH_3 (in atms), as a function of temperature²⁴ given in Eq. 1.

$$\log_{10} P_{NH_3}(T) = 27.376004 - \frac{1914.9569}{T} - 8.45983 \log_{10} T + 2.39309 \times 10^{-3} T + 2.955214 \times 10^{-6} T^2 . \quad (1)$$

Corrections of the McBain balance data for buoyancy, significant only for $P_{\text{NH}_3} > 1$ atm were made by determining the density of NH_3 gas from Van der Waals equation of state²⁵ with P_{NH_3} given in Eq. 1, and the volume of the sample as follows: The area of the sample could be calculated from the weight, density, and d-spacing or c-axis repeat distance of the host material HOPG. [Note that if the intercalant layers are disordered and/or unregistered with the graphite layers, then $d = [d_g + (n-1) 3.35] \text{\AA}$, where n is the stage number and 3.35\AA is the interplanar distance in pristine graphite.] The volume of the specimen can then be determined from the d-spacing of the NH_3 intercalated material which in turn is obtained from (00 l) X-ray diffraction measurements. After the sample was initially intercalated with NH_3 at room temperature, the bulk composition of the specimen was reversibly varied over the range $1.49 < x < 4.33$ (where x is the mole ratio of NH_3 to K) for 10^{-3} atms $< P_{\text{NH}_3} < 10$ atms. The McBain balance absorption data, corrected for buoyancy, is shown in Figure 1.

The second technique for weight-uptake measurements utilized a specially-designed high-pressure glass manifold, which was connected through a 3mm Ace glass-teflon valve to a vacuum system with an ultimate vacuum of 5×10^{-7} Torr. An NH_3 reservoir, a sample chamber, a standard volume, and a Datametrix Barocell Type 590D-100P-3P1-H5X-4D capacitance manometer were also connected to the manifold each through a separate 3mm glass-teflon valve. The volume of the manifold and each chamber was determined by a series of expansions at a known initial pressure of an inert gas such as argon from the standard volume into a previously evacuated manifold or chamber. From a measurement of the final pressure

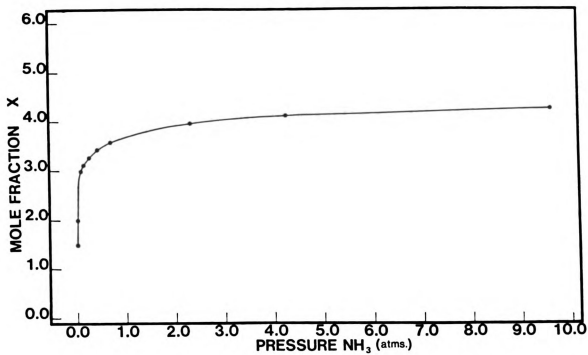


Figure 1. The dependence of the mole fraction x (x = mole ratio of NH_3/K) of $\text{K}(\text{NH}_3)_x\text{C}_{24}$ with P_{NH_3} , determined by a McBain balance¹⁹ method. Experimental points are indicated by solid dots (\bullet), the solid line is a guide to the eye.

resulting from the expansion, the volume of each chamber and manifold could be calculated and then averaged over several trials to yield an accuracy of $< 1\%$. By monitoring the pressure difference before and after intercalation, together with the predetermined volumes, the number of moles of NH_3 taken in by the graphite can then be calculated from Van der Waals equation.²⁵

This "gas-handling" technique, the results of which are shown in Figure 2 as solid dots for intercalation and open circles for deintercalation, compliments the McBain balance technique, the data of which are also shown as open triangles in Figure 2. The former allows access to the low P, low x region of the initial intercalation of KC_{24} with NH_3 . In fact, for our typical samples (mass ~50mg), the inclusion of the low pressure region of Figure 2 necessitated measuring the NH_3 content intercalated into graphite to an accuracy of $.1\mu$ mole. However, the "gas-handling" technique has a slightly higher error (1% vs. .2%) compared with the McBain balance method at the high pressure end. Note also that there was a small amount of adsorption of NH_3 onto the walls of the glass manifold that will affect the accuracy of x at low pressures ($< 10^{-2}$ atms), but this was minimal and should not change the qualitative feature of the weight-uptake curve of Figure 2.

All x-ray measurements and sample characterization reported here were accomplished utilizing a Huber model 430-440-512 4-circle diffractometer coupled through a vertically-bent graphite monochromator to a Rigaku 12-Kw rotating anode x-ray source equipped with a Mo anode. The x-ray signal from a Bicron NaI detector was fed into a Tracor-Northern 1710 Multichannel analyzer (MCA). Both the MCA and Huber diffractometer were controlled using a DEC-PDP-1103 digital computer,

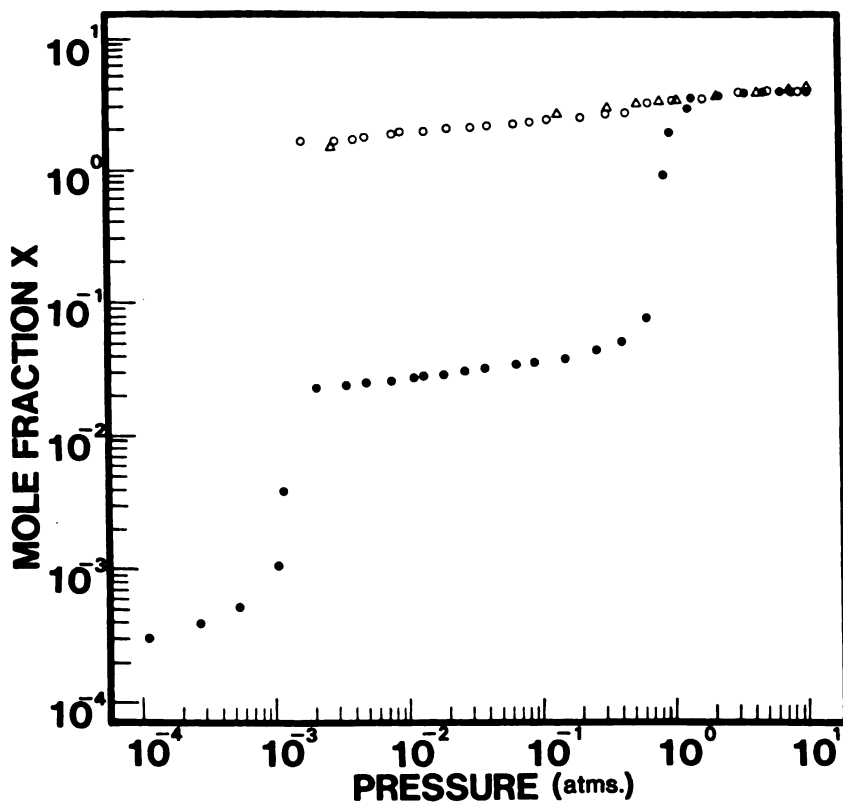


Figure 2. The variation of the mole fraction x with P_{NH_3} for the ternary GIC $\text{K}(\text{NH}_3)_x \text{C}_{24}$ as measured by a "gas-handling" technique (see text). Experimental points indicated with a solid dot (\bullet) represent the initial intercalation of NH_3 , those with open circles (\circ) are for deintercalation. The McBain balance data from Fig. 1 has been replotted as open triangles.

with specially-designed software for automatically repeated scans along any predetermined path in real or reciprocal space.

In situ x-ray diffraction studies as a function of P_{NH_3} were also performed on the ternary GIC $\text{K}(\text{NH}_3)_x\text{C}_{24}$. A KC_{24} sample (-.7mm x 6mm x 10mm) prepared in the manner described above, was placed in an 8mm pyrex tube with excess liquid NH_3 . The KC_{24} sample was initially intercalated with NH_3 at room temperature, and was found to be a pure stage-1 compound ($d = 6.633\text{\AA}$) with a stoichiometry $\text{K}(\text{NH}_3)_{4.33}\text{C}_{24}$ determined by weight-uptake measurements. We then maintained the sample at room temperature for all subsequent measurements, but in order to change the sample composition, i.e. change x in $\text{K}(\text{NH}_3)_x\text{C}_{24}$, we varied the temperature of the excess NH_3 as follows:

A dewar of ethyl alcohol was placed around the NH_3 end of the sample tube and the alcohol was slowly ($\approx 20^\circ\text{K}/\text{hour}$) cooled (to -110°C) to avoid exfoliation of the specimen. The ethyl alcohol was then replaced with liquid nitrogen as the low temperature bath. The dewar of liquid nitrogen was removed and a dewar containing an ethanol slush at -110°C was placed over the NH_3 end of the sample tube and allowed to warm up slowly ($\approx 4.4^\circ\text{K}/\text{hour}$) to room temperature. The ammonia pressure was again determined by monitoring the temperature of the excess NH_3 liquid and applying Eq. 1.

In situ x-ray (00 ℓ) diffraction scans were taken at one hour intervals as the NH_3 warmed. Representative scans are shown in Figure 3 which depicts the pressure evolution of the K-NH_3 GIC from stage 2 to stage 1. The pattern of Figure 3(d) is associated with a change in the color of the sample from dark metallic blue to a yellow-gold and reveals that the sample consisted of a mixed phase system composed mainly of the

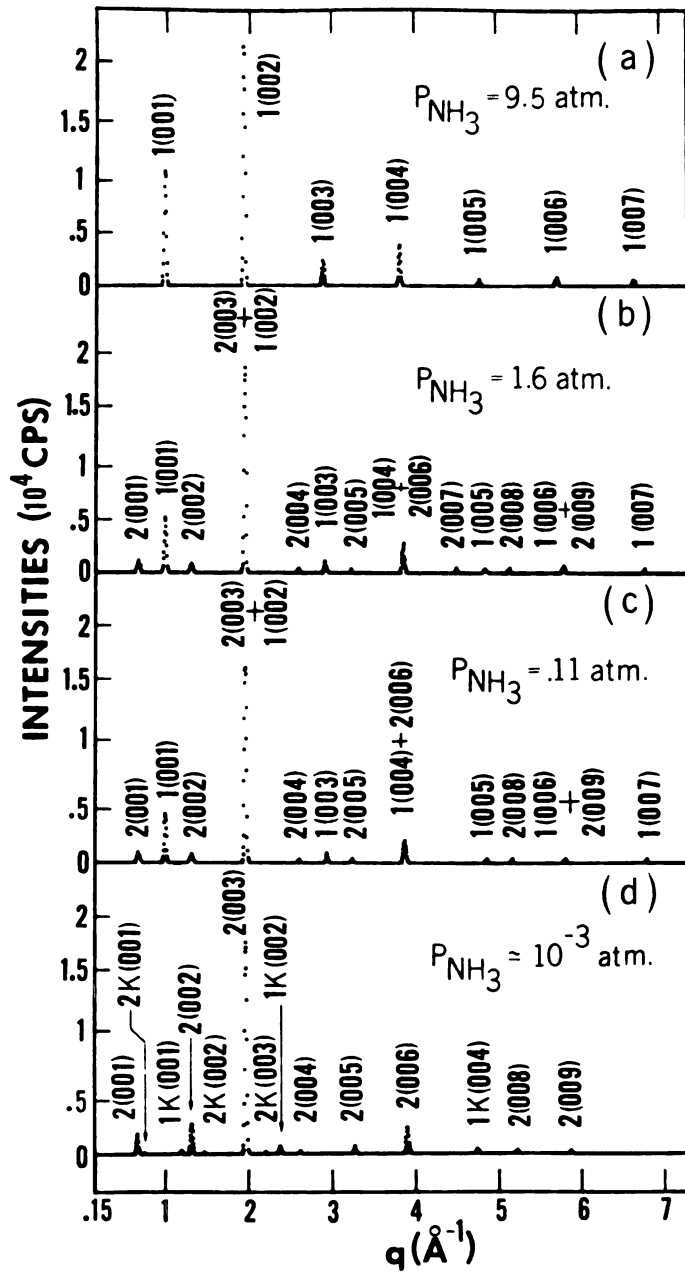


Figure 3. (a), (b), (c), and (d) represent the P_{NH_3} evolution of the $(00l)$ x-ray diffraction patterns of $\text{K}(\text{NH}_3)_x\text{C}_{24}$. Reflections associated with the stage n K-NH₃ ternary GIC's are labeled $n(00l)$. Those associated with the binary potassium GIC's are labeled $nK(00l)$.

stage-2 K-NH₃ ternary GIC with admixtures of the binary GIC's KC₂₄ (d = 8.67Å) and KC₈ (d = 5.33Å). The "yellowish" appearance of the sample surface is due to the presence of KC₈, which is normally gold in color. Observed reflections in each pattern are of instrument-limited width and thus, for the 1-mm slit settings used, indicate a c-axis correlation range of ~350Å.

Shown in Figures 4 and 5 are the d-spacings of stage 1 (d₁) and stage 2 (d₂) K-(NH₃) GIC's as a function of P_{NH₃}. The NH₃ pressure dependence of the intensities of the (001) reflection of stage 1 and the (002) reflection of stage 2 is shown in Figure 6 and clearly indicates a phase transition from stage-2 to stage-1 with increasing pressure. The inflections visible in the intensity data of Figure 6 at P_{NH₃} = 5.5 atms are due to compositional changes and will be discussed below. For P_{NH₃} > 6.5 atms, only the (001) and (002) reflections of the stage-2 region are detectable in the (00l) x-ray diffraction patterns. The (003) reflection of stage 2 is masked by the strong (002) reflection of stage 1. The large fluctuations visible in d₂ vs. P_{NH₃} of Figure 5 are due to inaccuracies associated with determining d₂ from only the two observable low-angle reflections cited above. The dashed line in Figure 5 is an extrapolation of the d₂ vs. P_{NH₃} curve to P_{NH₃} = 9.5 atms (corresponding to T_{NH₃} = room temperature) with d₂ = 9.930Å. Both the d-spacings of Figures 4 and 5 and the weight-uptake measurements of Figures 1 and 2 show rapid changes for P_{NH₃} < 1 atm and establish that the c-axis expansion of the K-NH₃ GIC is due to the influx of NH₃.

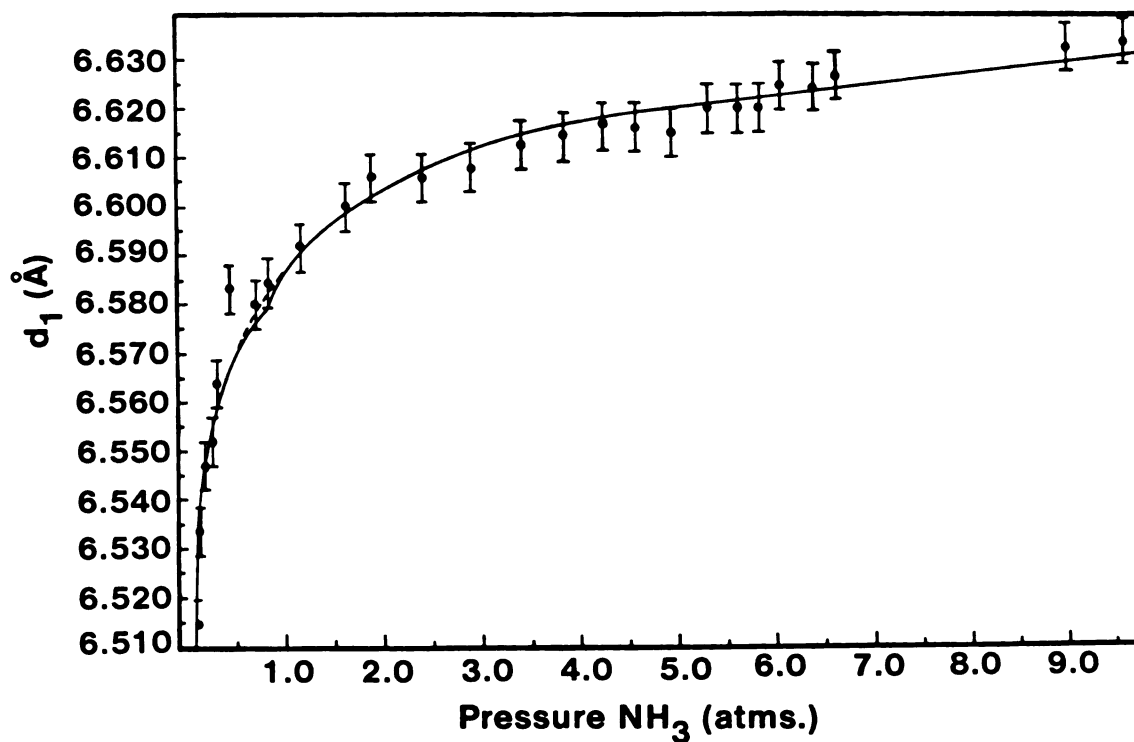


Figure 4. The variation of the d-spacing of stage-1 K- NH_3 GIC (d_1) with P_{NH_3} . The experimental points are shown as solid dots (o) with the indicated error bars, and the solid line represents a theoretical fit to the data using Eq. 18.

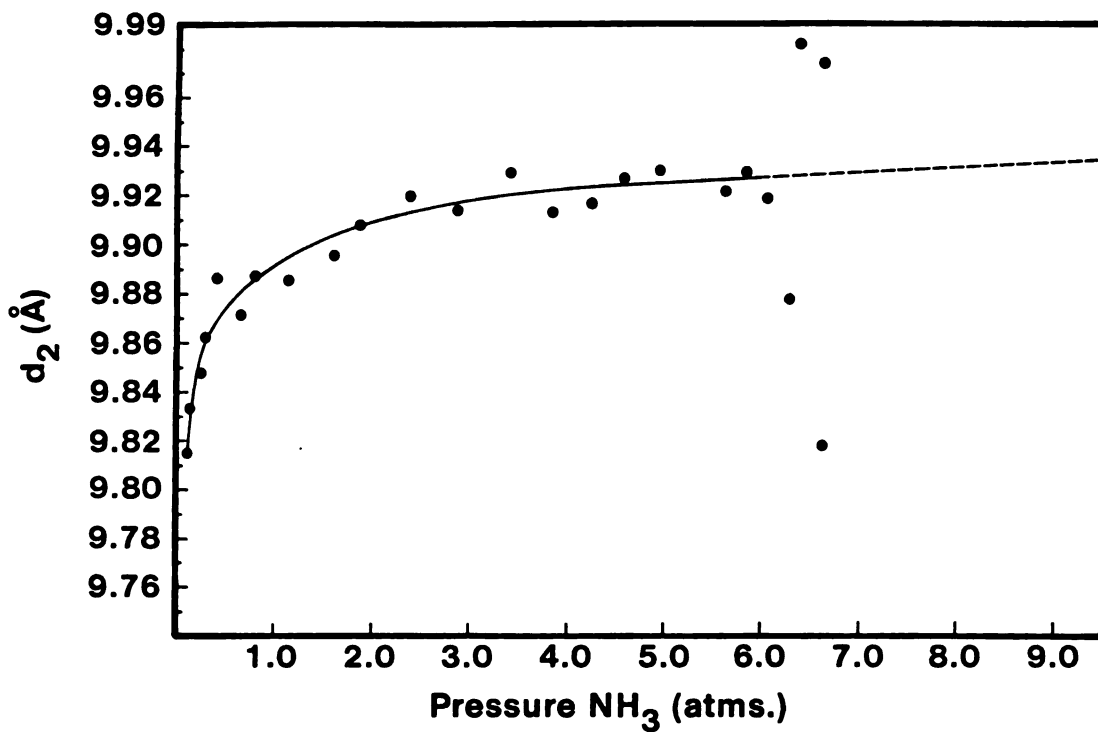


Figure 5. The dependence of the d-spacing of stage-2 (d_2) K- NH_3 GIC with P_{NH_3} . Experimental points are indicated with a solid dot (o), and the solid line is a guide to the eye. The dashed line is an extrapolation of the curve to $P_{\text{NH}_3} = 9.5$

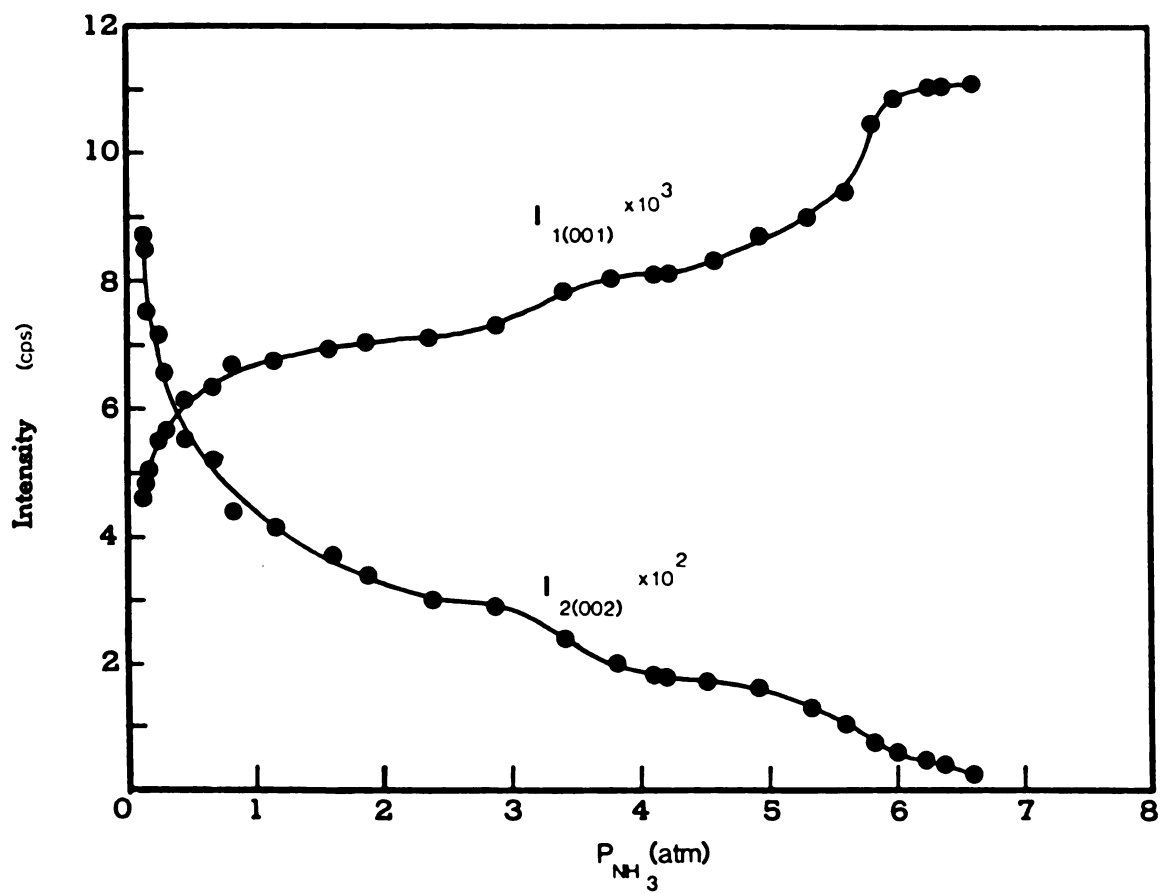


Figure 6. The dependence of the intensities of the (001) reflection of stage-1 and the (002) reflection of stage-2 K-NH_3 GIC's with P_{NH_3} (indicated with solid dots ●).

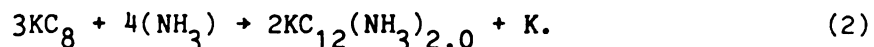
III. Discussion and Analysis

A. Comparison with Rudorff's Results on K-NH₃ GIC's

Before proceeding with the analysis of the above experimental data, it will be useful to discuss the stage-1 and stage-2 K-NH₃ GIC results of Rudorff and coworkers¹⁸ in order that comparisons can be made with our results. It will also be necessary to discuss the physical implications arising from the weight-uptake curve of Figure 2 and the x-ray diffraction pattern of Figure 3d before a method of analysis can be established.

Rudorff et al.¹⁸ showed, over 30 years ago, that metal ammonia solutions (M-NH₃ where M is any alkali metal) could be readily intercalated into graphite. They prepared a stage-1 K-NH₃ GIC via two techniques: The first technique was to directly immerse the binary GIC KC₈ into liquid NH₃. They found that upon intercalation of NH₃, K was expelled from the specimen. A second technique was to directly immerse graphite powder in a metal rich K-NH₃ solution. Both techniques, after the removal of excess absorbed NH₃ at 0°C, were reported to yield the ternary GIC K(NH₃)_{2.0}C₁₂ with a d-spacing of 6.5Å. A stage-2 K-NH₃ GIC was also prepared by controlling the concentration of the K-NH₃ solution into which the graphite powder was immersed. Rudorff et al.¹⁸ found, after the evacuation of NH₃, that only for a carbon/potassium molar ratio of 28 was a pure stage-2 compound formed with an average stoichiometry of K(NH₃)_{2.3}C₂₈ and d-spacing of 9.9Å.

From the results of Rudorff and coworkers, it seems energetically favorable at low NH_3 pressures, for $\text{K}(\text{NH}_3)_x\text{C}_y$ GIC's to acquire a carbon/metal ratio of 12 for stage 1 and 28 for stage 2, and an NH_3 /metal ratio of 2.0 for both (stage 2 may have a slightly higher NH_3 /metal ratio). Thus, potassium was expelled from the binary GIC KC_8 upon submersion into liquid NH_3 according to the reaction



Upon the removal of the absorbed NH_3 in a vacuum, both stage 1 and stage 2 K- NH_3 GIC's still retain large amounts of NH_3 ($x = 2.0$) in their respective galleries. Thus, at low pressures these K- NH_3 ternary GIC's are residue compounds.

We have also prepared pure stage-1 K- NH_3 GIC's in a manner similar to that of Rudorff¹⁸ (i.e. HOPG + K- NH_3 liquid and KC_8 + NH_3 liquid), except our samples have excess liquid NH_3 in the sample vessel. The (00 l) x-ray diffraction patterns of KC_8 + NH_3 liquid and HOPG + K- NH_3 liquid are shown in Figures 7a and 7b, and indicate that the resultant stage-1 ternary GIC's have very similar d-spacings of 6.516Å and 6.586Å, respectively. These values are in reasonable agreement with Rudorff's results of $d = 6.5\text{Å}$ for both methods. Furthermore, our KC_8 + NH_3 liquid samples upon intercalation exfoliated, a process which appears to be associated with the rapid expulsion of potassium as reported by Rudorff.¹⁸ Nevertheless, it is reasonable to question whether the stoichiometry of our stage-1 compounds prepared from HOPG + K- NH_3 liquid and KC_8 + NH_3 liquid is in fact the same as reported by Rudorff,¹⁸ since at high NH_3 pressure it is possible to either expell potassium or intercalate additional ammonia.

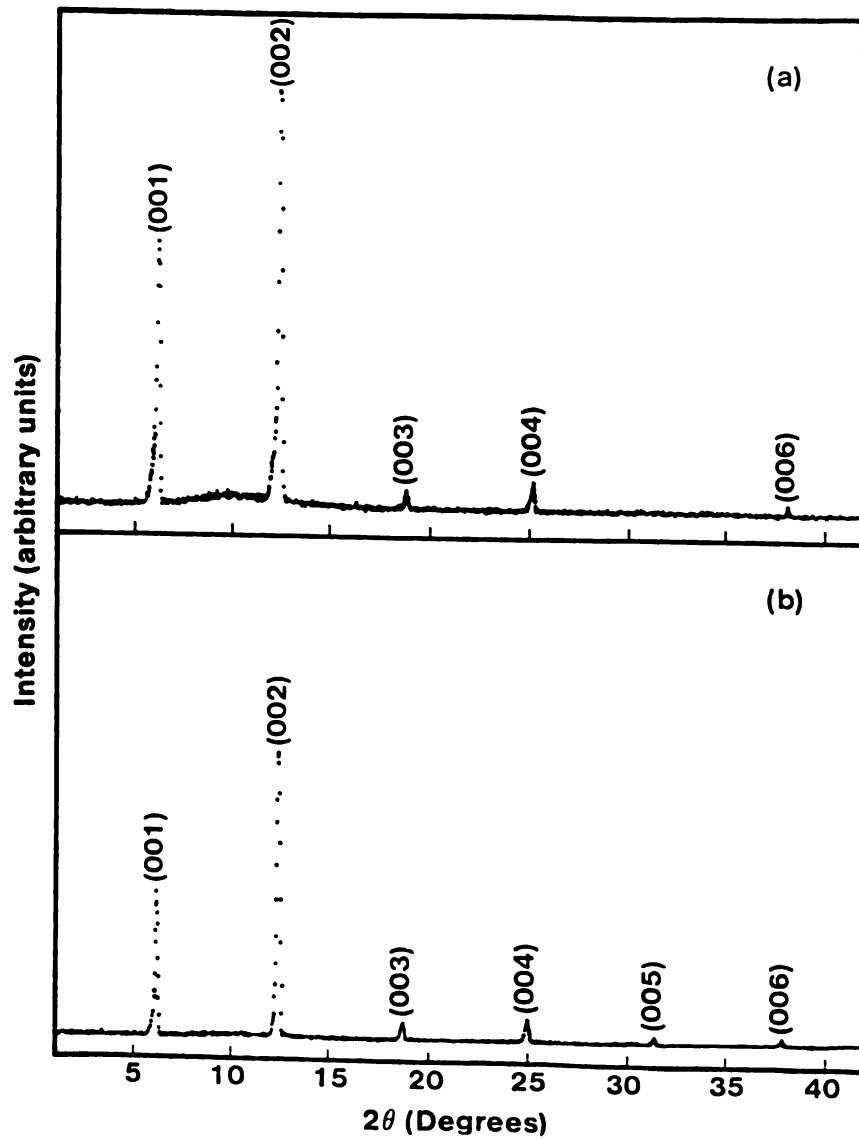


Figure 7. The room temperature (00 l) x-ray diffraction patterns of (a) stage-1 $\text{KC}_8 + \text{NH}_3$ liquid, and (b) stage-1 $\text{HOPG} + \text{K-NH}_3$ solution. The notation is the same as that of Fig. 3.

Given a fixed carbon/potassium ratio of 12, it is possible to estimate the maximum intercalation of NH_3 at 9.5 atms. The "effective" area of an NH_3 molecule can be estimated on the assumption that NH_3 completely fills the available area of the graphite gallery for stage-1 $\text{K}(\text{NH}_3)_{4.33}\text{C}_{24}$. The "available area" for the unit of composition $\text{K}(\text{NH}_3)_{4.33}\text{C}_{24}$ of stage 1 is $A = 56\text{\AA}^2$ and it was determined by subtracting the area of a potassium ion of radius 1.46\AA (see below) from the area of 24 carbon atoms. From $A = 56\text{\AA}^2$ and $x_{\text{max}} = 4.33$, the "effective area" of an NH_3 molecule A_{NH_3} is 13.07\AA^2 , which following a similar analysis leads to a value $x_{\text{max}} = 2.0$ for the compound $\text{K}(\text{NH}_3)_x\text{C}_{12}$. Thus, if no potassium is ejected, the $\text{K}(\text{NH}_3)_x\text{C}_{12}$ compound becomes saturated at the low pressure (vacuum) at which $x = x_{\text{max}} = 2$ and ingests no more NH_3 even when P_{NH_3} is raised to 9.5 atm.

The d-spacing of our stage-1 compounds prepared from HOPG + K-NH_3 liquid is $\approx 6.5\text{\AA}$ even with $P_{\text{NH}_3} = 9.5$ atm and lies very close to that reported by Rudorff¹⁸ ($d = 6.5\text{\AA}$). In contrast, our stage-1 $\text{K}(\text{NH}_3)_{4.33}\text{C}_{24}$ compound which was prepared by reacting KC_{24} with NH_3 has a d-spacing of 6.633\AA. Therefore, it is indeed evident that large amounts of potassium are not expelled from the $\text{K}(\text{NH}_3)_x\text{C}_{12}$ system when it is exposed to elevated NH_3 pressures.

B. The Absorption Isotherm

We will now describe and explain the physical implications of the weight-uptake curve of Figure 2 and the x-ray diffraction pattern of the residue compound of Figure 3d.

As P_{NH_3} is increased, the weight-uptake curve in Figure 2 (solid dots) shows that little intercalation takes place until a pressure of 10^{-3} atms is reached, then rapid intercalation sets in. This rapid influx of NH_3 could be attributed to an activation energy associated with separating the graphite layers enough to allow a small amount of NH_3 to enter. For ammonia pressures $>10^{-3}$ atms a plateau region is reached with $x = .03$. This plateau region extends from 10^{-3} atms to .6 atms and is followed by another rapid influx of NH_3 reaching another plateau region at $x = 4.0$. This transition at $P_{\text{NH}_3} = .6$ atms is also concurrent with a stage transformation from stage 2 to stage 1 (refer to Fig. 6) and is accompanied by a dilution of the inplane potassium density from KC_{12} to KC_{24} . At 9.5 atms the sample is a pure stage 1 with a stoichiometry of $\text{KC}_{24}(\text{NH}_3)_{4.33}$. As the pressure is lowered from 9.5 atms (open circles of Fig. 2), x now follows a new path and as $P_{\text{NH}_3} \rightarrow 0$, $x \rightarrow 1.49$, which is consistent with the fact that the compound which results from pumping off the NH_3 is a stage-2 residue compound.¹⁸

Akuzawa et al.²⁶ have also prepared K- NH_3 GIC's using quite different preparation techniques. They first prepared a stage-2 $\text{K}(\text{NH}_3)_{2.0}\text{C}_{28}$ using the methods of Rudorff,¹⁸ then evacuated the sample chamber at an elevated temperature and reintercalated to stage 1 with potassium vapor. Akuzawa and coworkers report a stage-1 compound with a d-spacing of 5.4Å, slightly larger than that of KC_8 of 5.35Å and a stoichiometry from chemical analysis of $\text{K}(\text{NH}_3)_{.03}\text{C}_6$. The exact composition of the samples prepared by Akuzawa et al. is somewhat in doubt since NH_3 has a tendency to decompose at the elevated temperatures used to reintercalate potassium. The similarity in the K/ NH_3 ratio $x =$

.03 of Akuzawa's sample and the x value of the first plateau region in Figure 2 is striking in light of the totally different preparation techniques involved. This similarity indicates that once this first plateau region at $x = .03$ is reached, the weight-uptake curve (see Fig. 2) is no longer reversible and subsequent desorption of NH_3 yields a stage-2 residue compound, $\text{K}(\text{NH}_3)_{.03}\text{C}_{24}$.

Although we have not as yet measured the d-spacing in that first plateau region of Fig. 2 at composition $\text{K}(\text{NH}_3)_{.03}\text{C}_{24}$, we expect to find a carbon-intercalant-carbon sandwich thickness similar to that of $\text{K}(\text{NH}_3)_{.03}\text{C}_6$ which according to Akuzawa et al.²⁶ is approximately $d = 5.4\text{\AA}$ as noted above. This similarity is not surprising since NH_3 sparsely populates the graphite galleries (for $x = .03$ the NH_3 - NH_3 distances are $\sim 100\text{\AA}$) and graphite can easily accommodate a sufficiently small density of local elastic distortions (due to intercalation) without altering significantly its sandwich thickness.²⁷

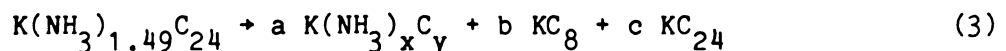
From the above discussion, a plausible explanation of the first rapid influx of NH_3 at 10^{-3} atms is as follows. The elastic energy of the carbon-(K- NH_3)-carbon sandwich is small since the sandwich thicknesses of $\text{K}(\text{NH}_3)_{.03}\text{C}_{24}$ ($d_s = 5.4\text{\AA}$) and KC_{24} ($d_s = 5.35\text{\AA}$) are nearly the same. Thus, even at these very low pressures, the NH_3 pressure is still large enough to overcome the energy associated with creating sparsely-populated elastic distortions, thereby intercalating .03 moles of NH_3 per mole of K into the galleries. The plateau region of $x = .03$ and the second rapid intercalation of NH_3 at $P_{\text{NH}_3} = 0.6$ atms can be explained in a similar fashion. Since NH_3 has a high mobility in the galleries of graphite,¹⁹ to significantly increase x beyond 0.03 may require the sandwich thickness on the average to be much larger (for

example, $d_s = 6.5\text{\AA}$ as measured on deintercalation at 0.6 atms.) than that of $\text{K}(\text{NH}_3)_{.03}\text{C}_{24}$ ($d_s = 5.4\text{\AA}$). Thus, the elastic energy involved with increasing x is large and the pressure to overcome this energy is also large. Thus, x remains constant at $x \sim .03$ for several decades of ammonia pressure until rapid intercalation sets in at the critical pressure of 0.6 atms.

C. The Residue Compound $\text{K}(\text{NH}_3)_{1.49}\text{C}_{24}$

As noted above, the residue compound represented in the pattern of Figure 3d contained three phases: stage-1 KC_8 , stage-2 KC_{24} , and the stage-2 $\text{K}(\text{NH}_3)_{1.49}\text{C}_{24}$. The bulk stoichiometry of the latter was established from the weight-uptake measurements shown in Figures 1 and 2. These results at first glance are not consistent with the stoichiometry of the stage-2 residue compound $\text{K}(\text{NH}_3)_{2.3}\text{C}_{28}$ prepared by Rudorff, but at this point, it is not clear that such a comparison can be made given the difference in the initial conditions of sample preparation.

Since no potassium is expelled from $\text{K}(\text{NH}_3)_x\text{C}_{24}$ as x is reduced the presence of KC_8 in the $x = 1.49$ residue compound requires that for a fixed carbon/potassium ratio of 24 there must also exist expanded regions of KC_y where $y > 24$. It is interesting to note that the formation of 75% of $\text{K}(\text{NH}_3)_2\text{C}_{28}$ is entirely possible just based on balancing the NH_3 content for the two compounds (i.e. 75% of $x = 2.0 \rightarrow x = 1.5$). From the above observations it is possible to describe the three phase system of Fig. 3d with the following reaction



The relative magnitudes of a , b , and c and the mole fractions x , y can be determined by simultaneously solving the three mass equations 4a, 4b, and 4c that balance Eq. 3 for K , C , and NH_3 , plus Eqs. 5a and 5b, which represent the ratio of the intensity of the (003) reflection of $K(NH_3)_x C_y$ to the (002) reflection of KC_8 , and the ratio of the (003) reflection of KC_{24} to the (002) reflection of KC_8 respectively.

$$1 = a + b + c \quad (4a)$$

$$24 = ay + 8b + 24c \quad (4b)$$

$$1.49 = ay \quad (4c)$$

$$\frac{a |S_2'(q'_{003}, x, y)|^2 LP(q'_{003})}{b |S_1(q_{002})|^2 LP(q_{002})} = \frac{I_2'(q'_{003})}{I_1(q_{002})} \quad (5a)$$

$$\frac{c |S_2(q_{003})|^2 LP(q_{003})}{b |S_1(q_{002})|^2 LP(q_{002})} = \frac{I_2(q_{003})}{I_1(q_{002})} \quad (5b)$$

Here q_{002} , q'_{003} , and q_{003} are the wave vectors ($q = 4\pi \sin\theta/\lambda$) associated with the (002) reflection of KC_8 , the (003) reflection of $K(NH_3)_x C_y$, and the (003) reflection of KC_{24} , respectively. Also shown in Eqs. 5a and 5b are the structure factors $S_1(q)$, $S_2'(q)$, $S_2(q)$ (which is also dependent on composition x, y), and the intensities $I_1(q)$, $I_2'(q)$, $I_2(q)$ for KC_8 , $K(NH_3)_x C_y$, and KC_{24} , respectively, as well as the combined Lorentz polarization factor $LP(q)$. Debye-Waller and absorption corrections were omitted from Eqs. 5a and 5b and are expected to produce only marginal differences in the results since $q_{002} \approx q_{003}$ and $q_{002} \approx q'_{003}$.

The parameters that result from simultaneously solving the above five equations are: $a = .71$, $b = .24$, $c = .05$, $x = 2.1$, and $y = 29.4$, which to within experimental uncertainty are consistent with $a = .75$, $b = .19$, $c = .063$, $x = 2.0$, and $y = 28$, so that Eq. 2 can be rewritten in the following form:

$$K(\text{NH}_3)_{1.5}\text{C}_{24} = .75 K(\text{NH}_3)_{2.0}\text{C}_{28} + .25 \text{KC}_{12} \quad (6)$$

where $\text{KC}_{12} = .75 \text{KC}_8 + .25 \text{KC}_{24}$.

Equation 6 suggests that our stage-1 $K(\text{NH}_3)_{4.33}\text{C}_{24}$ sample evolved as the pressure was decreased to the stage-1 and stage-2 Rudorff compositions given below.

$$K(\text{NH}_3)_{2.0}\text{C}_{24} = .75 \text{KC}_{28}(\text{NH}_3)_{2.0} + .25 \text{KC}_{12}(\text{NH}_3)_{2.0} \quad (7)$$

This reaction is expected to occur at $P_{\text{NH}_3} = 10^{-2}$ atm, as estimated from Figure 2 (i.e. for $P_{\text{NH}_3} = 10^{-2}$ atms, $x = 2.0$).

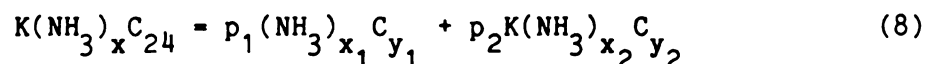
Upon further lowering of the ammonia pressure below 10^{-2} atms, a dynamic exchange of NH_3 between stage 1 and stage 2 and the environment may have caused the depletion of NH_3 in the stage-1 region yielding the unstable KC_{12} component which ultimately phase separated into KC_8 and KC_{24} .

A possible scenario for the depletion of NH_3 in stage 1 is the following: As P_{NH_3} is lowered below 10^{-2} atms, the composition evolves to $x < 2.0$; this is an energetically unfavorable situation for both stages. However, if as we show below, stage 2 has a higher affinity for NH_3 than does stage 1, it will "pull" the NH_3 across the graphite gallery from the stage-1 region. Then any excess in the stage 2 region,

above $x = 2.0$, will be desorbed. It has been established^{13,15,16} that stage-1 $K(NH_3)_{4.33}C_{24}$ is a donor GIC, thus, Rudorff's $K-NH_3$ compounds¹⁸ are also likely to be donors. If a direct comparison can be made between ternary alkali-ammonia and binary alkali donor GIC's which have charge exchanges of $f = 1$ and $f = .86$ for the stage-2 and stage-1 compounds, respectively, then the charge on the potassium ion of stage-2 $K(NH_3)_{2.0}C_{28}$ is greater than that for stage-1 $K(NH_3)_2C_{12}$. A greater charge on the potassium ion results in a stronger charge-dipole bond with NH_3 , which in turn requires that the stage-2 $K-NH_3$ GIC has a higher affinity for NH_3 than does stage-1. This would also explain the significantly higher NH_3 /metal ratios of the other stage-2 alkali and alkaline earth NH_3 -GIC's also reported by Rudorff.¹⁸

D. The Generalized Reaction of KC_{24} with NH_3

From the above discussion it is likely that the compositions of the two stages are pressure dependent and Eq. 7 should be generalized in the following manner



where y_n , x_n , and p_n are the mole ratios of carbon/potassium, NH_3 /potassium, and relative fraction of each stage n , all of which are pressure dependent and have yet to be determined.

To solve unambiguously for the above variables would require six independent equations. There are five equations that are readily at our disposal. These are the three mass equations that balance equation 8 for potassium, carbon, and NH_3 , listed in equations 9a, 9b, and 9c below, plus the two intensity equations 10a and 10b for the (001)

reflection of stage-1 $K(NH_3)_{x_1}C_{y_1}$ and the (002) reflection of stage-2 $K(NH_3)_{x_2}C_{y_2}$.

$$p_1 + p_2 = 1 \quad (9a)$$

$$p_1 y_1 + p_2 y_2 = 24 \quad (9b)$$

$$p_1 x_1 + p_2 x_2 = x \quad (9c)$$

$$p_1 |S_1(q_{001}, x_1, y_1, \gamma_1)|^2 LP(q_{001}) = \alpha I_1(q_{001}) \quad (10a)$$

$$p_2 |S_2(q_{002}, x_2, y_2, \gamma_2)|^2 LP(q_{002}) = \alpha I_2(q_{002}) \quad (10b)$$

Again, we have purposely left out absorption and Debye-Waller corrections because such corrections will only marginally influence the results and inevitably complicate the analysis. The constant α should only depend on the x-ray scattering geometry. It was determined so that the slope of x_1 vs. P_{NH_3} matched that of the weight-uptake measurements for $P_{NH_3} > 6.0$ atms since, to a very good approximation, $P_1 = 1.0$ in that region (see Fig. 6). The notation used in Eqs. 9 and 10 is the following: q_{00l} is the wavevector associated with the (00l) reflection of stage n , I_n , and P_n are the intensities and fraction of each stage, $LP(q)$ is the combined Lorentz polarization factor, and $S_n(q_{00l}, x_n, y_n, \gamma_n)$ is the structure factor for stage n , which depends on the wave vector q_{00l} , the composition (x_n, y_n) and a charge exchange parameter (γ_n) . Incorporated into the structure factors $S_n(q_n)$ are the charge exchange terms $f = 1 - \gamma_n(X_n - 4)$ where $\gamma_2 = 0$ and $\gamma_1 = .424$ were inferred from NMR measurements¹⁵ of $K(NH_3)_{4.33}C_{24}$. The charge exchange terms will be considered in more detail later.

In order to solve for the variables in eqs. 9 and 10 as a function of ammonia pressure an additional constraint is required. Such a constraint can be found by setting $x_2 = 2.3$. We have shown in earlier work¹² that x_2 is essentially pressure independent and $x_2 = 2.1$ at low pressures. However, small pressure dependent compositional changes in y_1 and y_2 were not previously considered, but do not alter the basic pressure insensitivity of x_2 . Therefore, since x_2 is pressure insensitive, y_2 can be expected to follow suit (this assumes of course that NH_3 completely fills the available gallery area determined by y_2).

Rudorff reported that at very low ammonia pressures the stage-2 K-NH_3 ternary GIC had an average stoichiometry of $\text{K}(\text{NH}_3)_{2.3}\text{C}_{28}$ ¹⁸ which is consistent with our ternary GIC represented in Fig. 3d. If y_2 remains constant at 28, we can estimate the value of $(x_2)_{\text{max}}$ by assuming that the stage-2 ternary GIC is maximally occupied by NH_3 , that is NH_3 completely fills the available interlayer space. From the effective area of an NH_3 molecule previously calculated, we find $(x_2)_{\text{max}} = .101$, $y_2 = .512$, and $(x_2)_{\text{max}} = 2.3$ for $y_2 = 28$. Therefore, to a good approximation, x_2 is pressure independent and equal to 2.3.

With the above constraint, y_n, p_n for each stage n , and x_1 can be determined by simultaneously solving Eqs. 9 and 10. This is accomplished by reducing these equations to a 6th degree polynomial of one variable. The resulting solutions for the variations of y_1 and y_2 with P_{NH_3} are plotted in Fig. 8. It can be seen from Fig. 8 that as P_{NH_3} is increased, y_1 increases from Rudorff's result of $y_1 = 12$ (open circle) to $y_1 = 24$, while y_2 remains relatively constant at Rudorff's value $y_2 = 28$ (open circle at low pressure) until $P_{\text{NH}_3} < 5.0$ atms, where

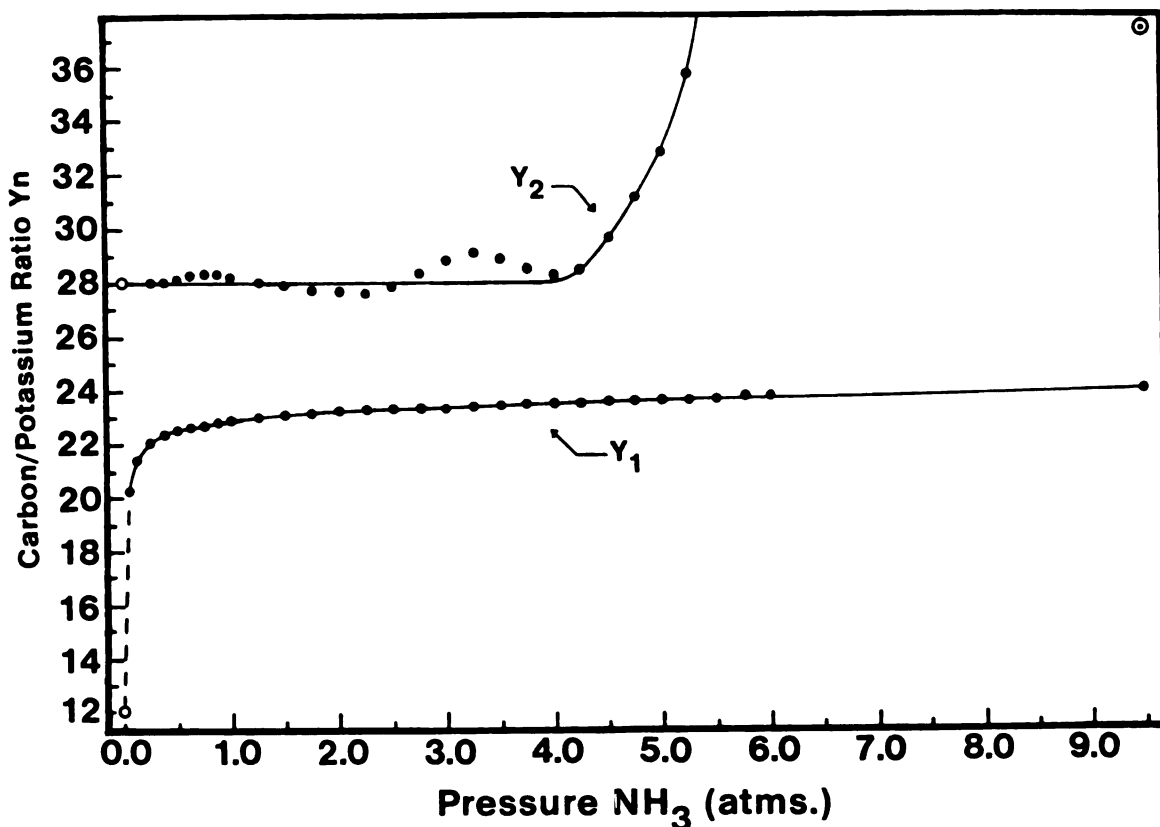


Figure 8. The dependence on P_{NH_3} of the carbon/potassium ratios y_n for each stage n K-NH₃ GIC. Analyzed data points are indicated with a solid dot (\bullet). The solid lines are a guide to the eye. The dashed line for the y_1 vs. P_{NH_3} curve is an extrapolation to the Rudorff¹⁸ C/K ratio $y_1 = 12$. The open circles represent the C/K ratios reported by Rudorff¹⁸ for stage 1 and 2 K-NH₃ GIC's. The solid dot with a concentric circle (\odot) represents an estimate of y_2 at $P_{\text{NH}_3} = 9.5$ atms based on an analysis of the x-ray data shown in Fig. 10 (see text).

it rises sharply. This sharp rise in y_2 for $P_{\text{NH}_3} \sim 5.0$ atms implies that our original assumption of the pressure insensitivity of y_2 is valid only in the range $P_{\text{NH}_3} < 5$ atms. However, our immediate concern is the pressure dependence of x_1 . With the present approach, x_1 should be accurate up to $P_{\text{NH}_3} < 5.0$ atms and also for $P_{\text{NH}_3} \geq 6.0$ atms. (see discussion of eqs. 9 and 10). Thus, the sharp rise in y_2 does not pose a serious problem for determination of $x_1(P_{\text{NH}_3})$.

Small fluctuations of y_1 and y_2 , visible in Fig. 8, are due to the artificial constraint of holding x_2 constant at 2.3 and can be largely removed by allowing small variations in x_2 . The larger fluctuation in y_2 at $P_{\text{NH}_3} = 3.2$ atms corresponds to an inflection in the intensities of the (001) reflection of stage 1 and the (002) reflection of stage 2 shown in Fig. 6. The dependence of the fractions p_1 and p_2 on P_{NH_3} deduced from the solutions of eqs. 9 and 10 is shown in Fig. 9. The rapid changes in which $p_1 \rightarrow 1$ and $p_2 \rightarrow 0$ at $P_{\text{NH}_3} = 5.5$ atm are associated with the sharp rise of y_2 at that pressure. Furthermore, the dashed line indicates an extrapolation to $p_2 = .75$ and $p_1 = .25$ (at low NH_3 pressure) which would be consistent with the formation of the stage 1 and 2 Rudorff compositions given in Eq. 6.

There are other indications that the value of y_2 should be in excess of 37 as indicated in Fig. 8. The room temperature ($P_{\text{NH}_3} = 9.5$ atms) (00 l) x-ray diffraction patterns of $\text{KC}_{36} + \text{NH}_3$ liquid are shown in Fig. 10 and represent a two-phase system composed mostly of a stage-2 K-NH_3 ternary GIC, but with small amounts of a stage-1 K-NH_3 GIC. An analysis identical to that used on the 3-phase system of Fig. 3d (see

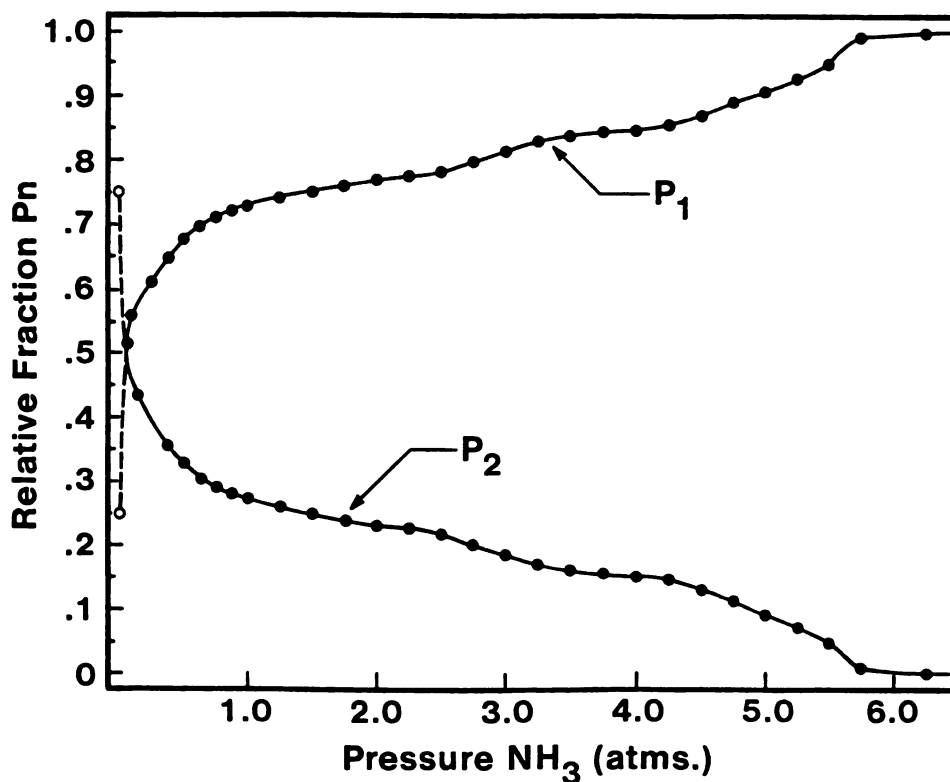


Figure 9. The dependence of p_n , the fraction of each stage n on P_{NH_3} . Analyzed data points are indicated with a solid dot (\bullet), and the solid line is a guide to the eye. The dashed line indicates an extrapolation from the p_n vs. P_{NH_3} curves to the values of $p_1 = 0.25$ and $p_2 = 0.75$ at $P_{\text{NH}_3} = 0$ atms (indicated with open circles), which would be consistent with the formation of the stage-1 and stage-2 Rudorff¹⁸ K-NH₃ GIC's (see Eq. 7 of the text).

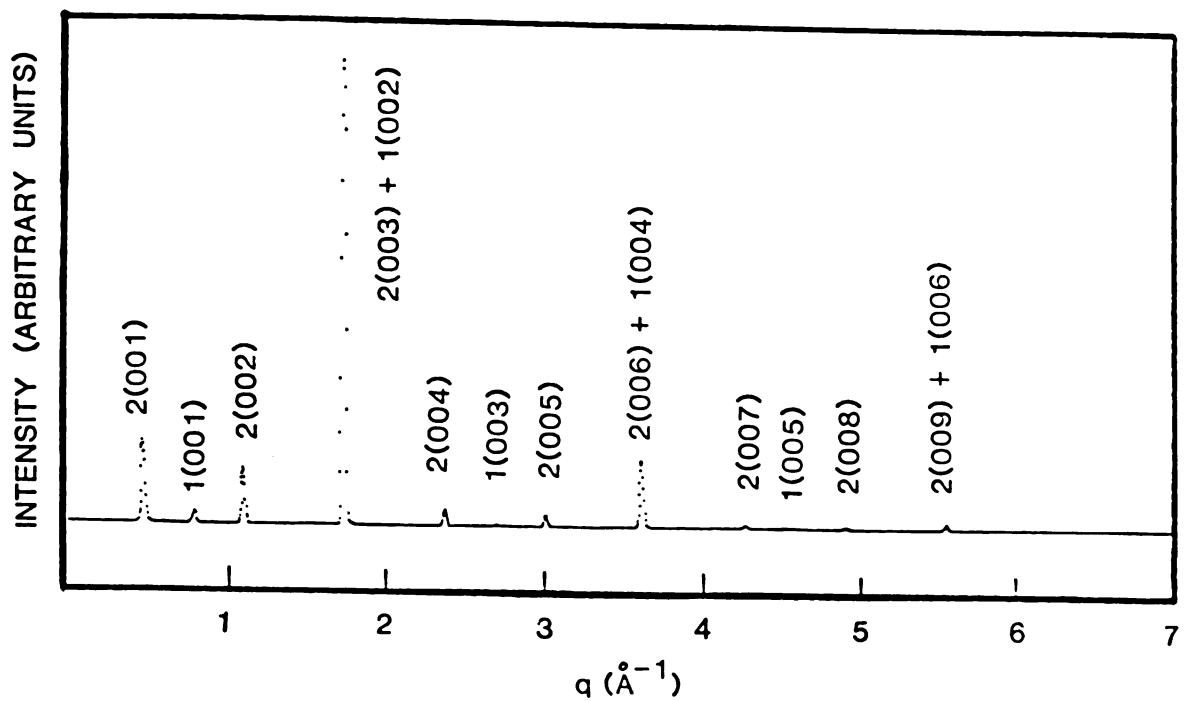


Figure 10. The room temperature ($P_{\text{NH}_3} = 9.5$ atms) (00 l) x-ray diffraction pattern of $\text{KC}_{36} + \text{NH}_3$ liquid. The notation is the same as that of Fig. 3.

Eqs. 4 and 5) was applied to determine the values of x_2 and y_2 for this 2-phase system. It was found by assuming for stage 1, $y_1 = 24$ and $x_1 = 4.33$ and for stage 2 a maximally-occupied gallery (i.e. $x_2 = 101$, $y_2 = 0.512$), that $y_2 = 37.2$ (shown as a solid dot with a concentric open circle in Fig. 8), which may indicate that at $P_{\text{NH}_3} = 9.5$ atms, $\text{K}(\text{NH}_3)_{3.2}\text{C}_{37}$ is a pure stage-2 K-NH₃ GIC.

E. x_1 vs. P_{NH_3} and the Fowler-Guggenheim Form

Figure 11 shows the variation with P_{NH_3} of x_1 (solid dots) for $\text{K}(\text{NH}_3)_{3.2}\text{C}_{37}$ and the corresponding fit to a Fowler-Guggenheim (FG) adsorption equation²³ (solid line in Fig. 1) given below

$$P_{\text{NH}_3} = \frac{\alpha x_1}{(\beta - x_1)} e^{\omega x_1} \quad (11)$$

with $\alpha = 0.496 \times 10^{-5} \pm 0.077 \times 10^{-5}$, $\beta = 4.40 \pm 0.06$, $\omega = 2.43 \pm 0.04$.

It is interesting to note that because the carbon/potassium ratios have been allowed to vary, the FG function now provides a better fit to the data of Fig. 11 than does the Langmuir function²⁸ which was previously applied.¹² The superiority of the FG form is not surprising since the Langmuir function is a zero-order approximation to adsorption and does not include the interaction between adsorbed atoms. However, the Fowler-Guggenheim equation given above includes this interaction and reduces to the Langmuir form where $\omega = 0$.

The fit of x_1 vs. P_{NH_3} shown in Fig. 11 yields the parameter ω which measures the interaction energy between NH₃ molecules. Fowler and Guggenheim derived the relation $\epsilon = \beta kT\omega/Z$ where for our use, Z is the

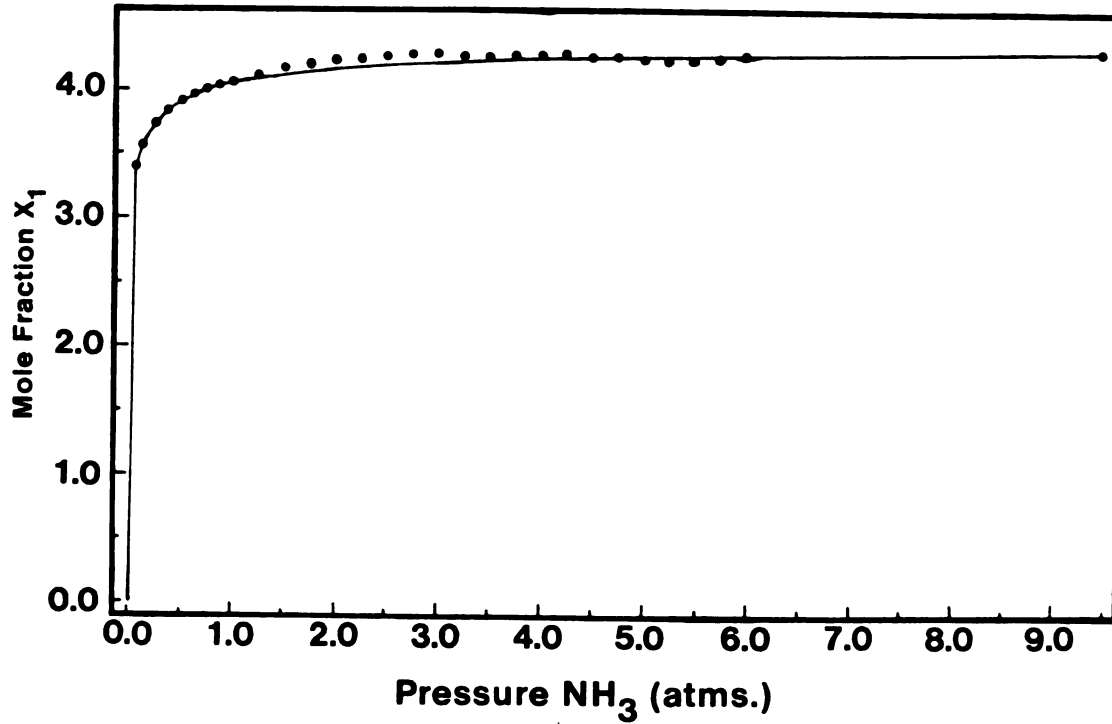


Figure 11. The variation of the mole fraction of stage-1 X_1 with P_{NH_3} . Analyzed data points are indicated with solid dots (\bullet). The solid line represents a least squares fit to X vs. P_{NH_3} using Eq. 11 of the text with $\alpha = 0.496 \times 10^{-5}$, $\beta = 4.40$, and $\omega = 2.43$.

number of nearest neighbor NH_3 molecules. The interaction energy between NH_3 molecules is ϵ , kT is the usual thermal energy, and β and ω are given above, with $\omega > 0$ indicating a repulsive interaction between molecules. We find $\omega > 0$ and for a maximum close-packed structure of six nearest neighbors $\epsilon_{\min} = +0.04$ eV.

An estimate can be made of the maximum repulsive energy of two interacting dipoles from $\epsilon_{\max} = \mu^2/r^3$.²⁹ Here, μ is the dipole moment and we have taken r as the close-packed hard sphere diameter of the NH_3 molecule. By using the known value for $\mu_{\text{NH}_3} = 1.5$ Debye²⁵ and $r = 3.41$ Å from diffuse x-ray scattering measurements of liquid NH_3 ,³⁰ we find $\epsilon_{\max} = .035$ eV which is, within error, in agreement with the repulsive energy found from the parameter ω .

A repulsive interaction between NH_3 molecules is contrary to physical intuition, since one would expect dipole alignment to be energetically favorable. However, it is known from NMR results¹⁹ that the NH_3 3-fold axis which is the dipole axis is dynamically tilted toward the potassium ion to which it is bound, thereby restricting the molecule's ability to orient itself. There are also steric constraints on the NH_3 molecule which are imposed by the graphite lattice as can be seen from Fig. 12. The inability of the NH_3 molecule to freely orient means that the probability for dipole-dipole alignment is low and that the dipole-dipole interaction could be repulsive. The accuracy of the magnitude of the interaction energy derived from Eq. 11 is not high, but its repulsive character ($\omega > 0$) is unambiguous.

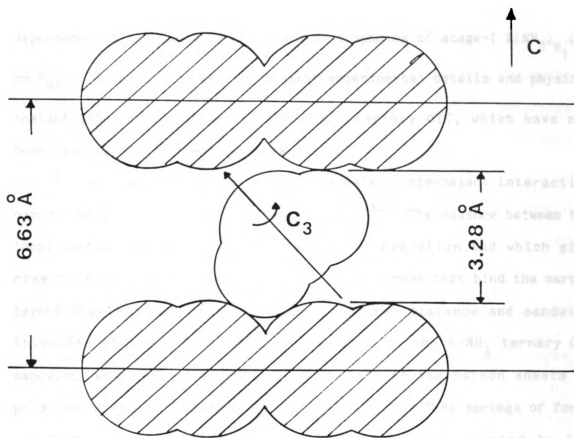


Figure 12. An inplane view of the surface of revolution of an NH_3 molecule about its C_3 axis in a plausible configuration in the stage-1 $\text{K}(\text{NH}_3)_{4.33}\text{C}_{24}$ sandwich. All atomic sizes are scaled relative to their Van der Waals radii:²¹ $r_{\text{carbon}} = 1.675\text{\AA}$, $r_{\text{nitrogen}} = 1.5\text{\AA}$, and $r_{\text{hydrogen}} = 1.2\text{\AA}$. Rotations about the C_3 axis cause the three hydrogens to form an annular ring. This ring is placed in the hexagonal cavity of carbon atoms with the C_3 axis tilted with respect to the c -axis of graphite. The carbon atoms of the graphite bounding planes are shaded.

F. The Model

We now focus on the theoretical model which we have used to fit the dependence of the sandwich thickness or d-spacing of stage-1 $K(NH_3)_{x_1} C_{y_1}$ on P_{NH_3} . In addition, we will present experimental details and physical insight into the properties of the K-NH₃ ternary GIC, which have not been discussed in our earlier work.¹²

It is known that for GIC's the intercalant-intercalant interaction can be mediated by elastic strain fields.^{4,5} The balance between the local distortions which are produced by intercalation and which give rise to these elastic strain fields and the forces that bind the carbon layers together determines the c-axis repeat distance and sandwich thickness of the resulting GIC. To describe the K-NH₃ ternary GIC sandwich, we have used a harmonic model in which the carbon sheets of pristine graphite which initially are "connected" by springs of force constant k_0 with equilibrium length d_0 are intercalated by the "insertion" of two additional springs representing K and NH₃ with force constants k_K and k_A and equilibrium lengths d_K and $d_A > d_0$.

The K-NH₃ intercalant of the stage-1 ternary GIC has been established to be of the donor type from x-ray measurements of the a-axis lattice parameter¹³ and from NMR¹⁹ and reflectivity measurements.²⁰ Most of the charge donated by potassium remains on the carbon sheets after NH₃ insertion, and for the purposes of this discussion, we assume that this charge is distributed uniformly, leaving behind a positively-charged K-NH₃ layer which is "sandwiched" between negatively charged carbon sheets. In actuality, for donor compounds such as the alkali-GIC's it has been shown³¹ that the charge on the carbon layers is not completely delocalized, but screens the positive ions by accumulating

around them. The carbon layers are also not rigid sheets, but can accommodate distortions perpendicular to the layer.²⁷ Nevertheless, a model which describes the K-NH₃ ternary sandwich as uniformly charged rigid carbon sheets separated by "atomic" springs, constitutes a sufficiently reasonable approximation to provide useful information. Following Hawrylak³ and Dahn³² the stage-1 sandwich energy E per carbon atom can be expressed as

$$E = -\alpha x_K^{3/2} + \Omega d_{s_1} x_K^2 f^2 + 1/2 k_o (d_{s_1} - d_o)^2 + 1/2 x_K k_K (d_{s_1} - d_K)^2 + 1/2 x_A k_A (d_{s_1} - d_A)^2 \quad (12)$$

Here α and Ω are constants, d_{s_1} is the equilibrium sandwich thickness of stage 1 and x_K and x_A are the concentrations of K and NH₃ in units of the number of carbon atoms, i.e. $x_K = N_K/N_C$ and $x_A = N_A/N_C$, where N_J is the number of atoms of type J in the bulk specimen for a particular stage.

In Eq. 12 the first term represents the binding or cohesive energy of a 2-dimensional free electron gas while the second term is the electrostatic energy associated with separated layers of charge. The remaining terms represent the elastic energies associated with pure graphite ($x_K = x_A = 0$) and potassium ($x_A = 0, x_K = 0$) and ammonia ($x_K = 0, x_A = 0$) GIC's. The equilibrium length d_K for the potassium intercalant is related to the size of the K species which in turn depends on the charge transfer, f , from the potassium ion to the carbon sheets through the relation³³

$$r_K = f r_{K^+} + (1 - f) r_{K^o} \quad (13)$$

where r_K is the radius of the K ion with charge exchange f , and r_K^+ and r_K^o are the ionic and atomic radii of potassium. Enoki et al.³³ have used this relationship to determine the size of K and Rb ions in alkali binary GIC's and were able to explain the differences they observed in the ESR signals of hydrogenated KC_8 and RbC_8 . In order to relate r_K in Eq. 13 to d_K , the ionic and atomic equilibrium lengths (or sandwich thicknesses) d_K^+ and d_K^o , respectively, must be established. To a very good approximation d_K^o and d_K^+ can be determined from the following relations:

$$d_K^o = 2r_K^o + R_o \quad (14a)$$

$$d_K^+ = 2r_K^+ + R_o \quad (14b)$$

where the geometrical factor $R_o = 2.69\text{\AA}$ was obtained from the experimental value of $d_K^+ = 5.35\text{\AA}$ with $r_K^+ = 1.33\text{\AA}$.³³ Using Eqs. 14a and 14b, Eq. 13 can be rewritten as

$$d_K = fd_K^+ + (1-f)d_K^o \quad (15)$$

where

$$d_K = 2r_K + R_o .$$

It can be expected that the charge exchange f in Eq. 15 is dependent on the NH_3 concentration x_A , since it is well known^{14,15,16} that NH_3 in metal-ammonia ($M-NH_3$) solutions has a strong affinity for electrons. Therefore, it is useful to review briefly below the properties of bulk 3-dimensional (3D) metal ammonia solutions which elucidate the relationship between f and x_A in the 2D analogue $K(NH_3)_x C_{24}$.

As alkali metal is added to liquid NH_3 to form a dilute 3D $M-NH_3$ solution^{14,15} the metal relinquishes its valence electron to the liquid NH_3 and (for $M = \text{potassium}$) is solvated or surrounded by six octahedrally coordinated NH_3 molecules. Solvation of the expelled

electron also occurs, and it forms what will be referred to as an electron-cage with surrounding NH_3 molecules. However, the number of NH_3 molecules required for electron-cage formation on the basis of energy considerations is not known exactly, but is estimated to be between four and six.³⁴ Ammonia is bound in $\text{M}(\text{NH}_3)_6$ complexes by charge-dipole forces, with each NH_3 molecule oriented so that its dipole points away from the metal ion. In contrast, the binding of NH_3 in electron cages is much weaker. Copeland et al.³⁴ have shown that electron cage formation may be brought about by the self-trapping of an electron in a cavity produced by NH_3 molecules through short-range interaction with NH_3 dipoles and by the long-range polarization of the NH_3 medium. When the metal concentration is increased enough to allow significant overlap in the wavefunctions of the individual electron cages, electron "hopping" from cage to cage occurs and a nonmetal to metal transition takes place.

According to the Mott criterion,³⁵ the critical electron concentration n for a nonmetal-metal transition is $n^{1/3} a_H = .25$, where a_H is the effective hydrogen-like radius of the electron-cage. For K-NH_3 solutions, the nonmetal-metal transition occurs at ≈ 4 mole percent metal (MPM = moles of metal / (moles of metal + moles of NH_3) $\times 100\%$). Increasing the metal concentration eventually leads to an insufficient amount of NH_3 molecules with which to solvate the expelled valence electron of the metal. For example, in the very dilute region, $\text{MPM} < 10^{-5}$, there is essentially an infinite number of NH_3 molecules for each electron, but at 10 MPM there are only 9 NH_3 molecules for each metal ion. Assuming 6 NH_3 molecules are bound to the metal ion, only three can couple to the electron. Thus, at high concentrations the expelled

valance electrons which cannot be solvated are forced into the conduction band, causing the M-NH₃ solution to behave as a liquid metal. In fact it has been shown³⁶ from reflectivity experiments that there is a gradual transition between electron cage formation and the conduction band regime. Also note that solvated cations and solvated electrons may interact to produce neutral species^{37,38} either by direct cation-electron interaction, in which there are no NH₃ molecules in between their respective centers, or by NH₃-shared ion-electron pairs, in which the solvated cation and solvated electron share one or more NH₃ molecules, but still retain their own identities.

It is clear from the above discussion that the amount of electron solvation in M-NH₃ solutions depends on the relative concentration of NH₃ to that of K which can be written as X, where $X = x_A/x_K$. There also exists a minimum concentration X_c below which electron solvation cannot occur.

As noted above, Rudorff showed several decades ago that metal-ammonia solutions could be intercalated into graphite.¹⁸ It is surprising that neither the structural or molecular form of the intercalant, nor its 2D metal-ammonia character viz-à-viz a 2D nonmetal-metal transition, have yet been explored.

The metal hexamine K(NH₃)₆ cannot be intercalated into graphite, since that would require a sandwich thickness of at least 10Å and the maximum value observed for the K-NH₃ ternary GIC's is 6.6Å. However, if a pair of NH₃ molecules which lie on the same 4-fold octahedral axis of K(NH₃)₆ are removed, leaving a planar 4-fold coordinated K(NH₃)₄ cluster, intercalation is possible. Given an interlayer space of 3.28Å, which is defined to be the difference between the carbon-K(NH₃)-carbon

sandwich thickness and the Van der Waals diameter of the carbon atoms that flank an intercalant layer, only a monolayer of NH_3 can occupy the interlayer gallery. This point is illustrated in Fig. 12. It is interesting to note that 4-fold coordination is also suggested by weight-uptake measurements of stage-1 $\text{K}(\text{NH}_3)_{4.33}\text{C}_{24}$, with the .33 NH_3 "spacer" molecules per $\text{K}(\text{NH}_3)_{4.0}$ cluster possibly involved in electron cage formation. In principle, other planar N-fold coordination possibilities exist with $N = 2, 3, 5, 6$. However, such N-fold configurations are very unlikely because of steric limitations and/or the fact that the potassium- NH_3 components do not adopt such planar arrangements in bulk M-NH_3 solutions. Moreover, only 4-fold coordination is consistent with recent inplane diffuse x-ray scattering experiments on $\text{K}(\text{NH}_3)_x\text{C}_{24}$.¹³

The entrance of NH_3 into the graphite galleries results in the solvation of both potassium and of electrons originally donated by potassium to the graphite layer. The electron solvation is a manifestation of the collateral extraction of charge out of the carbon sheets together with the formation of electron cages. For the most dilute case, which corresponds to stage-1 $\text{K}(\text{NH}_3)_{4.33}\text{C}_{24}$, the concentration of potassium relative to NH_3 is still = 19 MPM, well into the metallic region of a bulk 3D M-NH_3 solution with the same concentration. Thus, it is very likely that the K-NH_3 intercalant layer acts as a 2D liquid metal with delocalized electrons, which are collectively shared by each potassium ion.

From the above discussion, it can be expected that as NH_3 is added to KC_{24} , little if any electron solvation takes place, since NH_3 preferentially solvates the available potassium ions until a critical

concentration $X_c = 4.0$ is exceeded. It can be assumed to a first approximation and for simplicity that the charge exchange, f , varies linearly with the excess NH_3 above $X = X_c$. Thus,

$$f = \begin{cases} 1 & \text{for } X < X_c \\ 1 - \gamma(X - X_c) & \text{for } X > X_c \end{cases} \quad (16)$$

where $X_c = 4.0$ and the constant γ has yet to be determined.

By incorporating Eqs. 15 and 16 into Eq. 12 and minimizing the sandwich energy E with respect to the sandwich thickness d_{s_1} for a given x_K and x_A we find:

$$\frac{d_{s_1}}{d_{K^+}} = \frac{\left[1 + X_c \frac{k_o}{x_K k_K} \frac{d_o}{d_{K^+}} + X_c \gamma \left(1 - \frac{d_{K^+ o}}{d_{K^+}}\right)\right] + \left[\frac{k_A}{k_K} \frac{d_A}{d_{K^+}} \gamma \left(\frac{d_{K^+ o}}{d_{K^+}} - 1\right)\right] X_1}{1 + \frac{k_o}{x_K k_K} + \frac{k_A}{k_K} X_1} + \frac{\Omega x_K [1 - \gamma(X_1 - X_c)]^2}{k_K \left(1 + \frac{k_o}{x_K k_K} + \frac{k_A}{k_K} X_1\right)} \quad (17)$$

When pristine graphite is intercalated with potassium and ammonia, the resultant carbon interlayer distance increases by about a factor of two. As a result of this large expansion the carbon force constant k_o appropriate to Eq. 17 is not equal to that of pure graphite. In order to properly determine k_o and k_K in Eq. 17, a microscopic theory with appropriately chosen interaction potentials would have to be constructed and the force constants evaluated. However, a crude approximation can be made for k_o by describing the carbon-carbon interlayer interaction with a Lennard-Jones potential, the minimum of which is at $r_o = 3.35\text{\AA}$,

the interlayer distance in pristine graphite, and calculating the force constant (curvature) at $r = 6.63\text{\AA}$, the interlayer distance in $\text{K}(\text{NH}_3)_{4.33}\text{C}_{24}$. Using this approach, we estimate that k_o for $\text{K}(\text{NH}_3)_{4.33}\text{C}_{24}$ is a factor of ~ 200 smaller than that of pristine graphite. Similarly, we find that the value of k_k appropriate to $\text{K}(\text{NH}_3)_{4.33}\text{C}_{24}$ decreases only about a factor of 2 from that for KC_{24} which is not surprising since the sandwich thickness of $\text{K}(\text{NH}_3)_{4.33}\text{C}_{24}$ is only about 20% larger than d_{K^+} . The above method for estimating force constants is of course over-simplified and ignores effects such as charge exchange, which would tend to decrease even further the interlayer interaction. Thus, it is clear that to a good approximation $k_o/k_{K^+} \ll 1$, and that the value of k_k may be approximately determined from those measured for the potassium GIC's.

It should also be mentioned that the results of Hawrylak and Subbaswamy³ for KC_x are also consistent with $k_o/k_{K^+} \ll 1$. In addition, they found that the electrostatic contribution to d_s (second term in Eq. 17) is quite small and we also find it to be negligible. With $\Omega = 0$ and $k_o/k_{K^+} \ll 1$ equation 17 can be rewritten.

$$\frac{d_{s1}}{d_{K^+}} = \frac{[1 - \gamma X_c (\frac{d_{K^+}^o}{d_{K^+}} - 1)] + [\gamma (\frac{d_{K^+}^o}{d_{K^+}} - 1) + \frac{k_A}{k_K} \frac{d_A}{d_{K^+}}] X_1}{1 + \frac{k_A}{k_K} X_1} \quad (18)$$

where $X_c = 4.0$.

The force constant ratio k_A/k_K of the K-NH_3 GIC in Eq. 18, can be estimated from measurements of bulk potassium and bulk ammonia. The bulk compressibilities of the alkali metals K, Rb, and Cs, and of NH_3 are at least an order of magnitude higher than that of pristine

graphite. Therefore, a c-axis compression of the GIC sandwich results primarily in a deformation of the intercalant in K-NH₃ GIC's. The effective c-axis force constant of the sandwich can thus be approximated by the interatomic force constants determined from measurements of the bulk properties of the intercalants. For example, the c-axis force constant ratio determined from neutron scattering experiments³⁹ on KC₈ and RbC₈ is, within experimental error, equal to the value $k_K/k_{Rb} = 1.46$ obtained from ultrasonic measurements of the room temperature elastic constants of bulk potassium and rubidium metal.⁴⁰

From the compressibility of liquid potassium⁴¹ (C_K) and liquid NH₃¹⁵ (C_A) we find an approximate force constant ratio $(k_A/k_K) - (C_A/C_K)^{-1} = 0.56$. In addition, from the longitudinal sound velocities v_i for liquid potassium⁴¹ and for NH₃¹⁵ determined by ultrasonic measurements and the relation⁴² $v_i = \sqrt{k_i/\rho_i}$ where ρ_i is the density of the liquid species i , the force constant ratio is found to be $k_A/k_K = .77$.

An independent estimate of the force constant ratios k_A/k_K can be made from an expression given by Dresselhaus et al.³⁹ By fitting the phonon dispersion curves of several GIC's, they found an empirical relation between the force constant of an intercalant and the corresponding equilibrium sandwich thickness. Their result can be rewritten to determine the force constant ratio k_A/k_K as a function of d_A (defined above) and the inplane intercalant density, S . Thus,

$$\frac{k_A}{k_K} = \frac{17.11}{S} e^{\frac{-d_A}{4.48}} \quad (19)$$

Equation 19 was derived using a value of $k_K = 2.3^{39}$ (normalized to k_O of pristine graphite). To our knowledge NH_3 cannot be solely intercalated into graphite, therefore, we must estimate the values of d_A and S to be used in Eq. 19.

We know from recent NMR measurements¹⁹ of stage-1 $\text{KC}_{24}(\text{NH}_3)_{4.33}$ that the NH_3 molecule is rapidly rotating (on NMR time scales) about its c_3 axis which simultaneously precesses about the graphite c -axis (see Fig. 12). The motion of the NH_3 molecule is nevertheless constrained (i.e. it does not tumble freely) by the charge-dipole forces which bind it to the potassium ion and by steric forces imposed by the bounding graphite planes. In a fictitious binary "NH₃-GIC" the NH_3 molecules could freely rotate in the graphite galleries. Free rotations of the NH_3 molecules can be insured if the molecule occupies a volume determined by inscribing its surface of revolution about the c_3 axis (see Fig. 12) in a sphere of radius $r_{\text{NH}_3} = 2.14\text{\AA}$. If such a sphere fit precisely into the double hexagonal cavity of the bounding graphite planes, the resultant value of d_A would be $d_A = 7.08\text{\AA}$. With that value of d_A and $S = 5.46$ established from the inplane area $\pi r_{\text{NH}_3}^2$ we find from Eq. 19 that $k_A/k_K = 0.65$. This value of $k_A/k_K = 0.65$ is in excellent agreement with those obtained from measurements of the GIC compressibilities ($k_A/k_K = 0.56$) and of the sound velocities of the intercalants K and NH_3 in bulk form ($k_A/k_K = 0.77$), and constitutes the average of those measurements. We will, therefore, assume for the remainder of this paper that $k_A/k_K = 0.65$.

G. Comparison with Experiment

We have fit d_1 vs. P_{NH_3} in Fig. 4 ($d_{s_1} = d_1$ for stage 1) using the Fowler-Guggenheim form of x_1 vs. P_{NH_3} (see Eq. 11), $k_A/k_K = 0.65$, and Eq. 18, with only two adjustable parameters, which are the bracketed terms in the numerator of Eq. 18. The results of that fit are shown as a solid line in Fig. 4 and constitute excellent agreement between theory and experiment. The apparent cusp in the fit of d_{s_1} vs. P_{NH_3} at $P_{\text{NH}_3} < 1$ atm is expected, since we have assumed a charge exchange f that inherently has a discontinuity in slope at $x = 4.0$. This cusp is unphysical and should be smoothed (see dashed line in Fig. 4). From the fit of Eq. 18 to our data we find directly $\gamma = .143 \pm .013$ and $d_A = 7.05 \pm .04\text{\AA}$. The value of $d_A = 7.05\text{\AA}$ is surprisingly close to our estimate of $d_A = 7.08\text{\AA}$ which indicates a self-consistency in our approach. From $\gamma = 0.143$ we find for stage-1 $\text{K}(\text{NH}_3)_{4.33}\text{C}_{24}$ the charge exchange $f = 0.95$ which, given the uncertainty in determining f by any method, is in reasonable agreement with values obtained from measurements of reflectivity,²⁰ $f = 0.73$ and NMR,¹⁹ $f = 0.86$. It should be mentioned that different values of k_A/k_K were tried and the resultant value of f was insensitive to the choice of k_A/k_K , i.e. $f = 0.95$ for $0.3 < k_A/k_K < 0.9$, but a least squares fit with $f = 1.0$ could not be obtained.

The agreement between the charge exchange f obtained from NMR and reflectivity measurements, and that extracted from the fit of d_{s_1} vs. P_{NH_3} , can be improved by considering other mechanisms for electron solvation such as NH_3 shared ion-electron pairs. That is, it is possible for the NH_3 molecules of different 4-fold K-NH_3 clusters to

orient themselves to form a cavity in which they can bind an electron. This would imply that for $X < X_c$ (where presently $X_c = 4.0$) the charge exchange $f < 1$. It is probable that f varies nonlinearly with the number of 4-fold $K-NH_3$ clusters. This nonlinearity could be treated by adding additional terms and parameters to Eq. 16 or equivalently to Eq. 18. This would marginally improve the fit to the data of Fig. 4. However, such a procedure is not warranted because Fig. 18 contains the essential physics of the charge exchange process and the data of Fig. 4 does not vary rapidly enough with P_{NH_3} to allow additional parameters to be accurately determined.

For the purposes of illustration, let us assume that the current description of the charge exchange f given in Eq. 16 is applicable but because of the existence of other electron solvation mechanisms, the constraint $X_c = 4.0$ must be relaxed to permit smaller values of X_c . From the current fit of d_{s_1} vs. P_{NH_3} in Fig. 4, we find $\gamma X_c = .57$, and for a charge exchange $f = .80$ we estimate that $X_c = 3.2$. This indicates that the inclusion of other solvation mechanisms tends to lower X_c and brings the extracted charge exchange f into better agreement with values determined in other measurements.

From the parameter $(d_A/d_{K^+})(k_A/k_K) + \gamma(d_{K^0}/d_{K^+} - 1) = .908$, and $\gamma = .143$, obtained from the fit to d_1 vs. P_{NH_3} , we estimate that the relative elastic contribution of the charge transfer term $\gamma(d_{K^0})(d_{K^+} - 1)$ to the sandwich expansion is at least 6%. Furthermore, the fractional increase in the sandwich thickness of our stage-1 $K(NH_3)_{4.33}C_{24}$ ($d = 6.633A$) relative to Rudorff's stage-1 $K(NH_3)_{2.0}C_{12}$ ($d = 6.5A$) is 2%, which can be fully accounted for by a charge transfer coupled

elastic expansion. As a final point, x_2 is pressure insensitive (at least at low pressure), therefore, the variation of d_2 with P_{NH_3} (see Fig. 5) must depend more on the variation with x_1 than with x_2 . The "keying" of d_2 to d_1 is not surprising in view of the high mobility of NH_3 in the galleries of laterally contiguous stage-1 and stage-2 regions, as would exist in the Daumas-Hèrold (DH) model⁴³ of the layer structure of GIC's which is shown schematically in Fig. 13. In the DH model each gallery contains some intercalant which, however, may show lateral inhomogeneities in its distribution. Macroscopic regions of different stage are separated by kink dislocations as shown in Fig. 14. But an NH_3 molecule can dynamically sample contiguous stage-1 and stage-2 regions while still remaining in the same gallery.

The expanded stage-1 sandwich (d_{s_1}) imposes both a dynamic and static strain on the stage-2 sandwich (d_{s_2}) resulting in a small decrease in d_{s_2} as compared with d_{s_1} ($d_{s_1} - d_{s_2} = 0.05\text{\AA}$). In fact the strain between the stage-1 and stage-2 regions, as measured by the difference between d_2 and d_1 , remained constant over the pressure range $0.1 \text{ atm} < P_{\text{NH}_3} < 6.5 \text{ atm}$, with $d_2 - d_1 = 3.30\text{\AA}$. The extrapolated value of $d_2 = 9.93\text{\AA}$ (see dashed line in Fig. 5) also indicates that this strain persists even at $P_{\text{NH}_3} = 9.5 \text{ atm}$ (of course the extrapolation assumes that stage 2 still exists at that pressure). It is interesting to note that higher stage mixed phase K-NH_3 GIC's also show the same difference between d_{n+1} and d_n for stage n . For example, Fig. 10 shows the room temperature x-ray diffraction pattern of $\text{KC}_{36} + \text{NH}_3$, which indicates a stage-1 and stage-2 mixture with $d_1 = 6.638\text{\AA}$, $d_2 = 9.938\text{\AA}$,

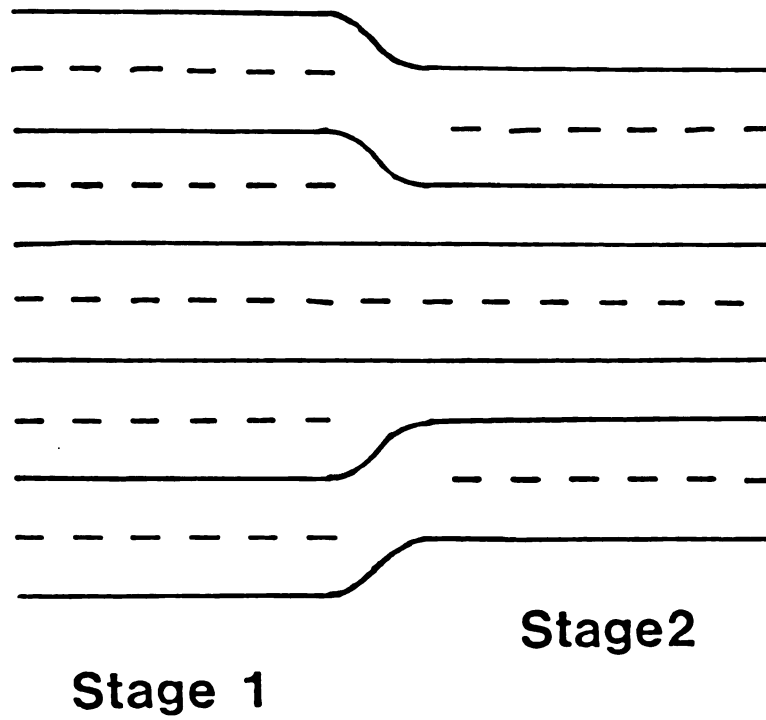


Figure 13. Daumas-Hèrold model⁴² of laterally contiguous layers of stage-1 and stage-2 regions present in a mixed stage graphite intercalation compound.

and $d_2 - d_1 = 3.300\text{\AA}$. Figure 14 shows that the room temperature (00 l) x-ray diffraction pattern of $\text{KC}_{48} + \text{NH}_3$ also indicates a mixed stage compound which in this case is composed mostly of stage-2 material ($d_2 = 9.984\text{\AA}$) with some stage-3 admixture ($d_3 = 13.29\text{\AA}$). Again, we find that $d_3 - d_2 = 3.306\text{\AA}$.

It is clear from the above discussion that for mixed phase K-NH₃ GIC's which are composed of 2 stages, n and $n+1$, the lower stage n imposes a strain on the higher stage $n+1$, and that this strain is insensitive to variations in P_{NH_3} . Moreover, the sandwich thickness of the stage n phase is essentially independent of that strain. To support this point, we note that the value of d_{s_2} for $\text{KC}_{48} + \text{NH}_3$ is 6.634\AA and is identical to the strain-free value of d_{s_1} for $\text{K}(\text{NH}_3)_{4.33}\text{C}_{24}$.

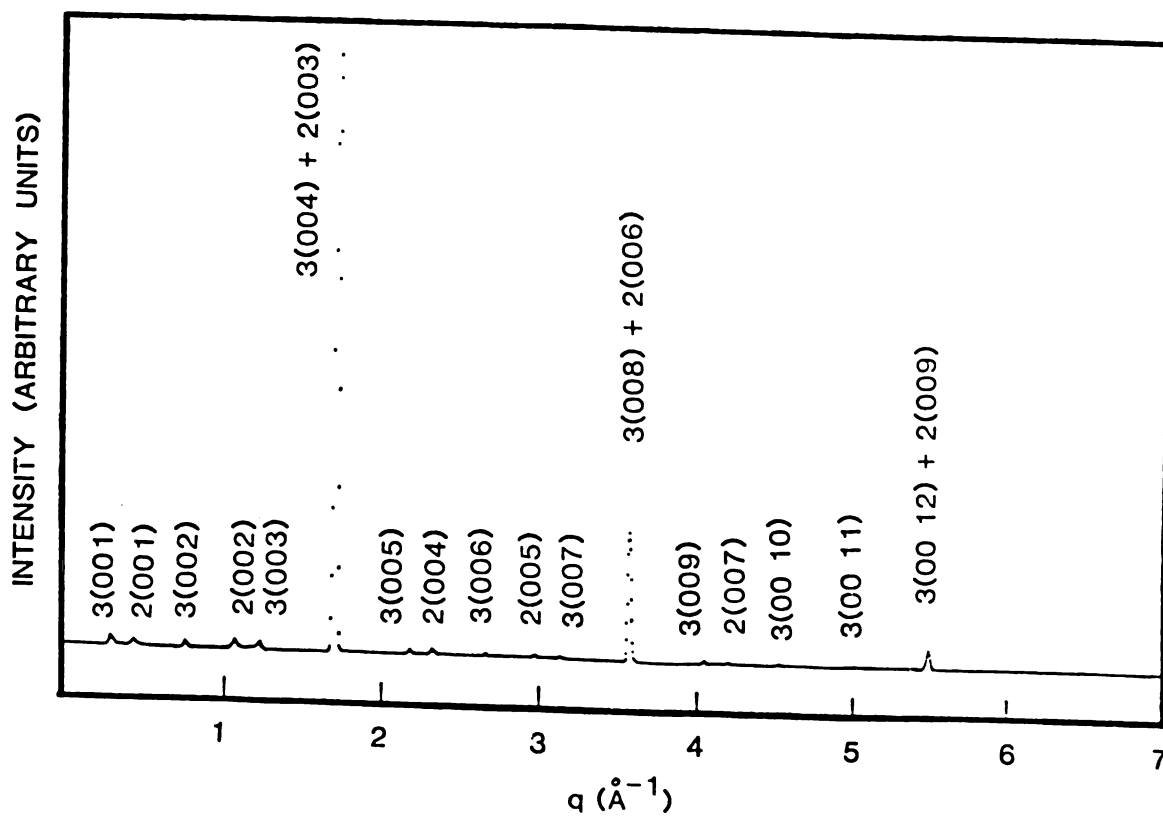


Figure 14. The room temperature ($P_{\text{NH}_3} = 9.5$ atms) (00 l) x-ray diffraction pattern of $\text{KC}_{48} + \text{NH}_3$ liquid. The notation is the same as that of Fig. 3.

IV. Summary and Concluding Remarks

We have found that as P_{NH_3} is lowered, the stage-1 $\text{K}(\text{NH}_3)_{4.33}\text{C}_{24}$ ternary GIC evolves to a mixed phase stage-1 $\text{K}(\text{NH}_3)_{x_1}\text{C}_{y_1}$ and stage-2 $\text{K}(\text{NH}_3)_{x_2}\text{C}_{y_2}$ system, with unexpected variations of the carbon/potassium ratios y_n (for stage n) with P_{NH_3} . At $P_{\text{NH}_3} = 9.5$ atms we find that $x_1 = 4.33$ and $y_1 = 24$ and estimate that $y_2 > 37$ and $x_2 > 3.2$. As the ammonia pressure is lowered, both y_1 and y_2 decrease and at $P_{\text{NH}_3} \sim 10^{-2}$ atms could be extrapolated to $y_1 = 12$ and $y_2 = 28$, which is consistent with the stoichiometry of compounds prepared by Rudorff,¹⁴ namely stage-1 $\text{K}(\text{NH}_3)_{2.0}\text{C}_{12}$ and stage-2 $\text{K}(\text{NH}_3)_{2.0}\text{C}_{28}$.

It was found that the sandwich of stage 1 imposed an elastic strain on the sandwich of stage 2 such that $d_{s_1} - d_{s_2} = 0.05\text{A}$ and that this strain was insensitive to variations in P_{NH_3} . Both d_{s_1} and d_{s_2} were found to depend on the variations of x_1 with P_{NH_3} , which was fit to a Fowler-Guggenheim equation for adsorption.

From x_1 vs. P_{NH_3} in Eq. 11 and the independently determined value of $k_A/k_K = 0.65$ we fit the d_1 vs. P_{NH_3} data in Fig. 4 using Eq. 18 with only two adjustable parameters. The resultant fit constitutes excellent agreement between theory and experiment. Both the sandwich thickness of the NH_3 -GIC and the charge exchange f could be independently extracted from the fit to d_1 vs. P_{NH_3} . The deduced value of $f = 0.95$ is in

reasonable agreement with values obtained from other measurements. The deduced charge exchange can be brought into closer agreement with reflectivity¹⁶ and NMR¹⁵ measurements by incorporating multiple electron solvation mechanisms into Eq. 16.

The physical origin of our results may be separated into three major effects: First, as NH_3 is added to the interlayer space containing K^+ ions, an expansion results from the size difference of NH_3 relative to K^+ (i.e. $d_A/d_{K^+} > 1$). Second, as NH_3 is ingested, some of the charge originally donated to the carbon layers is extracted back into the K-NH_3 layer, concurrent with electron cage formation, and is delocalized. Third, much of the delocalized charge resides near the potassium ions and increases their effective radii. This increased potassium radius generates additional elastic energy causing an increase in d_{s_1} .

The fractional increase of our stage-1 $\text{K(NH}_3)_{4.33}\text{C}_{24}$ ($d_{s_1} = 6.633\text{\AA}$) from rudorff's stage-1 $\text{K(NH}_3)_{2.0}\text{C}_{12}$ ($d=6.5\text{\AA}$) is 2%, which is very close to our estimate of the elastic contribution of the charge exchange term in Eq. 18 and suggests that the difference is entirely due to an elastic-charge transfer coupling.

Finally, the experimental results from several measurements^{1,12,13,19} can also be separated into three important effects: First, there is a significant extraction of charge from the graphite layers ($f = 1.0$ to $f = 0.80$) to the intercalant layer due to intercalated NH_3 , attributable to electron solvation. Second, the K-NH_3 intercalant forms a 2D liquid in the graphite gallery with the K ion forming a planar 4-fold coordinated cluster with the NH_3 molecule and the excess NH_3

molecules (0.33 per $\text{K}(\text{NH}_3)_4$ cluster at $P_{\text{NH}_3} = 9.5$ atms) lying in the plane defined by those clusters. Third, the relative potassium/ammonia concentration can be continuously varied from 19 MPM to 100 MPM with indications (see Fig. 8) that higher stages may provide a lower inplane potassium density than that corresponding to $y_1=24$ for stage 1. This would leave additional room for NH_3 and yield a lower minimum concentration.

These results for the K-NH_3 GIC are consistent with the formation of a 2D metal-ammonia solution in the gallery of graphite. Higher stages may provide the means of accessing the dilute region $< .1$ MPM, in which case the K-NH_3 ternary GIC's could be a novel and intrinsically interesting system for studying the 2D nonmetal/metal transition.

LIST OF REFERENCES

LIST OF REFERENCES

1. S.A. Safran, Phys. Rev. Lett. 44, 927 (1980).
2. S.E. Millman and G. Kirczenow, Phys. Rev. B26, 2310 (1982).
3. P. Hawrylak and K.R. Subbaswamy, Phys. Rev. B (in press).
4. S.A. Safran and D.R. Haman, Phys. Rev. B22, 606 (1980).
5. S.A. Safran and D.R. Haman, Phys. Rev. Lett. 42, 1410 (1979).
6. R. Clarke, N. Wada, and S.A. Solin, Phys. Rev. Lett. 44, 1616 (1980).
7. C.D. Fuerst, J.E. Fischer, J.D. Axe, J.B. Hastings, and D.B. McWhan, Phys. Rev. Lett. 50, 357 (1983).
8. K.D. Woo, W.A. Kamitakahara, D.P. DeVincenzo, D.S. Robinson, H. Mertwoy, J.W. McViker, and J.E. Fisher, Phys. Rev. Lett. 50, 182 (1983).
9. A. Metrot and J.E. Fischer, Syn. Metals 3, 201 (1981).
10. D.A. Neuman, H. Zabel, J.J. Rush, and N. Berk, Phys. Rev. Lett. 53, 56 (1984).
11. A. Hèrold, Proceedings of the International Conference on the Physics of Intercalation Compounds, edited by L. Pietronero and E. Tosatti (Springer-Verlag, New York, 1981), p. 7.
12. S.K. Hark, B.R. York, and S.A. Solin, Solid State Comm.
13. S.A. Solin, Y.B. Fan, and B.R. York, Bull. Mat. Res. Soc., in press.
14. J.L. Dye, Progress in Inorganic Chemistry 32 (1984).
15. J.C. Thompson, Electrons in Liquid Ammonia (Clarendon Press, Oxford, 1976).
16. J. Jortner and N.R. Kester, editors, Electrons in Fluids: The Nature of Metal-Ammonia Solutions (Springer-Verlag, New York, 1973).
17. J.C. Thompson, Rev. Mod. Phys. 40, 704 (1968).
18. W. Rudorff and E. Schultze, Angew. Chem. 66, 305 (1954).

19. H. Resing, B.R. York, and S.A. Solin, to be published.
20. D. Hoffman, A.M. Rao, G.L. Doll, P.C. Eklund, B.R. York, and S.A. Solin, *Bull Mat. Res. Soc.*, in press.
21. A. Hèrold, *Bull. Soc. Chim. Fr.* 999 (1955).
22. R.R. Dewald and J.H. Roberts, *J. Phys. Chem.* 72, 4224 (1968).
23. J.W. McBain and A.M. Baker, *J. Am. Chem. Soc.* 48, 690 (1926).
24. E.W. Washburn, editor, International Critical Tables of Numerical Data, Physics, Chemistry, Technology, first edition, Vol. III (McGraw-Hill, New York, 1928).
25. R.C. Weast, editor, Handbook of Chemistry and Physics 55th Ed. (CRC Press, Boca Raton, Florida, 1974).
26. N. Akuzawa, M. Ikeda, T. Ameniya, and Y. Takahashi, *Syn. Metals* 7, 65 (1983).
27. P. Chow and H. Zabel, *Syn. Met.* 7, 243 (1983).
28. R. Fowler and E. Guggenheim, Statistical Thermodynamics (Cambridge University Press, 1949).
29. Jackson, Classical Electrodynamics 2nd Ed. (John Wiley and Sons, New York, 1974).
30. A.H. Narten, *J. Chem. Phys.* 49, 1692 (1968).
31. N.A.W. Holzwarth, S. Louie, and S. Rabi, *Phys. Rev. Lett.* 47, 1318 (1981).
32. J.R. Dahn, D.B. Dahn, and R.R. Haering, *Solid State Comm.* 42, 179 (1982).
33. T. Enoki, M. Sano, H. Inokuchi, *J. Chem. Phys.* 28, 4 (1983).
34. D.A. Copeland, N.R. Kestner, and J. Jortner, *J. Chem. Phys.* 53, 3741 (1975).
35. N.F. Mott and E.A. Davis, Electronic Processes in Non-Crystalline Materials (Clarendon Press, Oxford, 1971).
36. T.A. Beckman and K.S. Pitzer, *J. Phys. Chem.* 65, 1527 (1961).
37. J.L. Dye, *Pure and Appl. Chem.* 49, 3 (1977).
38. W.A. Siddon, J.W. Fletcher, R. Catterall, and F.C. Sopchiphyn, *Chem. Phys. Letters* 48, 584 (1977).
39. G. Dresselhaus, R. Al-Jishi, J.D. Axe, C.F. Majkrzak, L. Passell, and S.K. Satija, *Solid State Comm.* 40, 229 (1981).

40. K.H. Hellwege, editor, Landolt-Börnstein Numerical Data and Functional Relationships in Science and Technology, Vol. II (Springer-Verlag, New York, 1979).
41. O.J. Kleppa, J. Chem. Phys. 18, 1331 (1950).
42. C. Kittel, Introduction to Solid State Physics, 2nd Ed. (John Wiley and Sons, Inc., New York, 1957).
43. N. Daumas and A. Hèrold, Bull. Soc. Chim. Fr. 5, 1598 (1971).

APPENDICES

Ternary Graphite Intercalation Compound KC_8C_{16} : An Ideal Layered Heterostructure

B. R. York, S. K. Hark, and S. A. Solin

Department of Physics and Astronomy, Michigan State University, East Lansing, Michigan 48824

(Received 28 February 1983)

An ideal ternary heterostructure graphite intercalation compound, KC_8C_{16} , which exhibits a stage-1 c -axis stacking sequence, $\dots\text{CKCCsCKCCs}\dots$, has been prepared. The stage, stacking sequence, and $(2 \times 2)R0^\circ$ in-plane structure have been confirmed by high-resolution x-ray diffraction studies which reveal a c -axis correlation range of $\sim 350 \text{ \AA}$. The structure factor and widths of the $(00l)$ reflections calculated on the basis of the proposed stacking sequence are in excellent agreement with experimental observations.

PACS numbers: 61.60.+m, 61.10.Fr

Heavy-alkali-metal ternary graphite intercalation compounds (GIC's), which were first synthesized more than a decade ago using powdered graphite, have become the focus of considerable recent interest^{2,3} in part because they represent potential model systems with which to study the structural properties of binary alloys in two dimensions. The ternary GIC's prepared to date have always been planar solid solutions $(A_xB_{1-x})_mC_{sxn}$, where n/m is the stage corresponding to the number of carbon layers separating nearest layers of intercalate ions, and $1/s$ is the areal number density of intercalate atoms relative to carbon atoms.⁴

We report in this Letter the first successful preparation of a ternary heterostructure GIC. The general form of such a compound can be stoichiometrically represented by the notation $(A_mC_{sxn})_l(B_nC_{s'yn})_{l'}$, where $m(m')$, $s(s')$, and $n(n')$ retain the definitions inferred above and $l(l')$ corresponds to the number of times the corresponding bracketed unit repeats in the minimum size c -axis stacking unit which defines the structure. The ternary GIC which we have prepared, $(\text{KC}_8\text{C}_{16})_1(\text{CsC}_8\text{C}_{16})_1$ or equivalently KC_8C_{16} , is the simplest such structure and can be represented by the repeat sequence $\dots\text{CKCCsCKCCs}\dots$. It is an ideal heterostructure because the potassium and cesium layers are commensurate with (i.e., epitaxial to) the carbon layer; the carbon, potassium, and cesium layers are atomically flat; there is no interdiffusion at the layer interfaces; and the stacked layers exhibit long-range order in both the c -axis and the a -axis directions. To our knowledge, such an ideal manmade heterostructure has not to date been prepared by use of sophisticated techniques such as molecular beam epitaxy.⁵

Samples were prepared in Pyrex with highly ordered pyrolytic graphite (HOPG) ($\sim 5 \times 10 \times 0.5 \text{ mm}^3$) by a sequential intercalation procedure.

A well-ordered pure stage-2 CsC_{24} compound⁶ was first obtained.⁷ The sample was then rapidly transferred in a glove box ($\leq 0.5 \text{ ppm O}_2$) to another Pyrex tube containing pure potassium metal. The tube was evacuated and sealed off in the usual manner. The tube was uniformly heated to 70°C and the CsC_{24} sample was immersed in liquid potassium. Periodically, to facilitate x-ray examination, the sample tube was placed in a centrifuge which was housed in an oven at 70°C , the excess liquid potassium was spun off, and the tube was quenched in air to room temperature. The diffraction patterns reported here were recorded using a 12-kW Rigaku rotating-anode x-ray source, a molybdenum target, and a Huber Model No. 430-440-512 four-circle diffractometer equipped with a vertically bent graphite monochromator. The maximum resolution of this instrument was measured with use of the (400) reflection of single-crystal germanium and found to be 0.003 \AA^{-1} .

Figure 1 shows the $(00l)$ x-ray diffraction patterns of the CsC_{24} starting material, after immersion and quenching for two hours, two days, and 12 days. The small diffuse background noticeable in Fig. 1 is due to the Pyrex envelope. The patterns of Fig. 1 have been indexed with the notation $(n/m)\delta(00l)$, where n/m is the stage and l is the order of the c -axis reflection. The symbol δ denotes the intercalate species. Thus $\delta = \text{K}$, Cs , or H , where H represents the heterostructure KC_8C_{16} . As can be seen from Fig. 1, the monophasic KC_{24} evolved to a three-phase system containing CsC_{24} , KC_{24} , and CsC_8 ; then to another three-phase system containing the KC_8C_{16} heterostructure, KC_8 , and KC_{24} ; and finally to a two-phase system of KC_8 and KC_8C_{16} .

In Fig. 2 we show a plot of the wave vector, q , versus the order of the reflections shown in Fig. 1(c). For a properly identified stacking structure such a plot should yield a straight line passing

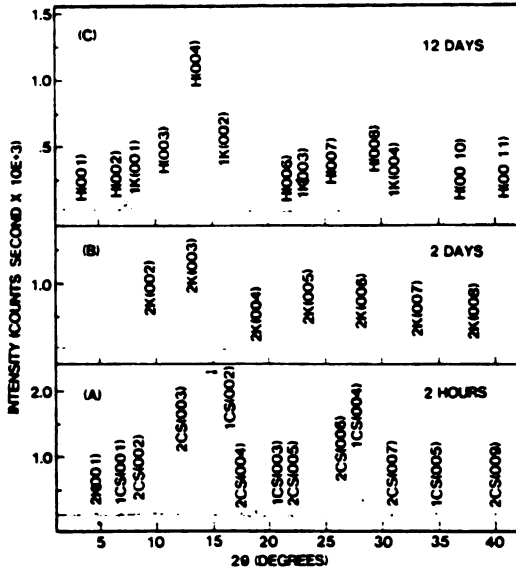


FIG. 1. (00l) diffraction patterns of stage-2 CsC₂₄ after immersion in liquid potassium. The reflections labeled H(00l) correspond to the heterostructure KC₈C₁₆. Those labeled nH(00l) correspond to a stage-n binary GIC intercalated with species θ. The diffraction patterns were acquired with Mo Kα radiation. Reflections which appear in more than one trace have been labeled only once. The ordinates of curves A and B have been truncated for presentation.

through the origin and with a slope 2π/d, where d is the minimum distance along the c axis (or sandwich thickness) which defines the stacking sequence.⁶ From Fig. 2 we find d_{KC₈} = 5.35 Å.

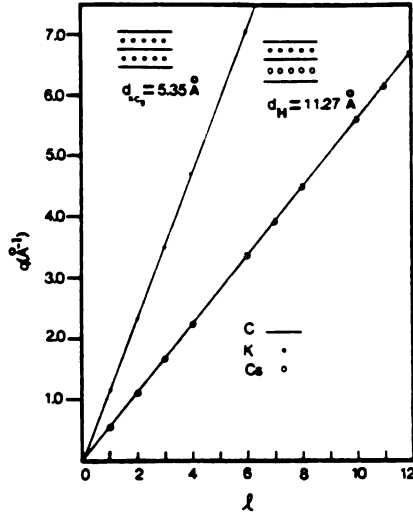


FIG. 2. A plot of the wave vector vs the order of the corresponding (00l) reflection for the KC₈ (dots) and KC₈C₁₆ (circled dots) components of Fig. 1(c). The basal spacings d_H and d_{KC₈} indicated were determined from the slopes of the straight (solid) lines which are least-squares fits to the data.

Similarly, from our measurements of CsC₈ we find that d_{C₁C₈} = 5.94 Å. Thus, to within experimental error, d_H = d_{KC₈} + d_{C₁C₈} as would be expected for the stacking sequence ...CKCCsCK...

To further confirm the heterostructure stacking sequence of KC₈C₁₆, we have calculated the (00l) x-ray intensity distribution I(q) vs q from the following equation⁸:

$$I(q) \propto \left| \sum_j f_j(q) \exp \left[-W_j \left(\frac{q}{4\pi} \right)^2 \right] \exp \left[-i(d_H \hat{z}_j) \cdot (q\hat{z}) \right] \right|^2 \left[\sum_l N^2 \exp \left(-\frac{(q - q_l)^2}{\Gamma^2/4 \ln 2} \right) \right] L_p(q). \quad (1)$$

Here L_p(q) is the combined Lorentz-polarization factor; \hat{z} is a unit vector; \hat{z}_j is the distance of the jth layer from the origin of the c-axis cell; f_j(q), j = C, Cs, K, are the q-dependent form factors⁹; and the reciprocal lattice vectors are $\hat{q}_i = (2\pi/d_H) l \hat{z}$. The appropriate values of W_j, the Debye-Waller factor, have been obtained from measurements of KC₈ and CsC₈.¹⁰ The square-bracketed term in Eq. (1) is the Gaussian approximation to the Bragg scattering term.⁸ The full width at half maximum of each reflection is $\Gamma = 4(1.4) \lambda d_H$. Here N is the number of cells of length d_H that are correlated along the c axis, the correlation range of which is λd_H.

In Fig. 3 we have plotted I(q), derived from

Fig. 1(c), and the theoretical diffraction pattern of Eq. (1) obtained with N = 31 and a Γ corrected for the instrument resolution. With the exception of the (001) peak, the experimental and theoretical curves of Fig. 3 are in excellent agreement. The discrepancy at low angle arises from the fact that at grazing incidence [μ = 1.3° for the (001) reflection] the effective sample cross section is only a small fraction of the incident beam cross section. For our sample configuration this geometrically induced cross section mismatch is absent for θ > 9° and has only a marginal effect on reflections which occur in the range 3° < θ < 9°.

The value of N used to compute I(q) was in fact

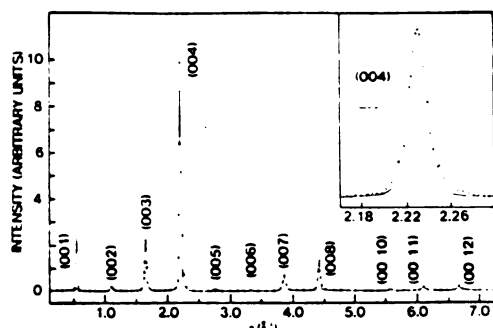


FIG. 3. The intensity of the (00 l) diffraction pattern of KCsC_{16} vs q . The solid line is the calculated reflection [see text, Eq. (1)]. The dots correspond to experimental results and are obtained from Fig. 1(c) after correction for the measured glass envelope background, subtraction of the stage-1 KC_8 pattern, and normalization to the theoretical curve at (004). The inset shows a high-resolution scan of the (004) reflection (vertical bars indicate the instrument resolution, 0.0045 \AA^{-1}).

deduced from the high-resolution x-ray scan shown in the inset of Fig. 3. From a Gaussian fit to the observed (004) heterostructure reflection we find, taking account of the instrument resolution of 0.0045 \AA^{-1} , a c -axis correlation range of $\sim 350 \text{ \AA}$. The corresponding correlation range for the KC_8 component of our sample was found from the (002) reflection to be $\sim 260 \text{ \AA}$. We also found that the width of the (00 l) reflections of KCsC_{16} were, to within experimental error, independent of q as expected when N is large.⁹ This q independence of the linewidth indicates that the staging of the heterostructure is "pure" over the $\sim 350\text{-\AA}$ correlation range with little or no statistical admixture of other stacking sequences (e.g., pristine HOPG or KC_8) as was recently found in pressure-induced fractional stages of KC_8 .⁴

The observation of phase-separated KC_8 and KCsC_{16} in the saturated compound which we have prepared is quantitatively consistent with two conditions which appear to govern the intercalation process during the initial period (0 to ~ 15 days) of intercalation, and at the immersion temperature of 70°C : (1) No cesium is expelled from the sample, and (2) potassium does not alloy with the Cs present in the sample. We have carried out a neutron activation analysis of the residual potassium used for immersion of CsC_{24} and find no cesium in excess of the impurity amount, < 50 ppm, present in our potassium.

Thus, the neutron activation analysis results support condition (1). Condition (2) is supported by the fact that intralayer Cs in CsC_{24} does not form a solid solution with potassium, but densifies to CsC_8 during the early stages of exposure [see Fig. 1(a)].

Conditions (1) and (2) above, together with our x-ray results, indicate that immersion intercalation of CsC_{24} by potassium is initially controlled by the reaction



the right-hand side of which is a saturated non-equilibrium state which appears to be metastable when the sample is cleansed of liquid potassium and quenched to room temperature. If the intercalation process was allowed to proceed to completion with the sample immersed in liquid potassium, the equilibrium product would probably be a ternary solid solution $\text{K}_x\text{Cs}_{1-x}\text{C}_8$. But there is evidence that such compounds are ultimately unstable¹¹ and further evolve into a phase-separated system composed of a ternary solid solution, KC_8 , and/or CsC_8 .³ Note, however, that the ternary solid solution and binary GIC components cited above would yield (00 l) diffraction patterns which are easily distinguished from those of the KCsC_{16} heterostructure.

Using Eq. (2) we calculate that the ratio of the peak intensity of $H(004)$ to $1K(002)$ should be 7.2. The corresponding observed ratio [see Fig. 1(c)] is 5.4, in good agreement with theory. In principle an alternative metastable saturated heterostructure of the form $(\text{KC}_8)_2(\text{CsC}_8)$, or equivalently $\text{K}_2\text{CsC}_{24}$ with the stacking sequence $\dots\text{CKCKCCsCKCKCCs}\dots$ could be generated by the admixture of CsC_{24} and potassium. Apparently such a structure has a higher free energy than the admixture of the higher-symmetry components KCsC_{16} and KC_8 .

The in-plane diffraction patterns of our ternary heterostructure KCsC_{16} have been carefully measured and confirm that both the potassium and the cesium layers form $(2 \times 2)R0^\circ$ (Ref. 6) commensurate superlattices with respect to the graphite host. We find no evidence for any other in-plane structure. We do, however, find a slight expansion of the a -axis lattice parameter of the host material from 2.46 \AA in the pristine form to 2.47 \AA when intercalated.

While KC_8 does make a contribution to the $(2 \times 2)R0^\circ$ in-plane diffraction pattern, we calculate on the basis of Eq. (2) that the contribution would be down by a factor of 17 for the (100) and (110)

reflections compared to the contribution from KCsC_{16} . These two reflections contain no carbon layer contributions.⁶ Therefore, we are confident that the KCsC_{16} does indeed exhibit a $(2 \times 2)R0^\circ$ in-plane superlattice structure. As a final note on this point, Raman scattering studies carried out on KCsC_{16} (Ref. 12) yield the unique spectra characteristic of an ordered $(2 \times 2)R0^\circ$ superlattice.¹³

The authors gratefully acknowledge useful discussions with P. Vora, T. Kaplan, and S. Mahanti. Thanks are also due to A. W. Moore for providing the HOPG used in this study. This work was supported by the National Science Foundation under Grants No. DMR80-10486 and No. DMR82-11554. The x-ray equipment was provided by the U. S. Office of Naval Research under Grant No. N00014-80-C-0610.

¹A. Héroid, in *Proceedings of the International Con-*

ference on the Physics of Intercalation Compounds, Trieste, 1981, edited by L. Pietronero and E. Tosatti (Springer-Verlag, New York, 1981), p. 7.

²M. E. Misenheimer, P. Chow, and H. Zabel, to be published.

³B. York, P. Vora, S. K. Hark, and S. A. Solin, *Bull. Am. Phys. Soc.* **28**, 348 (1983).

⁴C. D. Fuerst, J. E. Fischer, J. D. Axe, J. B. Hastings, and D. B. McWhan, *Phys. Rev. Lett.* **50**, 357 (1983).

⁵M. B. Panish, *Science* **208**, 916 (1980).

⁶S. A. Solin, *Adv. Chem. Phys.* **49**, 455 (1982).

⁷A. Héroid, *Bull. Soc. Chim. Fr.* **1955**, 999.

⁸A. Guinier, *X-Ray Diffraction* (Freeman, San Francisco, 1963).

⁹*International Tables for X-Ray Crystallography* (Kynoch, Birmingham, England, 1962), Vol. III.

¹⁰L. E. Campbell, G. L. Montet, and G. J. Perlow, *Phys. Rev. B* **15**, 3313 (1977).

¹¹A. Héroid, private communication.

¹²P. Vora, B. York, and S. A. Solin, unpublished.

¹³S. A. Solin, *Physica (Utrecht)* **99B**, 443 (1979).

Structure and Synthesis of the Ternary Alkali Graphite Intercalation
Compound KC_8C_{16} , An Ideal Layered Heterostructure

S. K. Hark,^{*} B. R. York and S. A. Solin

Department of Physics and Astronomy
Michigan State University
East Lansing, MI 48824

Abstract

We have prepared a stable two phase Graphite Intercalation Compound (GIC) containing KC_8 and KC_8C_{16} by immersing CsC_{24} into liquid K at 70°C . High resolution x-ray diffraction studies reveal that the KC_8C_{16} , which exhibits a stage one c-axis stacking sequence of . . . C K C Cs C K C Cs . . . is an ideal ternary heterostructure GIC with a c-axis repeat distance of $d_H = 11.27\text{\AA}$ and correlation range of 350\AA . The intensities of the $(00L)$ x-ray diffraction pattern calculated on the basis of the proposed c-axis repeat sequence are in excellent agreement with the experimental observations. The KC_8C_{16} in plane structure is a $(2 \times 2)\text{R}0^\circ$ superlattice with an in plane correlation range of 140\AA . The ordered intercalant layers stack along the c axis with an $\alpha, \beta, \gamma, \delta$ site sequence where for example $\alpha, \gamma = \text{K}$ and $\beta, \delta = \text{Cs}$ and stacking faults occur on average every 30\AA .

*Current Address: Xerox Corporation, Webster Research Center, Webster, NY.

I. Introduction

There is considerable current interest in studying ternary GIC's,¹⁻³ especially those involving alkali metals.^{4,5} These compounds represent potential model systems with which to study the properties of binary alloys in two dimensions, certain aspects of staging which can not be accessed by binary GIC's and novel aspects of superconductivity. The ternary GIC's prepared to date have, with one exception,⁶ been planar solid solutions, by which we mean that the intercalant layer is a homogeneous mixture of the 2 intercalant species. Recently, we discovered the possibility of synthesizing a structurally different ternary GIC, the alkali heterostructure KC_sC_{16} ,^{5,7} which possesses a c-axis layer stacking sequence of . . . C K C Cs C K C Cs . . .

There has been a vigorous effort over the past decade to fabricate such layered heterostructures, particularly in III-V semiconductor systems, using molecular beam epitaxy (MBE) techniques.⁸ While much progress has been made, an MBE derived ideal heterostructure, in our opinion, has yet to be achieved. From our point of view, an "ideal" layered heterostructure is one in which the adjacent layers at the layer-layer interface are epitaxial, exhibit no interdiffusion, are flat on an atomic scale, and also exhibit long range correlations in both the a-axis and c-axis directions. In this paper we shall present the detailed data which confirms our preliminary reports^{5,7} of the fabrication of such an "ideal" heterostructure the ternary GIC KC_sC_{16} . In addition we shall for the first time identify the c-axis stacking arrangement in KC_sC_{16} as $\alpha\beta\gamma\delta$ and we will show that the sequence is replete with epitaxial stacking faults.

II. Experimental Details

Samples of KC_sC_{16} were prepared in pyrex tubes with highly oriented pyrolytic graphite (HOPG) (~ 5 mm x 10 mm x .5 mm) by a sequential intercalation procedure. A well-ordered pure stage 2 CsC_{24} ⁹ compound was first obtained by the standard two-bulb

technique.¹⁰ The CsC_{24} sample was then rapidly transferred in a Vacuum Atmospheres Model MO-40-1 glove box (<0.5 ppm O_2) to another pyrex tube containing pure potassium metal (≤ 50 ppm impurities of Cs). The tube was evacuated and sealed off in the usual manner. The tube was uniformly heated to 70°C and the CsC_{24} sample was immersed in liquid potassium. Periodically, to facilitate x-ray examination, the sample tube was placed in a centrifuge which was housed in an oven at 70°C , the excess liquid potassium was spun off, and the sample was quenched in air to room temperature.

The diffraction patterns reported here were recorded using a 12 KW Rigaku rotating anode x-ray generator, a molybdenum target, and a Huber 430-440-512 four circle diffractometer equipped with a vertically bent graphite monochromator. The (004) reflection of graphite from the $\text{MoK}\alpha$ radiation was used as the incident x-ray beam for the sample. The harmonics of $\text{MoK}\alpha$ radiation were effectively removed by passing the signal, detected by a NaI scintillator, through a single channel analyser.¹¹ The maximum resolution of this instrument was determined using the (400) reflection of a single crystal of Ge to be $.003 \text{ \AA}^{-1}$. The instrument resolution used in the experiment, unless specified, was typically 0.02 \AA^{-1} .

III. Results and Discussion

The (00 ℓ) x-ray diffraction studies of the evolution of CsC_{24} into KCsC_{24} as a function of immersion time in liquid K at 70°C have been briefly reported.⁵ A more detailed description is given here. Before the immersion, the (00 ℓ) scan of CsC_{24} confirms that it is a pure stage 2 compound with c-axis repeat distance $d_{2\text{Cs}} = 9.29 \text{ \AA}$.⁹ Fig. 1 shows the (00 ℓ) x-ray diffraction patterns of the CsC_{24} starting material after immersion for 2 hrs, 2 days and 12 days and quenching. The small diffuse background noticeable in Fig. 1 is due to the pyrex envelope. The patterns of Fig. 1 have been indexed with the notation $nM(00\ell)$ where n is the stage index, $M = \text{K, Cs, H}$ (for heterostructure), and ℓ is the order of diffraction. As can be seen from Fig. 1, the pure

CsC₂₄ specimen evolves to a 3 phase system containing the original CsC₂₄ phase and additional KC₈ and CsC₈ phases, then to another 3 phase system containing KCsC₁₆ heterostructure, KC₈ and KC₂₄ phases, and finally to a 2 phase system of KC₈ and KCsC₁₆. The various phases except the heterostructure are identified from a comparison with the well known (00 ℓ) diffraction patterns of the corresponding pure binary compounds.⁹

Plots of the order, ℓ , versus the wave vector $|\vec{q}| = \frac{4\pi}{\lambda} \sin \theta$ of the reflections of the binary GIC phases present in Fig. 1 are shown in Fig. 2. The corresponding plot for the reflections of the heterostructure is shown in Fig. 3. For properly identified structures such plots should yield a straight line passing through the origin and with a slope $d/2\pi$, where d is the c -axis repeat distance which defines the structure along c -axis direction. From Fig. 2 we find for KC₈, $d_{1K} = 5.35 \text{ \AA}$ in agreement with previous measurements.⁹ From Fig. 3 for KCsC₁₆ we find $d_H = 11.27 \text{ \AA}$. Similarly from independent measurements of CsC₈ we find $d_{1Cs} = 5.94 \text{ \AA}$.⁵ To within experimental errors,

$$d_H = d_{1K} + d_{1Cs} \quad (1)$$

as would be expected for the c -axis repeat sequence . . . C K C Cs C K C Cs . . . Thus the heterostructure nature of the sample is in part confirmed.

To further confirm the heterostructure c -axis repeat sequence of KCsC₁₆, we have calculated the (00 ℓ) x-ray intensity distribution $I(q)$ versus q from the following equation,

$$I(q) = \left| \sum_j f_j(q) e^{-W_j \left(\frac{q}{4\pi}\right)^2} e^{-i(d_H \vec{Z}_j) \cdot (q\hat{Z})} \right|^2 B(q) L_p(q) \quad (2)$$

Here $f_j(q)$, $j = K, Cs, C$ are the q dependent atomic form factors, \hat{Z} is a unit vector along the c -axis direction, \vec{Z}_j is the distance of the j^{th} layer from the origin of the c -axis cell, and $q_{\ell} = \frac{2\pi}{d_H} \ell \hat{Z}$ are the reciprocal lattice vectors.

The appropriate choice of values of W_j , the Debye-Waller factors, is a delicate matter since there are no consistent values for carbon or intercalants in GIC's. For instance,

for GIC's the values for carbon depend on the intercalant species and the stage and vary by a great deal from one compound to another.

Nevertheless, it is found that the agreement between the calculated and experimental intensity distributions, when assessed by the residual of fit,¹¹ is not very sensitive to the actual values of W_j used. In our case, these values have been obtained from our x-ray measurements of KC_8 and from Mossbauer measurements of CsC_8 .¹² For example, the residuals are 0.12 when $W_C = 0.48$, $W_K = 1.66$, and $W_{Cs} = 1.24$ are used and 0.17 when W_j is completely neglected in the fitting.

The term $B(q)$ in Eq. (2) is a broadening factor which accounts for finite size and is given by¹³

$$B(q) = \frac{\sin^2(Nqd_H/2)}{\sin^2(qd_H/2)} \approx \sum_l N^2 \exp \left[-(q-q_l)^2 / (\Gamma^2/4 \ln 2) \right] \quad (3)$$

where Γ can be determined from the full width of a (00 l) reflection through the relation

$$\Gamma = 1.4/Nd_H \quad (4)$$

and N is the number of cells of length d_H that are correlated along the c -axis. Equation (4) was obtained by equating the full widths of the equivalent expressions for $B(q)$ given in Eq. 3. In determining Γ experimentally one must account for the instrumental contribution to the observed width. We do this by making the gaussian deconvolution

$$\Gamma^2 = \Gamma_{\text{observed}}^2 - \Gamma_{\text{instrument}}^2 \quad (5)$$

where $\Gamma_{\text{instrument}}$ is measured using the (400) reflection of single crystal germanium.

The term $L_p(q)$ in Eq. 2 is the combined Lorentz-Polarization factor which for our scattering configuration is given by

$$L_p(q) = \frac{1 + \cos \theta \cos \theta_1}{(1 + \cos^2 \theta_1) \sin 2\theta} \quad (6)$$

where θ_1 is the (004) Bragg angle setting of the graphite monochromator.¹⁴ All parameters, except Γ or equivalently N and the proportionality constant on the right hand side of Eq. 2 are known either experimentally or are available from standard tables.

To facilitate the calculation of the (00ℓ) diffraction pattern using Eq. 2, the value of N was independently determined from a high resolution (instrument resolution of 0.0045 \AA^{-1}) x-ray scan of the (004) heterostructure reflection. From a Gaussian fit to the observed reflection as shown in Fig. 4 we find, taking account of the instrument resolution in Eq. 5, a c-axis correlation range of $\Gamma = 350 \text{ \AA}$ or equivalently $N \cong 31$. In Fig. 6 we have plotted $I(q)$, derived from Fig 1(c), and the theoretical diffraction pattern of Eq. 2 obtained with $N = 31$. The proportionately constant in Eq 1 is fixed by normalizing the calculated intensity of the (004) reflection to the corresponding reflection in Fig. 1(c). The background from the pyrex envelope and diffraction peaks from KC_8 in Fig. 1c have been removed for clarity of comparison. The pyrex background scattering was measured in an independent study under similar experimental conditions. It was properly normalized and subtracted digitally from Fig. 1(c).

With the exception of the (001) peak, the experimental and theoretical curves of Fig. 3 are in excellent agreement. The discrepancy at low angles arises from the fact that for samples whose absorption is non-negligible and whose lateral size (5 mm) is larger than the x-ray beam crosssectional width (1 mm), there will be a discontinuous change in the scattering volume at the scattering angle for which the projected width of the sample on a plane normal to the incident x-ray beam is equal to the x-ray beam width. This artifact has not been properly treated in the theoretical calculation. For our sample configuration this geometrically-induced beam-sample crosssection mismatch is absent for $\theta > 9^\circ$ and has only a marginal effect on reflections which occur in the range $3^\circ \leq \theta \leq 9^\circ$.

With the observations that 1) $d_H = d_{1\text{Cs}} + d_{1\text{K}}$ and 2) the theoretical and experimental (00ℓ) diffraction patterns are in very good agreement, the heterostructure nature of our sample is thus clearly established.

The x-ray results cited above indicate that the immersion intercalation of CsC_{24} by liquid K is best described by the chemical reaction



The right hand side of Eq. 7 represents a metastable state since we expect the equilibrium phase to be a ternary solid solution of $\text{K}_{.5}\text{Cs}_{.5}\text{C}_8 + \text{KC}_8$ or the single phase substance $\text{K}_{.66}\text{Cs}_{.34}\text{C}_8$.¹⁵

Several facts indicate the Eq. 7 is applicable in the time period during which our sample synthesis was carried out. First note that Cs is not expelled from the CsC_{24} specimen on exposure to liquid K. Instead the entry of potassium causes the Cs to laterally coalesce into regions of CsC_8 (see Fig. 1A) from the less dense CsC_{24} . In addition, careful neutron activation analysis studies¹⁶ of the residual potassium in which CsC_{24} was immersed reveal that the level of cesium detected, < 50 ppm, was the same as that expected from the original purity of the potassium. Thus the bulk C/Cs ratio is preserved on exposing CsC_{24} to liquid K.

On the basis of Eq 3 we should be able to reasonably predict the relative intensity of say the (004) reflection of the heterostructure phase to the (002) reflection of the KC_8 phase. That relative intensity is given by

$$\frac{I_{\text{H}(004)}}{I_{\text{1K}(002)}} = \frac{\sum_j f_j e^{-W_j(q/4\pi)^2} e^{-i(d_{\text{H}}\vec{z}_j) \cdot (q_{\text{H}}\hat{z})^2} L_p(q_{\text{H}})}{\sum_j f_j e^{-W_j(q/4\pi)^2} e^{-i(d_{\text{1K}}\vec{z}_j) \cdot (q_{\text{1K}}\hat{z})^2} L_p(q_{\text{1K}})} = 7.2 \quad (8)$$

In fact the measured value of $I_{\text{H}(004)}/I_{\text{1K}(002)}$ as deduced from Fig. 1C is 5.4 in good agreement with the theoretical estimate based on Eq. 7.

While it is now obvious that Eq. 7 governs the chemical reaction of CsC_{24} with liquid potassium, it is worth mentioning the alternative reaction:



where the right hand side of Eq.4 also represents a ternary alkali GIC heterostructure but with the stage 1 stacking sequence . . . K C K C Cs C K C K C Cs C . . . Such a structure, while chemically viable, clearly has a higher degree of structural asymmetry than does the KCsC_{16} structure. Since $\text{K}_2\text{CsC}_{24}$ does not form it must also have a higher intercalant-intercalant layer interaction energy and thus a higher free energy of stacking.

The in plane $(hk0)$ diffraction pattern of the metastable two phase sample containing KC_8 and KCsC_{16} is shown in Fig. 6 and has been indexed according to the reflections of the $(2 \times 2)\text{RO}^\circ$ superlattice. We find no evidence of other in plane reflections. A plot of $(h^2 + k^2 + hk)^{1/2}$ versus the q values of each reflection of Fig. 6 is shown in Fig. 3. The slope of this plot yields the in plane lattice parameter, a , of the $(2 \times 2)\text{RO}^\circ$ cell. We find $a = 4.94 \text{ \AA}$ in good agreement with the expected value of $2 \times 2.46 \text{ \AA}$ ¹⁷ but a slight in plane expansion of the host graphite layer is evident. This expansion is consistent with those observed for KC_8 and CsC_8 .¹⁸ While KC_8 does make a contribution to the $(2 \times 2)\text{RO}^\circ$ in plane diffraction pattern, we calculate on the basis of Eq 2 and the difference in structure factors that its contribution would be reduced by a factor of 17 for the (100) and (110) reflections compared to the corresponding contributions from KCsC_{16} . These two reflections also contain carbon layer contributions. Therefore, we are confident that KCsC_{16} does indeed exhibit a $(2 \times 2)\text{RO}^\circ$ in plane superlattice. From the width of the (210) reflection, again taking account of the instrumental width, we determine an in plane correlation length of 140 \AA . The intercalant layers in KCsC_{16} are clearly commensurate with the graphite layers and exhibit long range order in the plane.

In order to determine the stacking sequence of intercalant layers in KCsC_{16} , we have examined $(hk\ell)$ reflections throughout the reciprocal space along constant levels ($h, k, \ell = \text{const.}$) and constant rows ($h = \text{const.}, k = \text{const.}, \ell$). Typical examples of constant level ($\ell \neq 0$) and constant row scans are shown in Fig. 7 and Fig. 8 respectively. Note from Fig. 7 that reflections associated with $k \neq 0$ appear. These reflections result from

the fact that HOPG and its intercalated derivatives yield a two-dimensional powder diffraction pattern for scattering configurations with $\vec{q} \perp \vec{c}$. It is also evident from Fig. 7 that the $(h k \ell = 1)$ reflections are relatively sharp and indicate the same a-axis correlation range ($\sim 140 \text{ \AA}$) as deduced from the $(hk0)$ pattern of Fig. 6.

In contrast to the sharp reflections of Figs. 6 and 7 the (11ℓ) constant row pattern of Fig. 8 yields reflections which are extremely broad and pseudo shifted from their expected interger positions. This pseudoshift results from the overlap of closely spaced broad bands superimposed on a continuum background. The pattern of Fig. 8 is a classic example of that expected for a layered system with stacking faults.¹⁹ From the widths of the observed reflections we estimate the c axis size of an unfaulted region to be $\sim 35 \text{ \AA}$.

The observed reflections from Figs. 5, 6, 7 and 8 and from a multitude of similar scans are summarized in Fig. 9. The reflections are indexed according to a cell which has a $(2 \times 2) \text{RO}^0$ in plane superlattice and a c-axis repeat distance of $2d_H = 22.54 \text{ \AA}$. The reflections observed are consistent with what could be expected from a polysynthetic crystal which is divided into domains corresponding to the different possible stacking sequences, $A\alpha A \beta A \gamma A \delta$, and those generated by permutation of $\alpha\beta\gamma\delta$. Here A refers to the c-layer and $\alpha\beta\gamma\delta$ to the intercalant layers where for example $\alpha\gamma = K$; $\beta, \delta = Cs$. Out of the 6 possible permutations of $\alpha, \beta, \gamma, \delta$ only 3 are distinct²¹ and energetically these stacking sequences are the same.

The square of structural factor $S^2(h, k, \ell)$ of such a crystal can be readily calculated. Neglecting the Debye-Waller factors, it is given by

$$S^2(h, k, \ell) = F_c^2(h, k, \ell) + \frac{1}{3} \sum_{\alpha\beta\gamma\delta} [F_I^2(h, k, \ell) + 2\text{Re}(F_c^*(h, k, \ell) F_I(h, k, \ell) e^{i\frac{2\pi d}{2d_H} \ell K})] \quad (10)$$

where

$$F_c(h, k, \ell) = \gamma F_c \cos\left(\frac{h-k}{6}\pi\right) \cos\frac{h}{2} \pi \cos\frac{k}{2} \pi [1 + (-1)^\ell] [1 + e^{i\ell d_{1K}/d_H}] \quad (11)$$

and

$$F_I = \left\{ \begin{array}{l} [1+(-1)^{h+k+l}][f_K+(-1)^k e^{i\ell\pi/2} f_{CS}], \alpha\beta\gamma\delta \\ [1+(-1)^{h+l}][f_K+(-1)^{h+k} e^{i\ell\pi/2} f_{CS}], \alpha\gamma\delta\beta \\ [1+(-1)^{k+l}][f_K+(-1)^h e^{i\ell\pi/2} f_{CS}], \alpha\delta\beta\gamma \end{array} \right\} \quad (12)$$

are the structure factors of the carbon and intercalant sublattices, respectively. The summation is over the 3 distinct permutations of $\alpha\beta\gamma\delta$. The final expression for S^2 is quite elaborate, but clearly predicts that for all $(hk0)$ other than $(0,0,\ell = 2n+1)$ ($n = \text{integer}$) there will be diffraction. Furthermore for $(h = 2n, k = 2m, \ell = 2p)$ (n,m,p integers) the intensity will strong and relatively weak for $(h = 2n+1, k, \ell = 2p)$. This is consistent with the observation that for $(1,1,\ell)$ and $(1,0,\ell)$ scans, the $\ell = 2p$ diffractions and for $(1,0,\ell)$ scans, $\ell = 2p + 1$ diffractions are, seemingly absent but do appear in various level scans (Fig. 9). In fact, this polysynthetic character is similar to that of KC_8 and RbC_8 and, as has been pointed out,²¹ could be a general property of the graphite intercalation compounds.

There are other possible stacking sequences, e.g. $A\alpha A\beta A\gamma A\alpha$, which are not energetically very different from $A\alpha A\beta A\gamma A\delta$, especially when only the next and third neighbor interactions are considered.¹³ Thus, it is not surprising that a c-axis stacking fault occurs approximately every one and one-half repeat distances. Nevertheless, the c-axis stacking faults do not disrupt the long-range layer heterostructure nature of $KCsC_{16}$.

Concluding Remarks

The compound $KCsC_{16}$ is not a unique example of a ternary GIC heterostructure. Indeed we have already presented preliminary evidence that the analogous compound $RbCsC_{16}$ can also be synthesized.⁷ Moreover Stump and coworkers have synthesized molecular ternary GIC heterostructures²⁰ but these compounds are unlikely to possess the high degree of in plane order (i.e. epitaxy) characteristic of their alkali counterparts. We

expect that KCsC_{16} is merely the first synthesized member of a large class of alkali ternary GIC heterostructures with considerably longer c-axis repeat distances and/or fractional stage²² behavior. For instance one can envision the sequential intercalation of stage 4 CsC_{48} with K to yield a stage 2 like compound KCsC_{48} with a c-axis stacking sequence . . . C K C C Cs C C K C C Cs . . .

Perhaps the most intriguing thing about KCsC_{16} and the class of potential new compounds which it represents are the novel physical properties and phenomena which they may be expected to exhibit. For example while the intercalant stacking sequences of KC_8 and CsC_8 are $\alpha\beta\gamma\delta$ and $\alpha\beta\gamma$ respectively, that of KCsC_{16} is $\alpha\beta\gamma\delta$. It would be very interesting to explore the c-axis order disorder stacking transition at elevated temperatures to determine what drives KCsC_{16} into a KC_8 like arrangement as opposed to a CsC_8 like arrangement. It would also be of considerable interest to probe the electronic eigenstates of KCsC_{16} which is, with respect to the c-axis, a novel one dimensional Kronig-Penny²³ like system.

Acknowledgements

We gratefully acknowledge useful discussions with P. Vora, T. Kaplan and S. Mahanti. Thanks are also due to A. W. Moore for providing the HOPG used in this study. This work was supported by the NSF under grants DMR 80-10486 and DMR 82-11554. The x-ray equipment was provided, in part, by the ONR under grant N 00014-80-C-0610.

References

1. A. Hérol, Proc. of the Intl. Conf. on the physics of intercalation compounds, ed by L. Pietroneso and E. Tosatti (Springer-Verlag, New York 1981) p. 7.
2. L. E. DeLong, V. Yeh and P. C. Ecklund, Solid State Commun. 44, 1145 (1982).
3. P. Vora, B. R. York and S. A. Solin, Syn. Metals, in press.
4. M. E. Misenheimer, P. Chow and H. Zabel, MRS Symposia Proc. 20, ed. by M. S. Dresselhaus et al., North Holland, 1983, p. 283.
5. B. R. York, S. K. Hark and S. A. Solin, Phys. Rev. Lett. 50, 357 (1983).
6. P. Lagrange, M. El Makrini, D. Guerard and A. Herold, Physica 99B, 473 (1980).
7. B. R. York, S. K. Hark and S. A. Solin, Syn. Metal, in press.
8. M. B. Panish, Science 208, 916 (1980).
9. S. A. Solin, Adv. in Chem. Phy. 49, 455 (1982).
10. A. Hérol, Bull. Soc. Chim. Fr. 999 (1955).
11. International Tables for X-Ray Crystallography, Kynoch Press (Birmingham, England 1962) Vol III, p. 150.
12. L. E. Campbell, L. G. Montet, and G. J. Perlow, Phys. Rev. B15, 3318 (1977).
13. A. Guinier, X-Ray Diffraction (W. H. Freeman, San Francisco, 1963).
14. H. P. Klug and L. E. Alexander, X-Ray diffraction procedures for polycrystalline and amorphous materials (John Wiley & Sons, New York 1974) p. 143.
15. B. R. York, S. K. Hark and S. A. Solin, Bull. Am. Phys. Soc., in press.
16. B. R. York, S. K. Hark and S. A. Solin, unpublished.
17. R.W.G. Wyckoff, Crystal Structures, Vol. I (Oxford University Press, London, 1962) p. 26.
18. D.E. Nixon and G. S. Perry, J. Phys. C 2, 1732 (1969); D. Guerard, C. Zeller and A. Hérol, C. R. Acad. Sci. Paris C 283, 437 (1976).

19. J. B. Hastings, W. B. Ellenson and J. E. Fischer, Phys. Rev. Lett., 42, 1552 (1979).
20. E. Stump, Physica B+C 105, 15 (1981).
21. A. Herold, D. Billand, D. Guerard, P. Lagrange and M. El. Makrini, Physica 105B, 253 (1981).
22. C. D. Fuerst, J. E. Fischer, J. D. Axe, J. B. Hastings and D. B. McWhan, Phys. Rev. Lett. 50, 357 (1983).
23. G. H. Wannier, "Elements of Solid State Theory" (Cambridge University Press, Cambridge, England 1960) p. 136.

Figure Captions

Fig. 1

(00 ℓ) diffraction patterns of CsC₂₄ immersed in liquid K at 70°C after a) 2 hours, b) 2 days and c) 12 days of immersion and quenching. The peaks belonging to the binary compounds are labeled according to nM(00 ℓ) where n is the stage and M = K or Cs. Those identified as belonging to the heterostructure is labelled H(00 ℓ).

Fig. 2

Plot of the q values versus the order, ℓ , of diffraction peaks for stage 1 and 2 K and stage 1 and 2 Cs graphite intercalation compounds. The slope of the straight line gives the d spacing for the corresponding compound.

Fig. 3

Plot of the order, ℓ , and $\sqrt{h^2 + k^2 + hk}$ of the diffraction peaks versus the corresponding q values for the (00 ℓ) and (hk0) scans of the heterostructure graphite intercalation compound. The slopes of the plots give respectively $d_H = 11.27 \text{ \AA}$ and $a = 4.94 \text{ \AA}$.

Fig. 4

High resolution scan (instrumental resolution = 0.0045 \AA^{-1} as indicated) of the (004) peak of the heterostructure. The dotted trace is the experimental data and the solid line is a Gaussian fit using $N = 31$ (see Eqs. 3 and 4 of text).

Fig. 5

Reproduction of the (00 ℓ) scan of the heterostructure after 12 days of immersion in liquid K. The background of the glass envelope and peaks due to KC₈ have been

removed. The dotted trace is the experimental result. The solid line is a theoretical fit to data using $N = 31$ and the (004) peak as the intensity normalizing peak.

Fig. 6

(hk0) scan of the in plane structure of the heterostructure. The peaks are indexed according to a $(2 \times 2)RO^{\circ}$ in plane unit cell.

Fig. 7

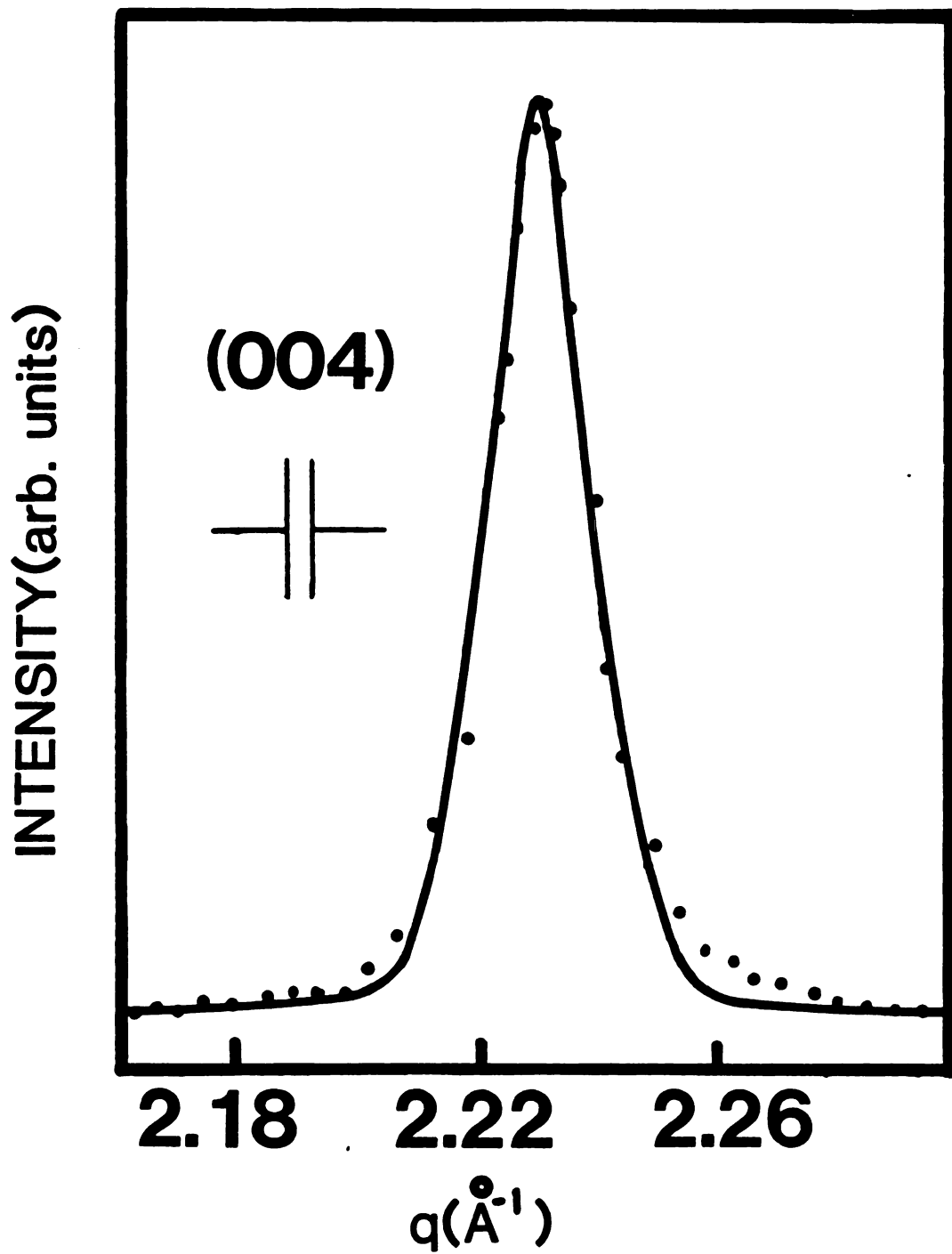
(hkl) scan of the heterostructure. The peaks are indexed according to the $(2 \times 2)RO^{\circ}$ in plane unit cell with a height $c = 2d_H$.

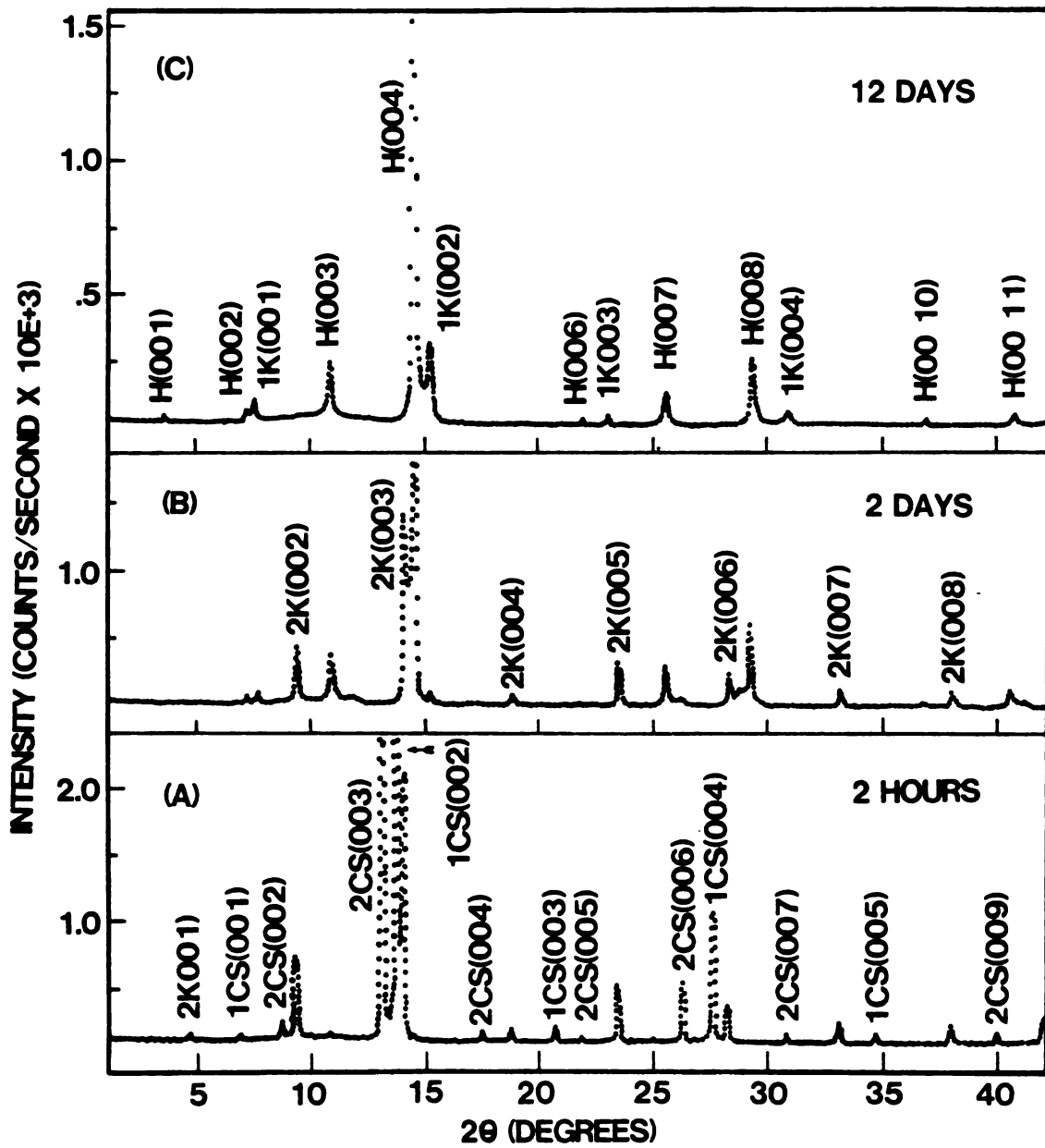
Fig. 8

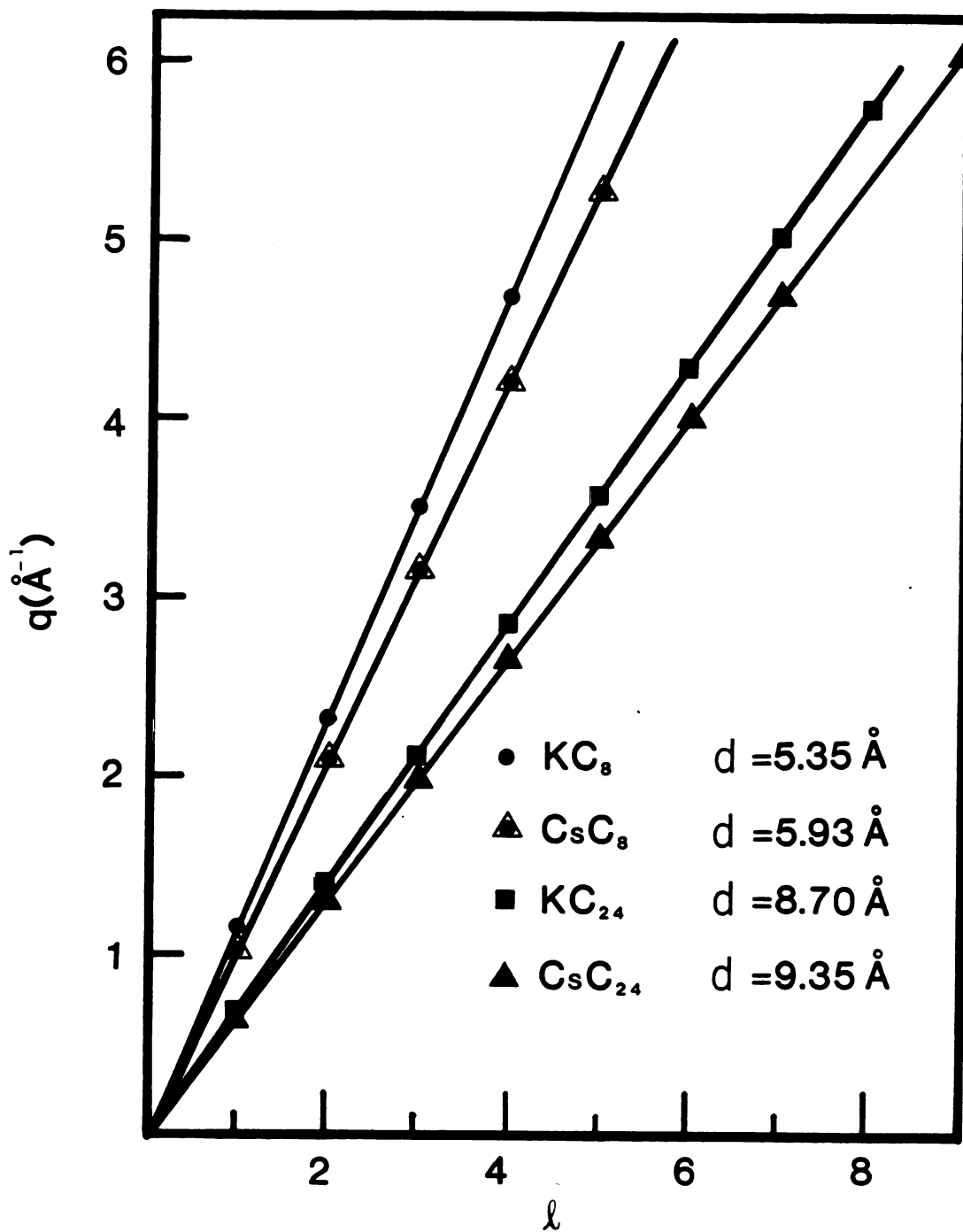
(11 ℓ) scan of the heterostructure.

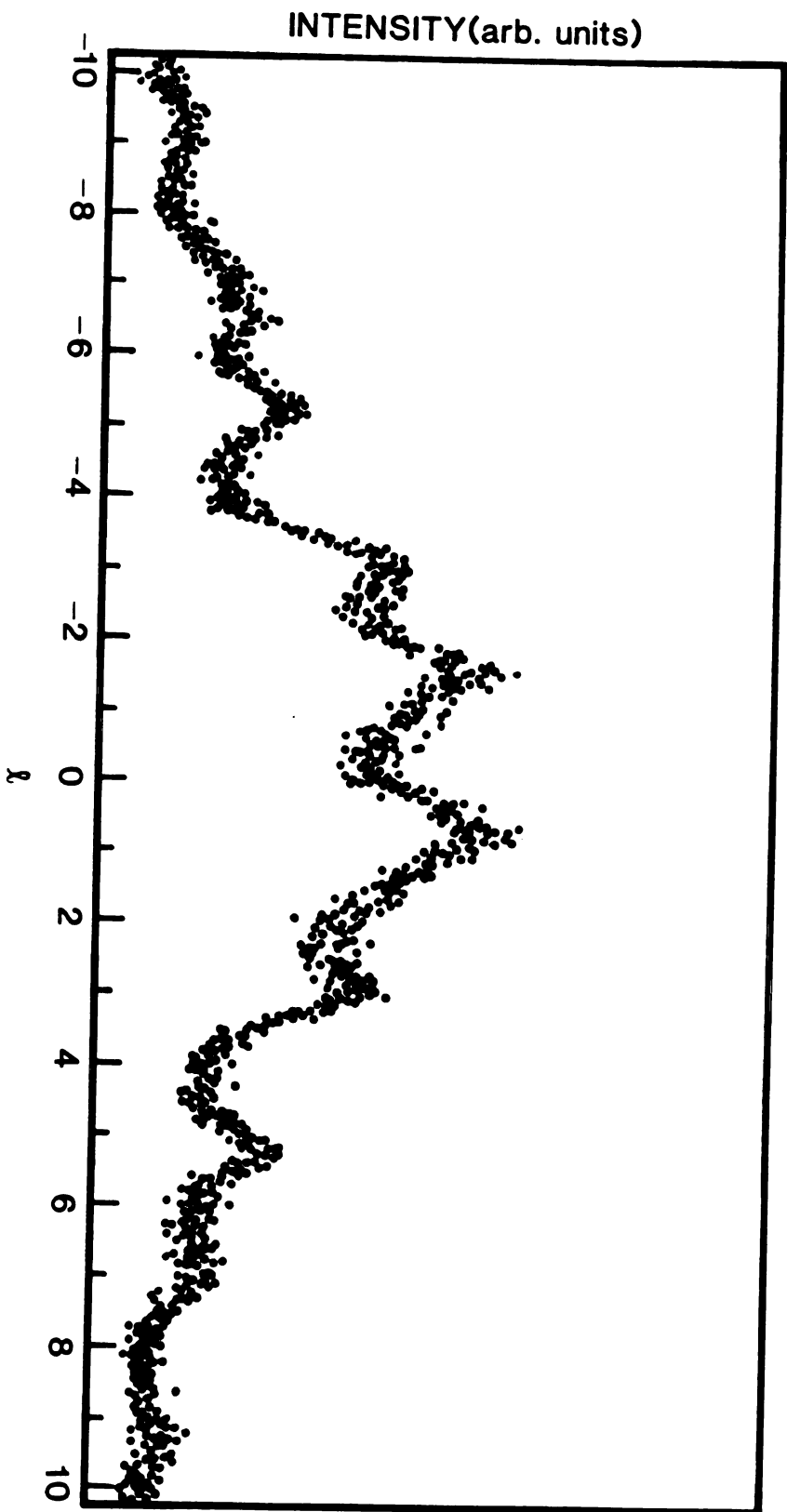
Fig. 9

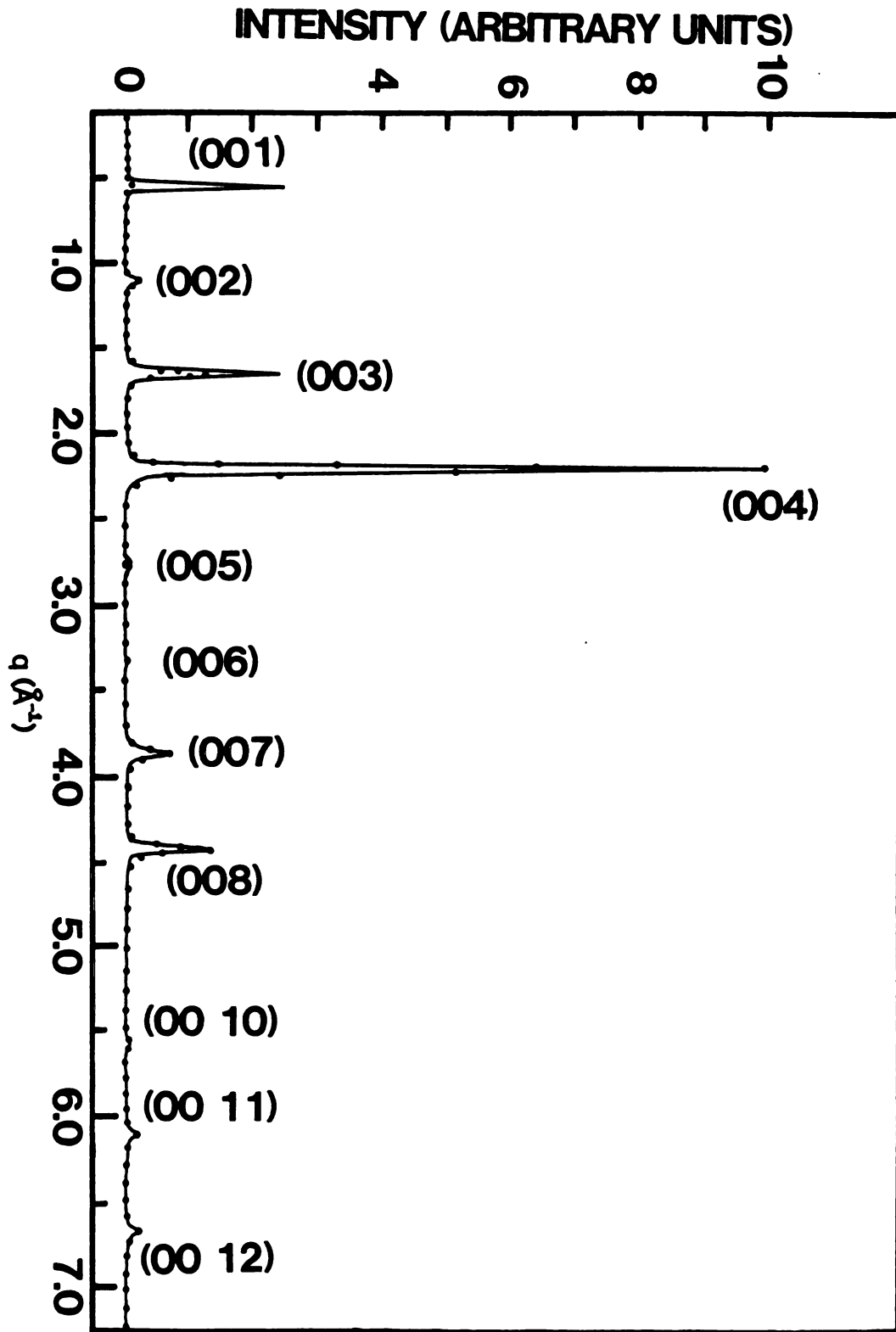
Summary of all the heterostructure diffraction peaks observed. (●) represents reflections observed while scanning along a constant level, ($h, k, \ell = \text{const}$), and (○) along a constant row ($h = \text{const}, k = \text{const}, \ell$).

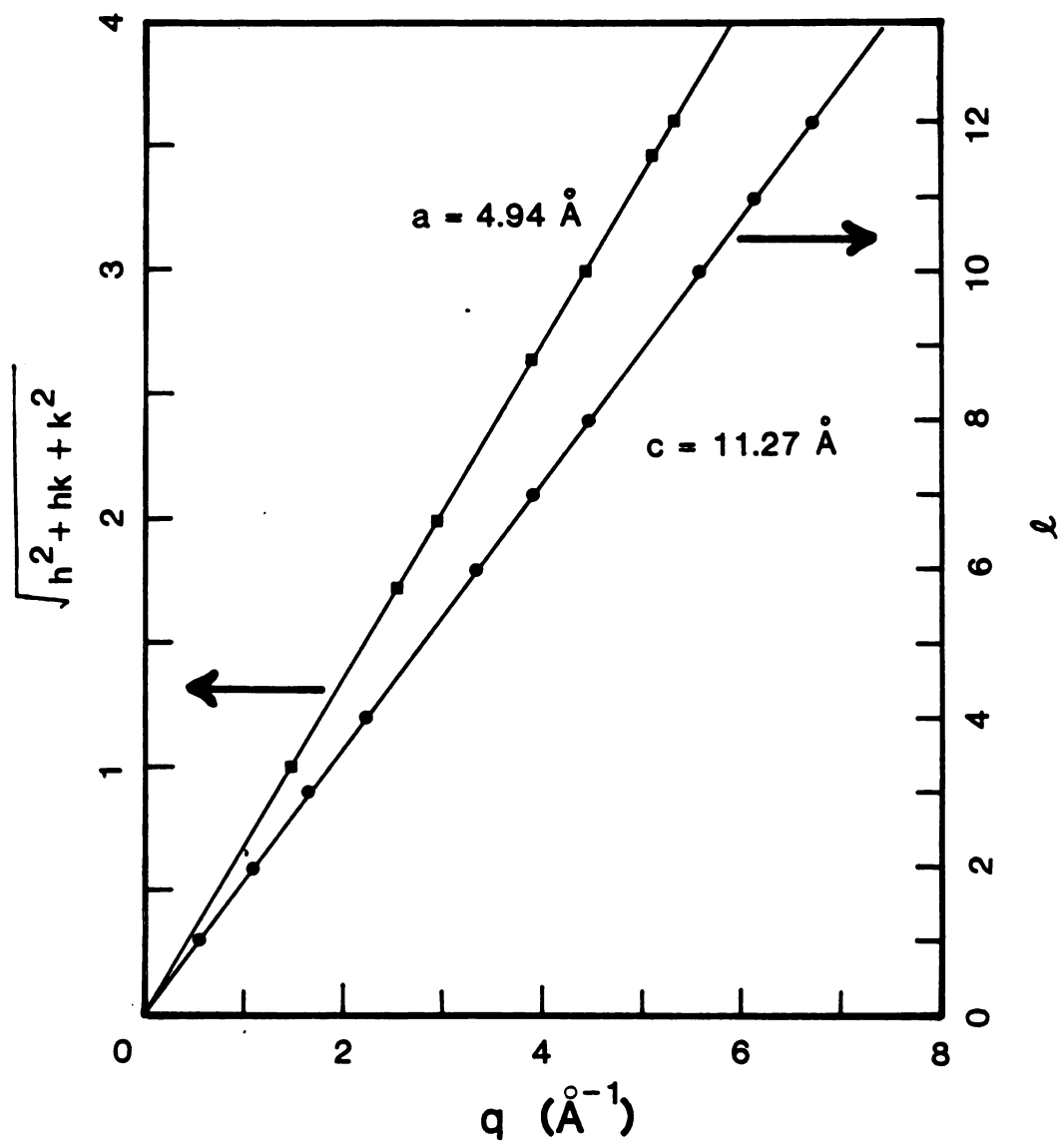


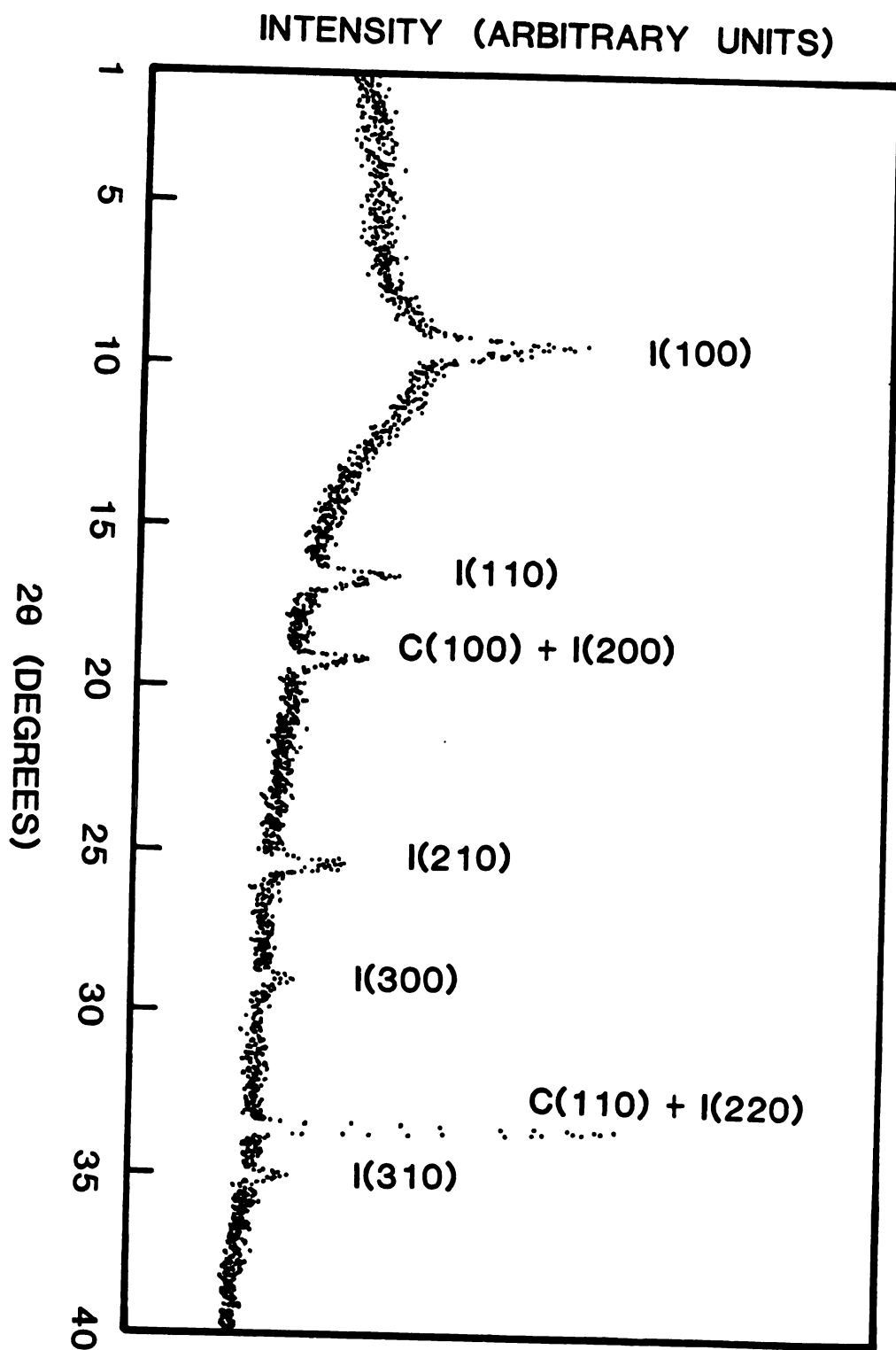












ALKALI TERNARY HETEROSTRUCTURE GICs: A NEW CLASS OF GRAPHITE INTERCALATION COMPOUNDS

B. R. YORK, S. K. HARK and S. A. SOLIN

Department of Physics and Astronomy, Michigan State University, East Lansing, MI 48824-1116 (U.S.A.)

Summary

We have prepared a stable, two-phase compound containing KCsC_{16} and KC_8 by exposing CsC_{24} to liquid potassium at 70°C . X-ray diffraction studies confirm that the KCsC_{16} is an ideal heterostructure GIC with the stacking sequence ...CKCCsCKCCs..., an in-plane structure that is $(2 \times 2)R0^\circ$, a c -axis correlation range of $\sim 350 \text{ \AA}$ and an in-plane correlation range of $\sim 140 \text{ \AA}$. The basal spacing of the heterostructure c -axis unit is $d_H = 11.27 \text{ \AA}$. Thus, to within experimental error, $d_H = d_{\text{KC}_8} + d_{\text{CsC}_8} = 5.34 \text{ \AA} + 5.94 \text{ \AA}$. We present evidence that a similar heterostructure compound, RbKC_{16} , with $d_H = 11.00 \text{ \AA}$ has also been prepared. These new compounds are physical realizations of an ideal heterostructure because their layers are atomically flat, epitaxial, exhibit long-range correlations in both the c -axis and a -axis directions, and exhibit no interdiffusion at the layer interfaces.

1. Introduction

During the past decade an enormous effort in manpower, and enormous sums of money have been expended to fabricate ideal man-made layered heterostructures using sophisticated molecular beam epitaxy (MBE) techniques [1]. While much progress has been made, an MBE derived ideal heterostructure has not yet, to the best of our knowledge, been synthesized. For our purposes, an "ideal" layered heterostructure is one in which the adjacent layers at the layer-layer interface are epitaxial, exhibit no interdiffusion, are flat on an atomic scale, and also exhibit long-range correlations in both the a -axis and c -axis directions.

In a recent letter [2] we reported the successful synthesis of an ideal layered heterostructure [3], the ternary graphite intercalation compound KCsC_{16} , which possesses a stacking sequence ...CKCCsCKCCs..., and which is one member of a new class of ternary GICs which can be stoichiometrically represented by the notation $(A_m C_{s \times n})_l (B_m C_{s' \times n'})_{l'}$ [2, 3]. Here A and B are different alkali metals, C is carbon, $l(l')$ represents the number of times a bracketed unit repeats in the minimum size c -axis stacking array which

defines the stacking sequence, $n/m(n'/m')$ is the stage designation within the bracketed unit and $1/s(1/s')$ represents the areal number density of intercalate atoms relative to carbon atoms.

In this paper we shall present (a) the first detailed data which confirm that the in-plane structure of KCsC_{16} is such that each metal layer forms a $(2 \times 2)R0'$ superlattice [4] with respect to the carbon layers, and (b) show preliminary evidence of the synthesis of another ternary GIC heterostructure, KRbC_{16} .

2. Experimental

Samples of KCsC_{16} were prepared in Pyrex with highly oriented pyrolytic graphite (HOPG) ($\approx 5 \times 10 \times 0.5 \text{ mm}^3$) by a sequential intercalation technique [2]. A well-ordered, pure [4] stage-2 binary GIC, CsC_{24} was rapidly transferred in a glove box ($< 0.5 \text{ ppm O}_2$) to a Pyrex tube containing pure potassium ($< 50 \text{ ppm}$ impurities). The tube was evacuated, sealed off in the usual manner, and heated to 70°C at which temperature it was inverted so as to immerse the CsC_{24} in liquid K. Periodically, the sample tube was placed in a centrifuge maintained at 70°C and the liquid potassium was spun off. After quenching to room temperature in air, high resolution (0.003 \AA^{-1}) X-ray diffraction patterns were acquired using apparatus which is described elsewhere [2]. The KRbC_{16} samples were prepared from RbC_{24} in a similar manner. Note, however, that the K-Cs heterostructure developed more rapidly (≈ 12 days) than did the K-Rb heterostructure.

3. Results and discussion

The $(00l)$ X-ray diffraction pattern of the CsC_{24} sample taken after 12 days of immersion in liquid potassium is shown in Fig. 1. As can be seen from that Figure, two sets of sharp reflections occur, one (labelled H) which corresponds to the heterostructure KCsC_{16} and one (labelled 1K) which

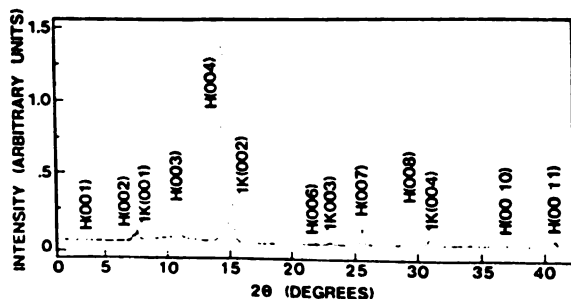


Fig. 1. $(00l)$ Diffraction pattern of stage-2 CsC_{24} after 12 days of immersion in liquid potassium. The reflections labelled H correspond to the heterostructure KCsC_{16} . Those labelled 1K correspond to stage-1 KC_8 . The diffraction patterns in the Figure and subsequent Figures were acquired with $\text{Mo K}\alpha$ radiation.

corresponds to stage 1 KC_8 . The intensities of the two sets of reflections shown in Fig. 1 are quantitatively consistent with the chemical reaction



which governs the initial period ($t \leq 20$ days) of the immersion intercalation reaction.

From a plot of the wave vector *versus* the order, l , of the H reflections, (solid circles of Fig. 2), the basal spacing, $d_{11} = 11.27 \text{ \AA}$, can be deduced. Within experimental error this basal spacing is equal to the sum of the basal spacings of KC_8 and CsC_8 , 5.35 \AA [5] and 5.94 \AA [6], respectively. Thus, the heterostructural nature of the sample is, in part, confirmed. In further support of that heterostructure form, we have calculated the structure factor for the H reflections assuming the ...CKCCsCKCCs... stacking arrangement. This calculation is described elsewhere [2] and yields results which are in excellent agreement with experiment. We find from the above cited calculation a *c*-axis stacking sequence correlation range of $\sim 350 \text{ \AA}$ which evidences a structure with long-range *c*-axis stacking order. Careful examination of (hkl) reflections [7] throughout reciprocal space along (hh, l -constant) and ($h = \text{constant}, k = \text{constant}, l$) scans indicates that the heterostructure adopts an $\alpha\beta\gamma\delta$ stacking sequence where $\alpha, \gamma = \text{K}; \beta, \delta = \text{Cs}$, similar to that of KC_8 but with a high probability of stacking faults (*i.e.*, $\alpha\beta\delta\beta, \alpha\delta\beta\gamma$, etc.) in the intercalate layer.

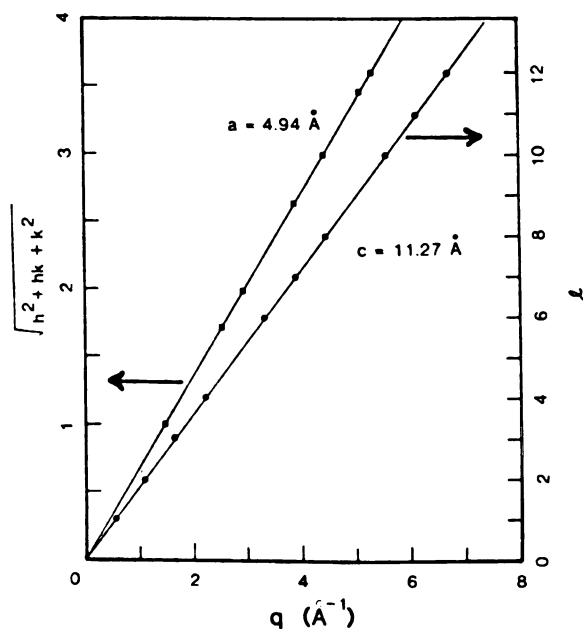


Fig. 2. A plot of the order, l , vs. wave vector, q , of the $(00l)$ heterostructure diffraction pattern of KC_8C_{16} (\bullet , right hand ordinate) and of a function of h and k (appropriate to a hexagonal $(2 \times 2)R0^\circ$ in-plane structure) vs. q (\blacksquare , left hand ordinate). Each of the solid lines shown represents a linear least-squares fit to the data.

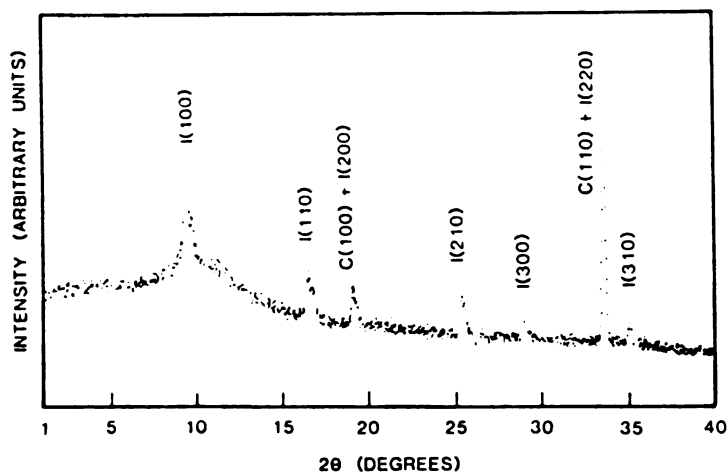


Fig. 3. In-plane ($hk0$) diffraction pattern of the KCsC_{16} heterostructure compound indexed with reference to the $(2 \times 2)\text{R}0^\circ$ superlattice. Reflections associated with the graphite layer are labelled with a "C" in the Figure. The diffuse scattering background is due to the glass envelope.

The in-plane ($hk0$) diffraction pattern of KCsC_{16} is shown in Fig. 3 and has been indexed according to the reflections of the $(2 \times 2)\text{R}0^\circ$ superlattice [4]. A plot of the q value of each reflection vs. $(h^2 + k^2 + hk)^{1/2}$ is shown in Fig. 2 (solid squares). The slope of this plot should yield the in-plane lattice parameter (a) of the $(2 \times 2)\text{R}0^\circ$ cell. We find $a = 4.94 \text{ \AA}$, in excellent agreement with the expected value $2 \times 2.47 \text{ \AA}$ [8], but nevertheless providing evidence of a slight in-plane expansion of the host graphite

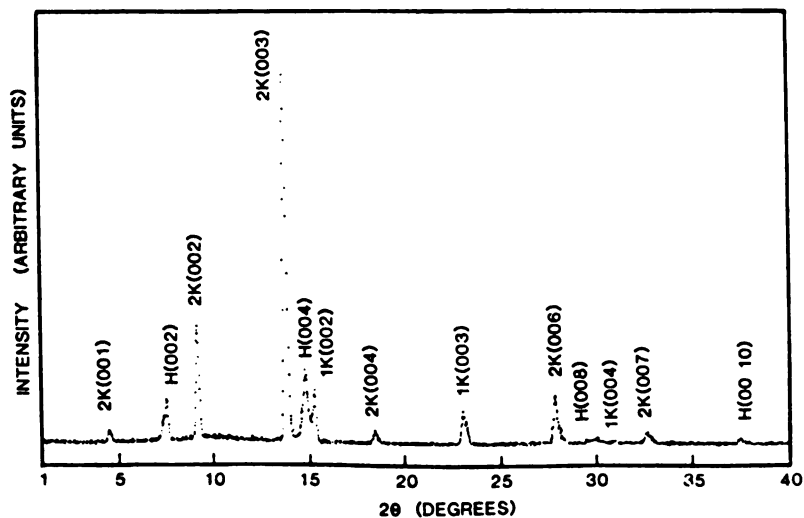


Fig. 4. $(00l)$ Diffraction pattern of stage-2 RbC_{24} after 4 h immersion in liquid potassium. Reflections labelled H are most likely due to a KRbC_{16} heterostructure, while those labelled 1K and 2K arise from stage-1 KC_8 and stage-2 KC_{24} .

layers. From the width of the (210) reflection (corrected for instrumental broadening) we determine an in-plane correlation length of 140 Å. Thus, the intercalate layers in KC_8C_{16} are clearly epitaxial to the graphite layers and also exhibit long-range in-plane order.

As noted in Section 2 above, we have attempted to synthesize KRbC_{16} by the same preparation methods as were used for KC_8C_{16} . Figure 4 shows the (00 l) diffraction pattern of RbC_{24} after immersion in liquid potassium for 4 h at 70 °C. The pattern contains three sets of reflections, labelled H, 1K, and 2K, and representing a heterostructure, stage 1 KC_8 , and stage 2 KC_{24} . By indexing the H reflections in the manner discussed for Fig. 2, we would deduce a heterostructure basal spacing of $d_H = 11.02$ Å, which is in excellent agreement with the sum of the basal spacings for KC_8 and RbC_8 , which are 5.35 Å and 5.65 Å, respectively. Only even orders of the (00 l) H pattern in Fig. 4 are detected, however. These reflections could also be indexed on a c -axis basal spacing of $11.02 \text{ Å}/2 = 5.51$ Å, a value which would

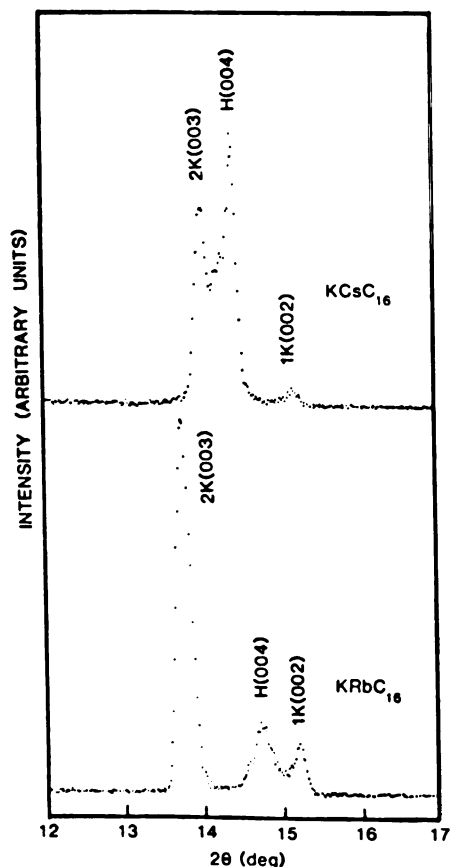


Fig. 5. Expanded (00 l) diffraction patterns of KC_8C_{16} and what is likely KRbC_{16} in the region of the heterostructure (004) reflection. See captions of Figs. 1 and 4 for a description of the labels used in this Figure.

infer that the compound examined was a solid solution [9], $K_xRb_{1-x}C_8$ with $x = 0.5$. Several facts argue against the solid solution interpretation: these are discussed below.

(i) Zabel and coworkers [10] have studied the $K_xRb_{1-x}C_8$ system [11] and have proposed a method by which x can be determined from the relative intensities of the (001) and (002) reflections. These would correspond to the (002) and (004) reflections of the heterostructure (double sized) cell. The ratio $I_{H(004)}/I_{H(002)}$ which we observe, however, is $\sim 3.5/0.7 = 5$, whereas for $K_{0.5}Rb_{0.5}C_8$, Zabel and coworkers [10] report $I_{002}/I_{001} \approx 2$. Even given the uncertainties attendant on measuring the intensities of low angle reflections from GICs [2], the discrepancy of a factor of 2.5 indicated above is well outside the bounds of experimental error and is evidence against the solid solution interpretation of the patterns of Fig. 4.

(ii) For the $KRbC_{16}$ heterostructure the odd order peaks ($00l = 2n + 1$) should be much weaker relative to, say, (004) than is the corresponding case for $KCsC_{16}$ because the atomic scattering factor for Rb is much closer to that of K than is the scattering factor for Cs. In the limit in which Rb assumed the scattering factor of K, (*i.e.*, the sample became KC_8) the odd order peaks would have identically zero intensity when indexed on the heterostructure double cell.

(iii) The K-Cs and K-Rb ternary immersion intercalation systems behave similarly during the intercalation process. This can be seen from Fig. 5 in which the diffraction patterns of the two systems are compared in the region of the H(004) reflection. The slight difference in the position of the $2K(003)$ reflections for the two compounds corresponds to slightly different KC_{24} basal spacings, 8.70 Å and 8.76 Å for the upper and lower traces, respectively.

4. Conclusions

We have confirmed unambiguously that one can prepare an ideal layered heterostructure, $KCsC_{16}$, by immersion intercalation of CsC_{24} in liquid potassium. We have also presented evidence that a similar heterostructure, $KRbC_{16}$, can be prepared using the same synthesis techniques. However, there is the possibility that the rubidium-based ternary GIC is a solid solution $K_{0.5}Rb_{0.5}C_8$ and further measurements will be necessary to definitely assess the structural character of the Rb-K-C immersion intercalation system.

Acknowledgments

We are grateful to R. D. Spence, Parul Vora, T. Kaplan, and S. Mahanti for useful discussions. Thanks are due to A. W. Moore for providing the HOPG used in this study. The research reported here was supported by the

National Science Foundation under grants DMR80-10486 and DMR82-11554. The X-ray equipment used in this research was provided by the Office of Naval Research under grant N00014-80-C-0610.

References

- 1 M. B. Panish, *Science*, **208** (1980) 916.
- 2 See B. R. York, S. K. Hark and S. A. Solin, *Phys. Rev. Lett.*, **50** (1983) 1470 and references therein.
- 3 A more complex hydrogen-potassium ternary heterostructure has been synthesized previously. See P. Lagrange and A. Hérold, *C. R. Acad. Sci., Ser. C*, **278** (1974) 701.
- 4 S. A. Solin, *Adv. Chem. Phys.*, **49** (1982) 455.
- 5 D. E. Nixon and G. S. Parry, *J. Phys. D*, **1** (1968) 291.
- 6 G. S. Parry, *Mater. Sci. Eng.*, **31** (1977) 99 and references therein.
- 7 S. K. Hark, B. R. York and S. A. Solin, to be published.
- 8 R. W. G. Wyckoff, *Crystal Structures*, Vol. I, Oxford Univ. Press, London, 1962, p. 26.
- 9 A. Hérold, in L. Pietronero and E. Tosatti (eds.), *Proc. Int. Conf. on the Physics of Intercalation Compounds*, Trieste, 1981, Springer, New York, 1981, p. 7, and references therein.
- 10 M. E. Misenheimer, P. Chow and H. Zabel, in press.
- 11 These ternary solid solutions were first synthesized by D. Billaud and A. Hérold, *Bull. Soc. Chim. Fr.*, (1971) 103.

X-RAY DIFFRACTION STUDIES OF POTASSIUM-AMMONIA ALKALI-MOLECULAR TERNARY GRAPHITE INTERCALATION COMPOUNDS

S. K. HARK, B. R. YORK and S. A. SOLIN

*Department of Physics and Astronomy, Michigan State University, East Lansing, MI
48824-1116 (U.S.A.)*

Summary

We report high resolution X-ray diffraction and gravimetric studies of potassium-ammonia ternary GICs. Both the weight uptake and the sandwich thickness of the intercalated layers vary with the vapor pressure of NH_3 to which the binary potassium-graphite compounds are exposed. A model is presented to account for these observations and to relate them to the degree of change exchange exhibited by the potassium ions.

Introduction

Research on graphite intercalation compounds (GICs) has been mainly concentrated on the binary systems formed from a single intercalated species and the graphite host. Much less attention has been devoted to the ternary GICs which contain two distinct intercalant species A and B and which can be represented as $\text{A}_x\text{B}_x\cdot\text{C}_n$. The intercalants can be a combination of two donor species, a donor and acceptor, or two acceptor species. Hérold [1] has distinguished between the "solution" ternaries in which the ratio $x/(x+x')$ can vary between wide limits without significant structural changes, and the "compound" ternaries in which mechanical, chemical or electronic constraints impose more or less narrow limits on the ratio $x/(x+x')$. Recently [2, 3] a new type of ternary, KCsC_{16} , which does not belong to either one of Hérold's classifications has been discovered. In this compound alternate layers of K and Cs were intercalated into HOPG to form a heterostructure.

We have prepared and studied a system of "compound" ternaries in which K and NH_3 constitute the intercalant species. Their preparation and X-ray diffraction studies will be presented in this report. In an accompanying report [4] Raman scattering studies will be discussed.

Stage 1 and Stage 2 alkali metal-ammonia ternary GIC systems which were prepared from the action of metal-ammonia solutions on graphite powder have been studied as early as 1954 by Rüdorff and coworkers [5]. They prepared a stage I compound with the composition $\text{K}(\text{NH}_3)_{2.1}\text{C}_{12.5}$ and a stage-2 compound $\text{K}(\text{NH}_3)_{2.8}\text{C}_{28.7}$. The respective c-axis repeat distances I_c

were determined to be 6.5 Å and 9.9 Å. We found that the composition and value of I_c are not unique, but for the K-NH₃ ternaries can vary over a wide range depending on the conditions under which the samples were prepared.

Materials preparation and experimental methods

The ternary GICs were prepared from a successive intercalation process using highly oriented pyrolytic graphite host material. Samples of different stages of K-GICs were first prepared from HOPG using the standard two-bulb technique [6] and the stages were confirmed by (00 l) X-ray diffraction scans. The well staged K-GICs were then transferred, in a glove box, into another glass tube which was subsequently evacuated to $< 10^{-5}$ Torr. Anhydrous NH₃ which was precleaned with sodium [7] was distilled into the sample tube which was then sealed off. Sufficient NH₃ was transferred to ensure that the K-GICs were exposed to a saturated vapour throughout an NH₃ temperature range $77 \text{ K} < T < 300 \text{ K}$. Ammonia intercalated rapidly at room temperature, as indicated by the expansion of the sample thickness. For all our samples, there was always some initial liquid condensation on the sample surface. There were indications that the liquid might play a role in assisting the intercalation process. Ternaries prepared from stage-2 and higher stage K-GICs were unexfoliated, their mosaic spreads are comparable with those for typical binary K-GICs. In the case of NH₃ reacting with KC₈, the sample

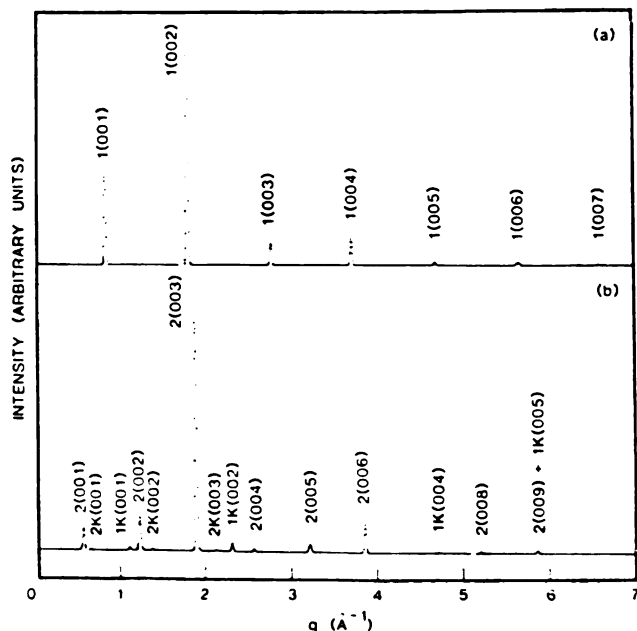


Fig. 1. (00 l) X-ray diffraction of ternary compounds formed from the reactions of KC₂₄ and NH₃ at a vapour pressure (a) 10 atm and (b) lowered to 0.1 Torr. Reflections of stage n ($n = 1, 2$) K-NH₃ ternary GIC were indexed as $n(00l)$. Reflections of stage m ($m = 1, 2$) binary K-GIC were indexed as $mK(00l)$. The pattern shown in this and the following Figure were acquired using Mo K α radiation.

had a tendency to exfoliate and expel potassium which dissolved in the liquid NH_3 to produce a light blue K-NH_3 solution.

The stages of the ternaries prepared were determined from $(00l)$ X-ray diffraction using the $\text{Mo K}\alpha$ line. In-plane $(hk0)$ scans were used to determine the in plane order of the K-NH_3 ternary.

Gravimetric measurements reported here were made using a two step procedure [8]. The graphite specimen (typical mass 60 mg) was weighed before and after intercalation of potassium (accuracy $50 \mu\text{g}$). It was then loaded in a glove box into an evacuable cylinder fitted with a McBain balance. The McBain balance was used to measure the mass uptake of NH_3 .

Results and discussion

When NH_3 at a vapor pressure of ~ 10 atm corresponding to room temperature was allowed to react with KC_{24} , a pure stage 1 ternary compound, $\text{K}(\text{NH}_3)_x\text{C}_{24}$, resulted, as determined by the X-ray $(00l)$ scan, Fig. 1(a). In the cases of KC_{36} and KC_{48} reacting with NH_3 , a phase separated mixture of stages 1 and 2 (Fig. 2(a)) and stages 2 and 3 (Fig. 2(b)), respectively, were obtained. The instrument limited widths of the diffraction peaks indicate that the ternaries are pure stage [9] compounds which exhibit long range

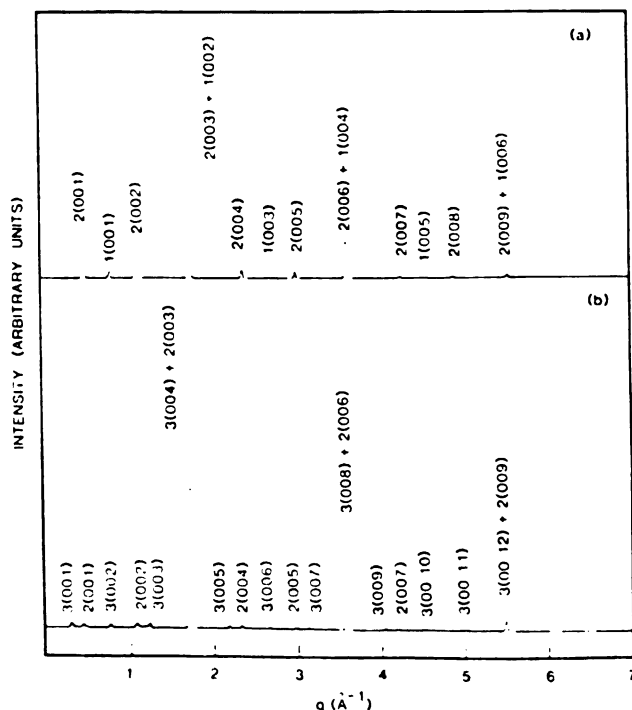


Fig. 2. $(00l)$ X-ray diffraction of ternary compounds formed from the reactions of NH_3 (vapour pressure, 10 atm) and (a) KC_{36} and (b) KC_{48} . Reflections of stage n ($n = 1, 2, 3$) K-NH_3 ternary GIC were indexed as $n(00l)$.

order ($> 200 \text{ \AA}$) in the c -axis direction. The c -axis repeat distances, I_c , of the stage-1 K-NH₃ ternary GICs, and of the stage 2 and 3 compounds prepared in a similar manner by reacting NH₃ at 10 atm with KC₂₄, KC₃₆ and KC₄₈, were determined to be 6.63, 9.94, and 13.30 Å, respectively. Thus, the intercalation of NH₃ into the KC_{12 n} compounds involves a decrease in stage. Similar decreasing stage changes have been observed by Béguin and coworkers [10] and have recently been confirmed by us [11] in the case of furan, and tetrahydrofuran interacting with KC_{12 n} . Such stage changes at room temperature are easily interpreted using the Daumas-Hérolld model [12].

Our stage-1 ternaries gave $I_c = 6.63 \text{ \AA}$ rather than the 6.56 \AA quoted by Rüdorff (for a sample with the composition K(NH₃)_{2.1}C_{12.5}). Furthermore, stage 1 ternary samples prepared in our laboratory from the reaction of KC₈ and NH₃, although exfoliated, gave $I_c = 6.54 \text{ \AA}$, which agrees with the value reported by Rüdorff who pumped off NH₃ from his samples after intercalation. Using a method suggested by Setton [13], the value of x in the formula K(NH₃) _{x} C _{y} can be estimated from the intercalation volume available for NH₃ molecules if y and the volume of the K ion are known. For a sample with a measured value of $y = 23.86$ we calculate that for the saturated stage 1 compound (NH₃ vapor pressure of ≈ 10 atm surrounding the sample) the weight uptake of NH₃ should yield x in the range $4.48 \leq X \leq 5.64$ where the lower and upper limits correspond to a potassium radius of 2.29 \AA (atomic radius deduced from K metal) and 1.33 \AA (ionic radius deduced from potassium halides), respectively. The measured value of x deduced from a McBain balance was 4.45, corresponding to a stage-1 sample with composition K(NH₃)_{4.45}C_{23.86}.

As the temperature of the excess liquid NH₃ in the sample tube is reduced, thereby reducing the NH₃ vapor pressure, so also is the measured value of x . When the excess liquid NH₃ was frozen at liquid nitrogen temperature, the pure stage 1 ternary NH₃-K GIC phase separated into a three phase system containing pure stage 2 NH₃-K GIC and small amounts of pure KC₈ and KC₂₄ as indicated by the (00 l) X-ray diffraction pattern of Fig. 1(b). The stage-2 ternary component has a c -axis repeat distance of $I_c = 9.65 \text{ \AA}$, which not surprisingly is different from the corresponding value reported by Rüdorff [5]. If we again apply Setton's procedure [13] to calculate the expected value of x for the stage-2 NH₃-K GIC (NH₃ vapor pressure < 0.1 Torr for excess ammonia at 77 K), we find, using the same extreme values of the K radius noted above, that $1.23 \leq X \leq 2.39$, while the measured value of x is 1.66 yielding now a stage-2 sample of composition K(NH₃)_{1.66}C_{23.86}.

Concurrent with the changes in weight uptake with NH₃ vapor pressure we have observed that the value of I_c for stages 1 and 2 K-NH₃ GICs can be *continuously* tuned by adjusting the NH₃ vapor pressure over the sample [14]. Thus the differences in the value of I_c between our samples and those of Rüdorff relate to the fact that they have different compositions. Presumably, NH₃ (which is known to solvate K), when intercalated into KC_{12 n} competes with the graphite layer to receive the donated charge. The amount of intercalated NH₃ thus affects the degree of charge transfer to the graphite

layer. This, in turn, changes the electrostatic interaction between layers and causes the system to adjust its equilibrium value of I_c . For the stage-1 compound $K(NH_3)_{4.46}C_{23.86}$, the K is only weakly ionized (*i.e.*, has a large radius) and the sandwich thickness of the intercalate layer (which is equal to I_c for the stage-1 compound) is considerably larger than the sandwich thickness of the stage 2 $K(NH_3)_{1.66}C_{23.86}$ compound in which the K is more strongly ionized (*i.e.*, has a smaller radius).

We have also examined the in-plane structure of the stage-1 ternary NH_3 -K GIC using X-ray ($hk0$) scans. Only diffraction peaks corresponding to glass and to the graphite in-plane lattice were found. Both the intercalated K and NH_3 are in a disordered state at the saturated vapour pressure of NH_3 at room temperature. The disorder is consistent with the fact that the compound is nonstoichiometric and, in the case of the stage 1 ternary there is only one K ion for every 24 C atoms in the layer. If the compound formed an in-plane superlattice at all, at a certain NH_3 vapour pressure and sample temperature, that superlattice would be considerably larger than the $(2 \times 2) R0^\circ$ structure of the binary KC_8 [15].

Conclusion

We have shown that NH_3 -K ternary GICs exhibit unique properties not found in other binary or ternary GICs. The compounds which Rüdorff studied in 1954 were specific NH_3 -K ternary GICs prepared under a specific set of conditions. By contrast, there is a whole range of possible states of NH_3 -K ternary GICs which have the same stage but varying composition.

Acknowledgements

Thanks are due to P. Vora and especially to T. J. Pinnavaia and R. D. Spence for useful discussions. We also thank A. W. Moore for supplying the graphite used in this work. This research was supported by the NSF under contracts DMR80-10486 and DMR82-11554. The X-ray equipment was provided by the Office of Naval Research under contract N00014-80-C-0613.

References

- 1 A. Hérol, in F. A. Lévy (ed.), *Intercalated Layered Materials*, Vol. 6, Reidel, Dordrecht, 1979, p. 323.
- 2 B. R. York, S. K. Hark and S. A. Solin, *Phys. Rev. Lett.*, **50** (1983) 1470.
- 3 B. R. York, S. K. Hark and S. A. Solin, *Synth. Met.*, **7** (1983) 25.
- 4 P. Vora, B. R. York and S. A. Solin, *Synth. Met.*, **7** (1983) 355.
- 5 W. Rüdorff and E. Schulze, *Angew. Chem.*, **66** (1954) 305. W. Rüdorff, *Adv. Inorg. Chem. Radiochem.*, **1** (1959) 323.
- 6 A. Hérol, *Mater. Sci. Eng.*, **31** (1979) 1.

- 7 J. V. Acrivos and J. Azebu, *J. Magn. Reson.*, **4** (1971) 1.
- 8 J. W. McBain and A. M. Bakr, *J. Am. Chem. Soc.*, **48** (1926) 690.
- 9 S. A. Solin, *Adv. Chem. Phys.*, **49** (1982) 455.
- 10 F. Béguin and R. Setton, *Carbon*, **13** (1975) 293. F. Béguin, L. Gatineau and R. Setton, *Proc. 6th London Int. Carbon and Graphite Conf.*, 1983, p. 97.
- 11 S. K. Hark, B. R. York and S. A. Solin, *Bull. Am. Phys. Soc.*, **28** (1983) 348.
- 12 N. Daumas and A. Hérold, *Bull. Soc. Chim. Fr.*, **5** (1971) 1598.
- 13 R. Setton, F. Béguin, J. Jegoudez and C. Mazières, *Rev. Chim. Miner.*, **19** (1982) 360.
- 14 S. K. Hark, B. R. York and S. A. Solin, to be published.
- 15 S. A. Solin, *Adv. Chem. Phys.*, **49** (1982) 455, and reference therein.

RAMAN SCATTERING STUDY OF ALKALI-MOLECULAR TERNARY GRAPHITE INTERCALATION COMPOUNDS

P. VORA, B. R. YORK and S. A. SOLIN

Department of Physics and Astronomy, Michigan State University, East Lansing, MI 48824-1116 (U.S.A.)

Summary

We have studied the room temperature Raman spectra of several stages of ternary GICs prepared by sequential intercalation of potassium-binary GICs with either furan, THF or NH_3 . A Raman study, which detects the shift of the graphite intralayer vibrational frequency due to intercalation, provides a useful tool for the probe of charge transfer of these novel materials. For all three stage 1 compounds, we have observed an intralayer graphite vibrational frequency at $\sim 1606 \text{ cm}^{-1}$ (upshifted from the pure graphite peak at 1582 cm^{-1}), which is Fano broadened and has a Raman profile similar to that exhibited by LiC_6 and EuC_6 . These results are compared and contrasted with those for the alkali binary GICs.

1. Introduction

The study of graphite intercalation compounds (GICs) continues to be an exciting field of interest [1, 2]. These interests stem primarily from the possibility of studying 2D systems and their corresponding phase transitions. Another aspect, which has been the subject of considerable debate, has been the nature and quantitative value of the charge transfer to the host lattice [3].

Most work to date on GICs has been on binary systems where there is an intercalation of only one species in the graphite host. For a ternary GIC, however, there exists the possibility of an even richer variety of phases and also of intercalation of competing (donor *versus* acceptor) species. This, in turn, may give a better understanding of 2D phase transitions and the nature of the interaction between the intercalant and the host [3].

In this paper, we present the Raman spectra for three different graphite ternary systems; K-furan, K-THF and K- NH_3 GICs. X-Ray studies [4 - 8] on these materials have shown that these ternaries exhibit different stages and also undergo interesting staging phase transitions. Our Raman results

supplement the X-ray data and also give further insight into the above mentioned aspects of intercalant-host bonding. We compare and contrast our results with corresponding binary potassium GICs.

2. Sample preparation and experimental procedure

The molecular ternaries were prepared by exposing the potassium binary GICs (previously made by using the standard two-bulb technique) [9] to the molecular species involved (*i.e.*, furan, THF and NH_3). A long glass tube with a break seal initially isolated the molecular liquid from the graphite-potassium system. After preparation of the alkali binary, the seal was broken and the sample exposed to the molecular liquid. Intercalation took place through the molecular vapor or through direct contact with the liquid. The tube was then further sealed to isolate the ternary GIC with just the molecular liquid to avoid interactions of the bare potassium with the liquids (furan and THF react with potassium over a period of time). Several samples were made in this manner with starting binaries of stages 1, 2 and 3. With NH_3 , a ternary was also made with an initial potassium stage 4 binary. Table 1 indicates the stages of the resulting ternaries which resulted from intercalation of the various initial binaries.

An argon ion laser provided the incident beam ($\lambda = 4880 \text{ \AA}$) for the scattering studies. The power of the beam was measured at $\sim 30 \text{ mW}$ near the sample. A Jarell-Ash double grating monochromator was used for the analysis of the scattered light. Alignment of the sample consisted of focussing a line image of the beam onto the GIC surface. The scattered light was collected and focussed on the spectrometer slit in the back scattering 90° geometry arrangement. The incident beam was polarized in the scattering plane to obtain a maximum coupling of the incident radiation to the sample.

TABLE 1

Stages of the ternary GICs produced with different initial potassium binary GICs

Initial K binary	Stage of resulting ternary after intercalation*		
	Furan	THF	NH_3
KC_8	—	—	1
KC_{24}	2	1	1**
KC_{36}	2	2	1 + 2
KC_{48}	—	—	2 + 3

* Verified by X-rays.

** A different stage 1 from the one made by KC_8 .

3. Results and discussion

The Raman spectra of graphite (or HOPG) has been known for some time [10, 11]. There are two Raman active bands corresponding to a low frequency shear mode at 42 cm^{-1} and a prominent intralayer mode at 1582 cm^{-1} . The changes of the 1582 cm^{-1} mode due to the intercalation of potassium in different stages have also been well studied [12]. Recently, the vibrational modes of the intercalant have also been observed directly [13, 14].

Figure 1(a) shows a spectrum for the KC_8 stage 1 GIC. The 1582 cm^{-1} band has been considerably Fano broadened [12] due to an electronic continuum arising from the strong coupling between the potassium donor and the host [15]. There also exists a low frequency 563 cm^{-1} band arising from both disorder induced scattering and the $(2 \times 2)\text{R}0^\circ$ ordering of the potassium in the plane [16]. However, the spectrum of a stage 1 ternary GIC, K-THF in this case, is noticeably different and is shown in Fig. 1(b). The sample was prepared by the intercalation of KC_{24} with THF vapor, as indicated in Table 1, and also characterized by X-rays to be a pure stage. Note from Fig. 1(b) that the intralayer mode has been shifted to 1606 cm^{-1} and is considerably narrower. The spectrum in fact is more like that of stage 2 KC_{24} or stage 1 EuC_6 [17]. Indeed, the color of the sample here is a deep blue, as in KC_{24} , rather than the gold expected of KC_8 . The narrowness of the peak ($\Delta\bar{\nu} \sim 22\text{ cm}^{-1}$) implies a weaker coupling between the 1582 cm^{-1} mode and the continuum than in the KC_8 case. Interestingly, this peak is even narrower than in KC_{24} ($\Delta\bar{\nu} \sim 29\text{ cm}^{-1}$). The disappearance of the low frequency 563 cm^{-1} band is consistent with the X-ray observation [7] of disorder in the plane.

A similar comparison has been made of the spectrum for the ternary (K-furan) C_{24} . Here, the resulting ternary prepared from KC_{24} (see Table 1) is also stage 2. Again, the carbon intralayer mode of the ternary is sharper ($\Delta\bar{\nu} \sim 23\text{ cm}^{-1}$) than that in KC_{24} , as shown in Fig. 2. Since one would not expect any appreciable change in the graphite phonon modes in the two cases, the width seems to be related to the charge transfer between the host and intercalant. We suggest that the furan molecule, being an acceptor, reduces the charge transfer to the host from the potassium donor. There is no appreciable shift in frequency between the two compounds.

Studies performed on the $(\text{K-NH}_3)\text{C}_{24}$ system are shown in Fig. 3. Here, again, the ternary was prepared *via* the NH_3 intercalation of KC_{24} . At room temperature, where the vapor pressure of NH_3 surrounding the sample is $\approx 10\text{ atm}$ (there is an excess amount of NH_3 liquid in the sample tube), the ternary is a pure stage 1 [8]. It has been shown from the X-ray results [8] that as the vapor pressure of the NH_3 is reduced by maintaining the excess NH_3 at liquid N_2 temperatures, for which the vapor pressure surrounding the sample is $< 0.1\text{ Torr}$, the sample evolves into a three phase system containing KC_8 , KC_{24} and pure stage-2 $\text{K}(\text{NH}_3)_{1.66}\text{C}_{23.86}$. These changes are clearly reflected in the Raman spectra as well. The appearance of

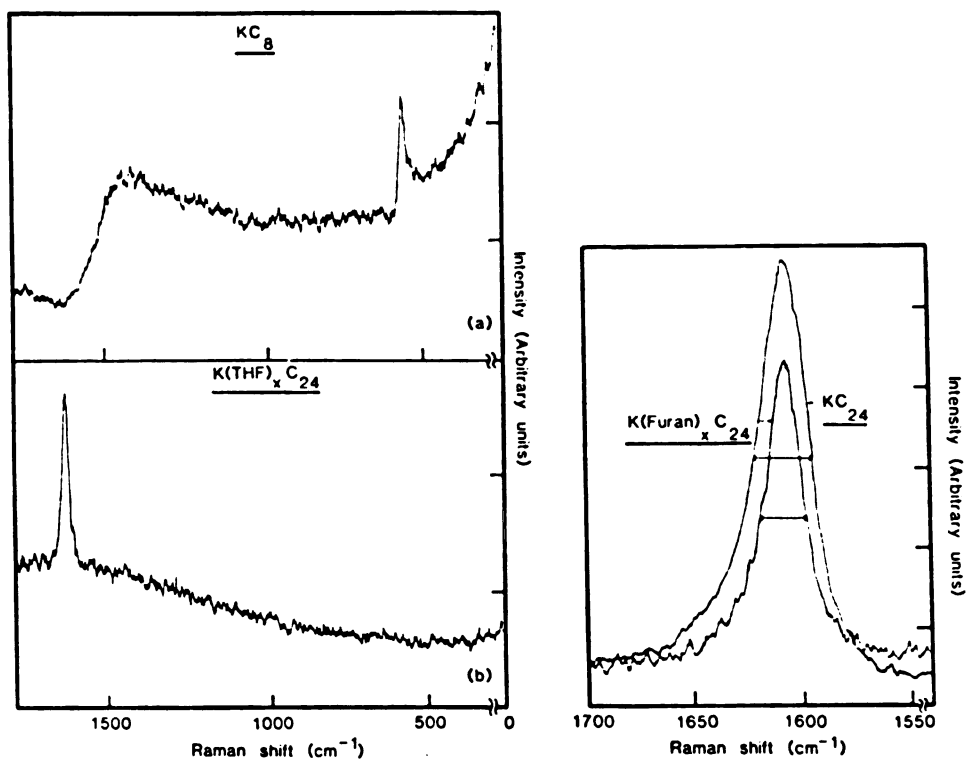


Fig. 1. The Raman spectra of an (a) stage 1 KC_8 and (b) stage 1 ternary $\text{K}(\text{THF})_x\text{KC}_{24}$. The abscissa in this Figure and the Figures which follow is linear in wavelength rather than wavenumber.

Fig. 2. Comparisons of the widths of the graphite intralayer mode for samples KC_{24} ($\Delta\tilde{\nu} = 29 \text{ cm}^{-1}$) and $\text{K}(\text{furan})_x\text{C}_{24}$ ($\Delta\tilde{\nu} = 23 \text{ cm}^{-1}$).

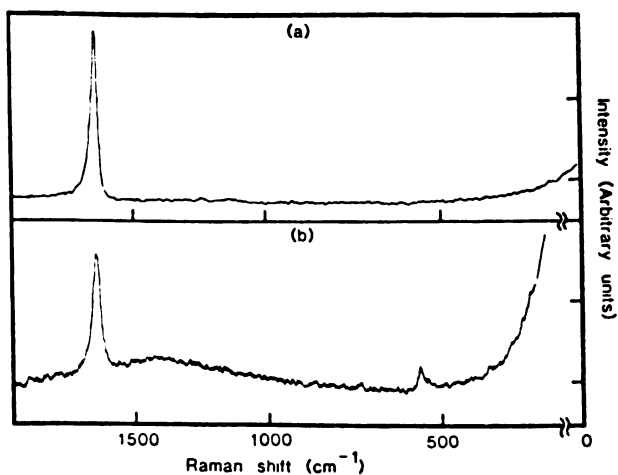


Fig. 3. The room-temperature Raman spectra of (a) stage 1 $\text{K}(\text{NH}_3)_{4.38}\text{C}_{23.86}$, excess NH_3 at room temperature, and (b) stage-2 $\text{K}(\text{NH}_3)_{1.66}\text{C}_{23.86} + \text{KC}_8 + \text{KC}_{24}$, excess NH_3 at 77 K.

the 563 cm^{-1} peak is an indication of the presence of KC_8 which, with KC_{24} , tends to reside on the sample surface. The superposition of the intralayer mode at slightly different wavenumber shifts for KC_{24} and $\text{K}(\text{NH}_3)_{1.66}\text{C}_{23.86}$ has resulted in the broadening of the $\sim 1580\text{ cm}^{-1}$ peak. Similar staging phase transitions may occur in the furan and THF systems as a function of intercalant vapor pressure as well.

Other higher stage phase transitions in the K-NH_3 ternary GIC system, as seen by X-ray [18], have also been evident in the corresponding Raman spectra. Figure 4 shows the change to a stage 2 + 3 (K-NH_3) ternary from a stage 4 KC_{48} sample. Similar results were also seen for the THF and NH_3 samples [19]. The relative intensities of the members of the doublets shown are consistent with the stage 4 and stage 2 + 3 designations.

It can be clearly seen that the results presented here indicate a richness in variety of possibilities for a better understanding of GIC systems. The Raman scattering results have also thrown light on understanding the width of the graphite intralayer mode. The Raman results are consistent with, and supplementary to, the X-ray results.

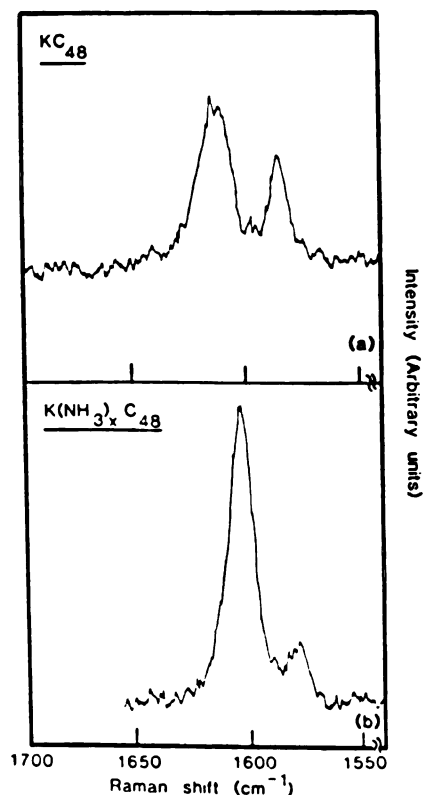


Fig. 4. Raman spectra showing the transformation of a stage 4 KC_{48} binary GIC to a stage 2 + 3 $\text{K}(\text{NH}_3)_x\text{C}_{48}$ ternary GIC.

Acknowledgments

We are grateful to S. K. Hark for useful discussions. Thanks are due to A. W. Moore for providing the graphite host material used in this study. This work was supported by the National Science Foundation under grants number DMR80-10486 and DMR82-11554.

References

- 1 S. A. Solin, *Adv. Chem. Phys.*, **49** (1982) 455.
- 2 M. S. Dresselhaus and G. Dresselhaus, *Adv. in Phys.*, **30** (1981) 139.
- 3 M. S. Dresselhaus and G. Dresselhaus, *Top. Appl. Phys.*, **51** (1982) 3.
- 4 F. Béguin, J. Jegoudez, C. Mazières and R. Setton, to be published.
- 5 F. Béguin, L. Grataineau and R. Setton, to be published.
- 6 W. Rüdorff and E. Schulze, *Angew. Chem.*, **66** (1954) 305; W. Rüdorff, *Adv. Inorg. Chem. Radiochem.*, **1** (1959) 323.
- 7 S. K. Hark, B. R. York and S. A. Solin, *Bull. Am. Phys. Soc.*, **28** (1983) 348.
- 8 S. K. Hark, B. R. York and S. A. Solin, *Synth. Met.*, **7** (1983) 257.
- 9 A. Hérold, *Mater. Sci. Eng.*, **31** (1979) 1.
- 10 R. J. Nemanich, G. Lucovsky and S. A. Solin, in M. Balkanski (ed.), *Proc. Int. Conf. on Lattice Dynamics*, Flammarion, Paris, 1978. R. J. Nemanich, G. Lucovsky and S. A. Solin, *Solid State Commun.*, **23** (1977) 117.
- 11 F. Tuinstra and J. L. Koenig, *J. Chem. Phys.*, **53** (1970) 1126.
- 12 S. A. Solin and N. Caswell, *J. Raman Spectrosc.*, **10** (1981) 129.
- 13 N. Wada, M. V. Klein and H. Zalul, in L. Pietronero and E. Tosatti (eds.), *Physics of Intercalation Compounds*, Springer, Berlin, 1981.
- 14 P. C. Eklund, J. Giergiel and P. Boolchand, in L. Pietronero and E. Tosatti (eds.), *Physics of Intercalation Compounds*, Springer, Berlin, 1981.
- 15 H. Miyazaki and C. Horie, *J. de Phys.*, **42** (1981) C6-335.
- 16 D. M. Hwang, S. A. Solin and D. Guérard, in L. Pietronero and E. Tosatti (eds.), *Physics of Intercalation Compounds*, Springer, Berlin, 1981.
- 17 D. M. Hwang and D. Guérard, *Solid State Commun.*, **40** (1981) 759.
- 18 S. K. Hark, B. R. York and S. A. Solin, to be published.
- 19 P. Vora, B. York and S. A. Solin, to be published.



TUNEABLE SANDWICH THICKNESS IN POTASSIUM-AMMONIA GRAPHITE INTERCALATION COMPOUNDS

S.K. Hark*, B.R. York, S.D. Mahanti, and S.A. Solin

Department of Physics and Astronomy, Michigan State University,
 East Lansing, MI 48824-1116, USA

Received 27 February 1984 by J. Tauc

We have studied the composition dependence of the sandwich thickness, d_s , in stages 1 and 2 ($n = 1, 2$) $K(NH_3)_x C_{24}$ ($0 < x \leq 4.48$) using high resolution x-ray diffraction. The variation of d_s with x is accurately predicted with a model of the sandwich energy⁵ which accounts explicitly for charge exchange, f , and for size and stiffness differences between the NH_3 and K species. Surprisingly, the reduction of f with increasing x markedly increases the elastic energy of the K ion.

The most fundamental and intrinsically interesting characteristic of graphite intercalation compounds (GIC's) is their ability to form pure stages.¹ Detailed theoretical models of the physics of the staging phenomena have only recently been presented.^{2,3,4} A key ingredient of those models is the contribution of the sandwich energy to the free energy from which the equilibrium stage is established. The sandwich energy is the energy which, when minimized, determines the perpendicular distance or sandwich thickness, d_s , between the bounding carbon layers which flank an intercalate layer.

Any acceptable model of staging must account for the dependence of sandwich thickness on composition and charge exchange. Yet, to date, insufficient experimental data exist with which to test theoretical predictions for the variation of d_s with those parameters. For instance, Metrot et al.⁵ noted that d_s was dependent on the electrochemical overcharging of stage 1 H_2SO_4 GIC's, but focused on the chemical implications of their measurements and did not explore in depth the very weak dependence of d_s on charge exchange. Similarly, Fisher and coworkers⁶ noted a very small (0.3%) composition dependent change in d_s for stage 2 LiC_{12} in comparison with stage 2 LiC_{18} . But the fixed stage composition of those compounds as well as of other alkali GIC's cannot be conveniently varied experimentally. Large variations (~5%) of d_s with composition x have been reported for $K_xRb_{1-x}C_8$,^{7,8} but such variations are predominantly elastic in origin⁸ and preclude an examination of the role of charge exchange.

In this paper we present the first detailed experimental study in which the variation of d_s with charge exchange, f , and composition, x , are explored. The subjects of this study are stages 1 and 2 $K(NH_3)_x C_{24}$,^{9,10} for which x and f can be varied over a wide range. We present a theoretical model for the x, f dependence of d_s which accounts well for our experimental measurements. This model also yields the surprising result that charge transfer between the carbon layers

and intercalate layers in $K(NH_3)_x C_{24}$ significantly effects d_s by altering the elastic contribution of the K ion to the sandwich energy.

Specimens of stage 1 and stage 2 potassium ammonia GIC's were prepared by exposing pure stage 2 highly oriented pyrolytic graphite $KC_{24+\Delta}$ ($0 \leq |\Delta| < 1.2$) to saturated NH_3 vapor, the pressure of which, P_{NH_3} , was controlled by adjusting the temperature of excess liquid NH_3 . The GIC was always maintained at room temperature. After the initial intercalation of NH_3 at ≈ 9 atm., the bulk composition of the specimen could be reversibly varied over the range $2.0 = 0.5 < x \leq 4.33$ for $77K \leq T_{NH_3} \leq 300K$.

The x-ray measurements which we report here were made using a Huber 4-circle diffractometer coupled through a vertically bent graphite monochromator to a Rigaku 12kw rotating anode x-ray source equipped with a Mo anode. In situ studies of the (00 ℓ) diffraction patterns as a function of P_{NH_3} were made "on the fly" by allowing the NH_3 end of the sample tube to slowly (<4.4K/hour) warm up to 300K from 77K.

The (00 ℓ) x-ray diffraction patterns of $K(NH_3)_x C_{23.5}$ are shown in Fig. 1. The observed reflections in each pattern are of instrument limited width and thus for the 1 mm slit settings used indicate a c-axis correlation range $\geq 300A$. At $P_{NH_3} \approx 9$ atm., the entire specimen consists of a pure stage 1 compound with composition $K(NH_3)_{4.33} C_{23.5}$. As P_{NH_3} is reduced, a second set of reflections corresponding to a pure stage 2 potassium-ammonia compound appear. For $P_{NH_3} \leq 10^{-3}$ torr the specimen is essentially a pure stage 2 compound with $x = 2.0 = .5$. Detectable admixtures of KC_{24} and KC_8 are evident in the 10^{-3} torr pattern of Fig. 1; however, these binary GIC phases are sufficiently minute to be ignored in the discussions which follow.

The intensities of the (002) and the (001) reflections of the stage 2 and stage 1 regions, respectively, are shown in Fig. 2 as a function of P_{NH_3} . The inflection evident at $P_{NH_3} \approx 5.5$

*Present Address: Xerox Corporation, Webster Research Center, 800 Phillips Road, Webster, NY 14580.

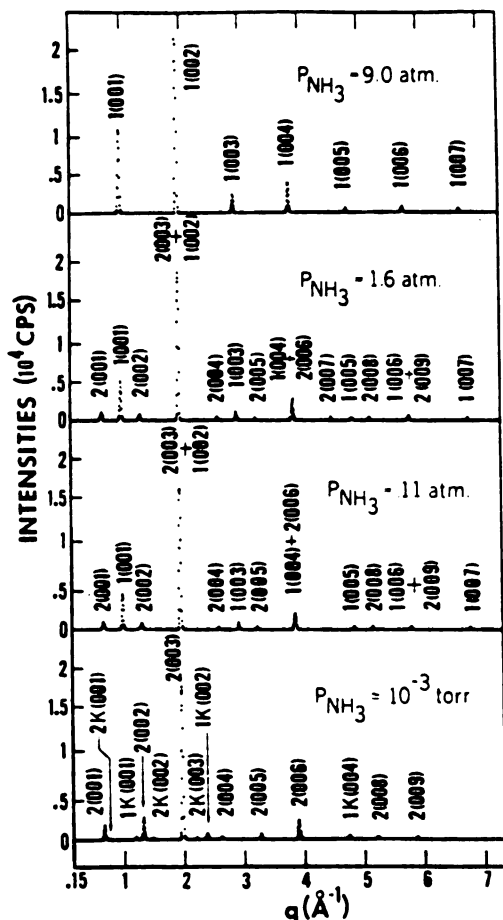


Fig. 1. (002) diffraction pattern of $K(NH_3)_x C_{23.5}$ as a function of the vapor pressure of ammonia. Reflections associated with the stage n potassium-ammonia ternary GIC are labeled $n(002)$. Those associated with potassium binary GIC's are labelled $nK(002)$.

atm., particularly for the (001) reflection of stage 1, corresponds to a staging phase transition which is accompanied by rapid changes in both the fractions of stages 1 and 2¹¹ and their inplane NH_3 densities. This phase transition exhibits several novel features and will be discussed in detail elsewhere.¹¹ Therefore, in the following discussion we address the pressure range $0 < P_{NH_3} \leq 5$ atm.

The exchange of intensities between stage 1 and stage 2 reflections evidenced in Figs. 1 and 2 is accompanied by a continuous variation of d_s . The x-ray derived values of d_s , $n = 1, 2$, (where the second subscript indicates n stage number) are

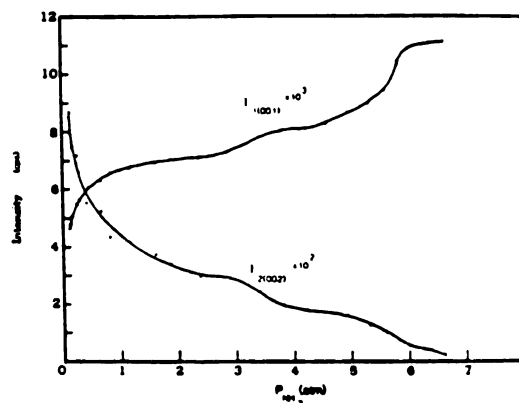


Fig. 2. The dependence of the intensity of the 1 (001) and 2 (002) reflections on ammonia vapor pressures (see caption of Fig. 1 for notation).

plotted in Fig. 3 as a function of P_{NH_3} . These sandwich thicknesses show a large $\sim 21\%$ variation (5.35 \AA to 6.61 \AA for d_{s1}) with P_{NH_3} . Also shown in Fig. 3 (inset) are the variations of $x_n = (x_A/x_K)_n$, $n = 1, 2$, with P_{NH_3} . Here x_K and x_A are the layer concentrations of the K and NH_3 species measured in units of the number of carbon atoms in a given layer. The relationship between x_n and P_{NH_3} was established using a procedure to be described below. Note from Fig. 3 that x_1 conforms very well to the Langmuire function¹² $x_1 = 4.49 P_{NH_3} / [0.0447 + P_{NH_3}]$. In contrast, x_2 is essentially pressure independent at low pressure and for $P_{NH_3} \rightarrow 0$, $x_2 \rightarrow 2.0$. These results are consistent with the fact that the compound which results from pumping off ammonia⁹ is a stage 2 residue compound.^{9,11} Our focus in this letter is the d_s vs.

P_{NH_3} data of Fig. 3. In order to explain that data, we write the total stage 1 sandwich energy E per carbon atom²⁻⁴ as

$$E = -\alpha x_K^{3/2} + \beta d_s x_K^2 f^2 + \frac{1}{2} k_O (d_s - d_O)^2 + \frac{1}{2} x_K k_K (d_s - d_K)^2 + \frac{1}{2} x_A k_A (d_s - d_A)^2 \quad (1)$$

For clarity, the second subscript, 1, has been dropped. In Eq. (1) the first term represents the cohesive energy of the sandwich, the second term is the electrostatic energy and the remaining terms represent the elastic energies associated with pure graphite ($x_K = x_A = 0$), and potassium ($x_A = 0, x_K \neq 0$) and ammonia ($x_K = 0, x_A \neq 0$) GIC's. Here k_O , k_K and k_A are the carbon, potassium and ammonia elastic force constants, respectively. The equilibrium separation of potassium intercalant depends upon d_s , which in turn is related to the charge transfer

through the relation¹³

$$d_K = (1 - f)d_{K^0} + fd_{K^+} \quad (2)$$

The ratio d_{K^0}/d_{K^+} depends on the ionic (r_{ion}) and atomic (r_{atom}) radii of K and can be determined from the relations $d_{K^+} = (2r_{ion} + r_0)$ and $d_{K^0} = (2r_{atom} + r_0)$ where r_{ion} and r_{atom} have the values 1.33Å and 2.29Å respectively and $r_0 = 2.69Å$ is obtained from the experimental value of $d_{K^+} = 5.35Å$. The charge transfer per K atom is a function of x_A since NH_3 , when in situ between the layers, tends to solvate the electrons initially given up by potassium to the carbon layers. For simplicity we assume that

$$f = 1 - \gamma x_A, \quad (3)$$

where γ is a constant.

By minimizing E with respect to d_s for a given x_K and x_A , we find (using $k_K x_K/k_0 \gg 1$ for x_K of interest⁴)

$$\frac{d_{s1}}{d_{K^+}} = \frac{1 + \left[\frac{d_A}{d_{K^+}} \cdot \frac{k_A}{k_K} + \gamma x_K \left(\frac{d_{K^0}}{d_{K^+}} - 1 \right) \right] x_1}{1 + \frac{k_A}{k_K} x_1} - B \frac{x_K^2 (1 - \gamma x_K x_1)^2}{k_K + k_A x_1} \quad (4)$$

Hawralak and Subbaswamy⁴ found that for KC_8 , the electrostatic contribution to d_s is quite small and we also find it to be negligible. Thus we have fit d_{s1} vs. P_{NH_3} of Fig. 3 using the Langmuire form of $x_1(P_{NH_3})$ given above and Eq. (4) with only two adjustable parameters which are the coefficients of x_1 in the numerator and denominator of the first term. The results of that fit are shown in Fig. 3 and constitute very good agreement with experiment. The small deviation between theory and experiment evidenced in the expanded plot of d_{s1} vs. P_{NH_3} of Fig. 3 shows that the latter exhibits a slightly larger slope in the plateau region. This discrepancy cannot be removed by including the electrostatic term of Eq. (4) and may be due to nonlinear effects in Eq. (3) and/or to a variation in the force constants with f .

From the fit of Eq. (4) (1st term) to our data, we find directly a ratio for the ammonia and potassium force constants of $k_A/k_K = .86$ indicating that the NH_3 molecule is softer than the K^+ ion as expected. Knowing k_A/k_K and the fact that $x_K = 1/24$ we can determine the relative elastic contributions of the size difference term, $d_A/d_{K^+} \cdot k_A/k_K$, and charge transfer term $\gamma x_K(d_{K^0}/d_{K^+} - 1)$ in Eq. (4) provided that we can establish a value of γ . The proper value of $\gamma = 4.8$ and the data of Fig. 3 (inset) were determined as follows: For a given P_{NH_3} we know $I_n(002)$ [Fig. 2], d_s [Fig. 3] and the³ gravimetrically measured^{11,14} NH_3 uptake x .

Calculated I_n depend on x_n , d_s and γ . Also, $x = \rho_1 x_1 + \rho_2 x_2$, where ρ_n is the fraction of stage n and $\rho_1 + \rho_2 = 1$. For fixed γ , ρ_n and x_n ($n = 1, 2$) can be found from the simultaneous equations for I_n and ρ_n . Trial γ 's were tested for compatibility with Fig. 2. The best fit was obtained with $\gamma = 4.8$ and Fig. 3 (inset) for x_n vs. P_{NH_3} is based on that value. As independent confirmation of this choice of γ , we note that the maximum values of x_1 and x_2 deduced from $\gamma = 4.8$ are in very good agreement with the saturation weight uptakes derived using the well established "volume available" criteria of Setton and coworkers.¹⁵

From the above cited parameters and Eq. (4) we find that although the size difference term dominates (70% contribution), the charge transfer term accounts for fully 30% of the sandwich expansion. These results have the following physical origin: As NH_3 is added to the layer interspace which contains K^+ ions, there are

three major effects: First, some sandwich expansion results from the size difference of ammonia (A) relative to ionized potassium (K^+) i.e. $d_A/d_{K^+} > 1$. Second, as ammonia is ingested, the charge originally donated to the carbon layers is extracted back into the $K-NH_3$ layer and delocalized. Much of the delocalized charge resides near K^+ ions leading to an increase in their effective radii. The increased radii of the potassium ions generates additional elastic energy which leads to an increase in d_{s1} . Third, NH_3 entrance is concurrent with a dilution of the K-C layer stoichiometry from KC_{12} to KC_{24} evidencing a stage 2 \rightarrow stage 1 transition at constant K composition.

As a final point we consider the d_2 vs. x_2 data of Fig. 3. Clearly d_2 is keyed more to the variation of d_1 with x_1 than to x_2 since x_2 is essentially residue-like and pressure insensitive at low P_{NH_3} . The keying of d_2 to d_1 is not surprising in view of the expected high mobility of NH_3 between laterally contiguous stage 1 and stage 2 regions as would exist in the Daumas-Hérolt model¹⁶ of the layer structure of GIC's. Thus, the expanded stage 1 regions impose both a dynamic and static strain on the layers of the stage 2 regions which accordingly acquire a separation d_{s2} only slightly less than d_{s1} .

Acknowledgement--We gratefully acknowledge useful interactions with T.J. Pinnavaia, J.L. Dye, R. Setton, K.R. Subbaswamy, and especially P.

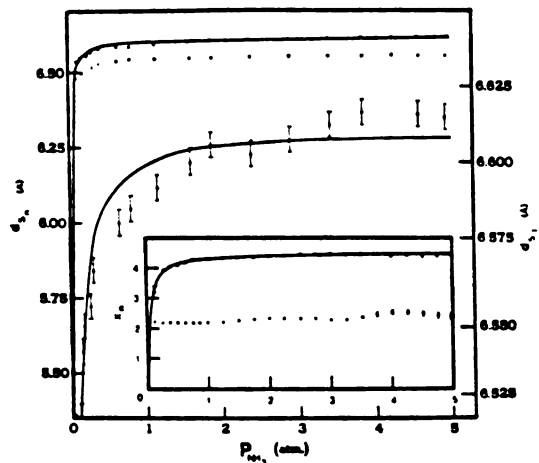


Fig. 3. The dependence of sandwich thickness, d_s^n , on P_{NH_3} displayed on a normal (left-hand ordinate) and expanded (right-hand ordinate) scale. Experimental points including one at the origin of the normal scale, are indicated by solid dots (\bullet) and open circles (\circ) for $n = 1$ and $n = 2$, respectively. The solid line is a fit to the data using Eq. 4 with the following parameters: $B = 0$, $d_{K^+} = 5.35 \text{ \AA}$, $d_{K^0} = 7.27 \text{ \AA}$, $d_A = 6.47 \text{ \AA}$, $k_A/k_K = 0.86$, $\gamma = 4.8$, $x_K = 1/24$. (Inset) The dependence of x_n for $n = 1$ (\bullet) and $n = 2$ (\circ) on P_{NH_3} . The solid line is a fit to the data using the Langmuire equation (see text) $x_1 = 4.49 P_{NH_3} / (.0447 + P_{NH_3})$. Unless otherwise indicated, error bars are smaller than the dots.

Vora, who assisted with some data acquisition and made major contributions to sample preparation. Thanks are also due to A.W. Moore for

providing the HOPG used in this study. This work was supported by the NSF under grants DMR 82-11554 and DMR 81-17297.

REFERENCES

1. S.A. Solin, *Advances in Chemical Physics* **49**, 455 (1982).
2. S.A. Safran and D.R. Hamann, *Physical Review B* **22**, 606 (1980).
3. S.E. Millman and G. Kirczenow, *Physical Review B* **26**, 2310 (1982).
4. P. Hawrylak and K.R. Subbaswamy, *Physical Review* (in press). See also J.R. Dahn, D.C. Dahn, and R.R. Haering, *Solid State Communications* **42**, 179 (1982).
5. A. Metrot and J.E. Fischer, *Synthetic Metals* **3**, 201 (1981).
6. K.C. Woo, W.A. Kamitakahara, D.P. Divincenzo, D.S. Robinson, H. Mertwoy, J.W. McKibben, and J.E. Fischer, *Physical Review Letters* **50**, 182 (1983).
7. A. Hérolid, *Proceedings of the International Conference on the Physics of Intercalation Compounds*, edited by L. Pietronero and E. Tosatti (Springer-Verlag, New York, 1981), p. 7.
8. M.E. Misenheimer, P. Chow, and H. Zabel, *Materials Research Society Proceedings* **20**, edited by M.S. Dresselhaus, et al. (North Holland, New York, 1983), p. 283.
9. W. Rudorff and E. Schultze, *Angew. Chem.* **66**, 305 (1954).

10. S.K. Hark, B.R. York, and S.A. Solin, *Synthetic Metals*, in press.
11. B.R. York, S.K. Hark, S.D. Mahanti, and S.A. Solin, to be published.
12. T.L. Hill, *Statistical Mechanics, Principles and Selected Applications* (McGraw-Hill, New York, 1956).
13. T. Enoki, M. Sano, and H. Inokuchi, *Journal of Chemical Physics* **78**, 2017 (1983).
14. J.W. McBain and A.M. Baker, *Journal American Chemical Society* **48**, 690 (1926).
15. F. Beguin, R. Setton, L. Facchini, A.P. Legrand, G. Merle, and C. Mai, *Synthetic Metals* **2**, 161 (1980).
16. N. Daumas and A. Hérol, *Bulletin Society Chim. Fr.* **5**, 1598 (1971).

NOVEL PROPERTIES OF ALKALI-METAL AMMONIA GRAPHITE INTERCALATION COMPOUNDS

S.A. SOLIN,* Y.B. FAN,* AND B.R. YORK*

*Department of Physics and Astronomy, Michigan State University, East Lansing, MI.

The ternary alkali-metal ammonia graphite intercalation compounds (GIC's) $M(NH_3)_x C_{12n}$ where $M = K, Rb, Cs$, and $n = 1, 2, \dots$ have been shown to have unusual staging transitions when the binary GIC is exposed to ammonia.¹ These staging transitions have been studied using (00 l) x-ray diffraction methods¹ and Raman scattering techniques.² In this paper we will report the inplane (hk0) patterns of the saturated potassium ammonia GIC $K(NH_3)_{4.38}C_{24}$ which is a pure stage-1 compound with long-range c-axis correlations. We will show that the K-NH₃ intercalants actually form a two-dimensional (2-D) liquid in the graphite galleries. This liquid is the 2-D analog of the well-known³ 3-D K-ammonia solution which has been heavily studied vis-à-vis the metal-insulator transition.

The $K(NH_3)_{4.38}C_{24}$ samples studied here were prepared by exposing KC_{24} to NH₃ vapor at a pressure of ~10 atm. The KC_{24} was prepared from highly oriented pyrolytic graphite (HOPG) using the usual two-bulb method.⁴ It was transferred in a glove box (≤ 0.5 ppm O₂, H₂O) to a pyrex tube into which dry NH₃ was condensed at liquid nitrogen temperatures. The end of the pyrex tube was epoxied to a thin-walled ($< .005$ ") aluminum can which contained the sample and was capable of simultaneously withstanding high NH₃ pressure, yet providing high transmittance of the incident and diffracted photons. The sample tube was sealed under vacuum at $\sim 10^{-5}$ torr and the NH₃ was allowed to warm to room temperature, thus acquiring an equilibrium vapor pressure of ~ 9 atm. and intercalating the KC_{24} specimen. Note that since no potassium was expelled during the insertion of NH₃, the potassium layer stoichiometry in the resultant stage-1 compound is KC_{24} corresponding to a reduced K density in comparison to the KC_{12} layer stoichiometry of the KC_{24} binary GIC.

The diffraction data reported here were acquired with incident MoK α radiation from a Rigaku 12 kw rotating anode source coupled to a vertically bent graphite monochromator and a computer-controlled Huber 4-circle diffractometer. A NaI scintillation detector was also used.

In Fig. 1 is shown the corrected inplane diffraction pattern ($\vec{q} \parallel \vec{c}$) for $K(NH_3)_{4.38}C_{24}$ acquired at room temperature. The solid line of Fig. 1 results from applying several correction factors to the as recorded data. Let $I_{exp}(q)$ be the observed (hk0) diffraction pattern. This contains Bragg reflections associated with the powder pattern of the aluminum sample can and the ordered carbon layers. A reference (hk0) pattern acquired from a sample free region of the aluminum can was recorded, appropriately scaled to and subsequently subtracted from $I_{exp}(q)$. The Bragg peaks associated with the carbon layers were removed (for clarity) from the resulting pattern to yield $I'_{exp}(q)$ which is the observed diffuse scattering. The pattern $I'_{exp}(q)$ was further corrected⁵ for absorption, and the Lorentz polarization factor to yield $I(\vec{q})$ as follows:

$$I'(q) = I'_{\text{exp}}(q) [(T/\cos\theta)\exp(-\mu T/\cos\theta)]^{-1} \times [(1 + \cos^2 2\theta' \cos^2 2\theta)/(1 + \cos^2 2\theta')]^{-1} \quad (1)$$

Here T is the sample thickness, μ is the effective absorption coefficient, θ is the diffraction angle, and θ' is the graphite monochromator diffraction angle for the (004) MoK_α reflection. The corrected diffuse scattering function $I'(q)$ which is shown in Fig. 1 was scaled to oscillate about the incoherent scattering contribution

$$I_{\text{Inc}}(q) = \sum_{uc} f_m^2 + i(m) \quad (2)$$

(shown as a dashed line in Fig. 1) at high q and from this scaling the ordinate scale of Fig. 1 (in electron units) was established. In Eq. (2), f_m

is the atomic scattering factor of the m^{th} atom, $uc \rightarrow$ unit of composition which in our case is $\text{K}(\text{NH}_3)_{4.38}\text{C}_{24}$ and $i(m)$ is the Compton modified scattering from the K, N, H, and C atoms.

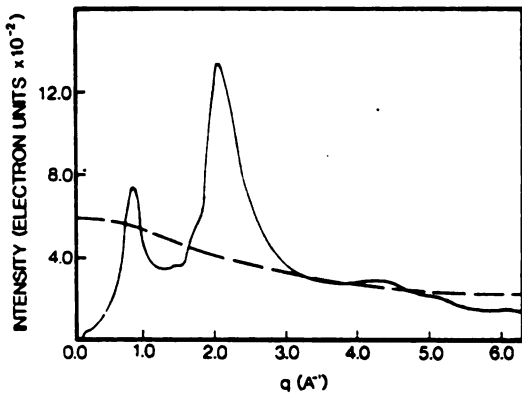


Fig. 1. The diffuse inplane ($q_{\parallel c}$) scattering $I'(q)$ from $\text{K}(\text{NH}_3)_{4.38}\text{C}_{24}$ (solid line) and the incoherent contribution (dashed line) as described in the text.

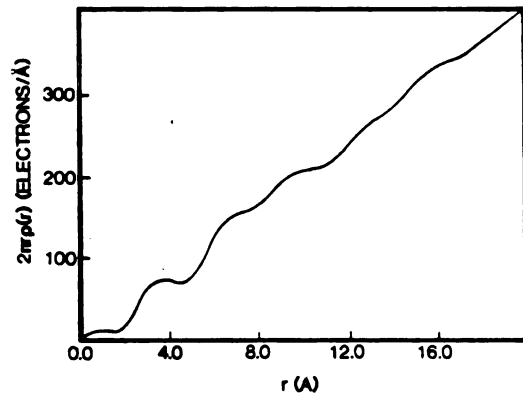


Fig. 2. The pair distribution function $2\pi r\rho(r)$ deduced by applying Eqs. 2 and 3 (see text) to the data of Fig. 1 with $\mu = 5.0 \text{ mm}^{-1}$, $\alpha = 0.7 \text{ \AA}$, and $T = 1.0 \text{ mm}$.

We have deduced the two-dimensional pair distribution function $2\pi r\rho(r)$ of the K-NH_3 liquid using a Bessel function transform of $I'(q)$, namely

$$2\pi r\rho(r) = 2\pi r\rho_0 + r \int_0^{q_m} [I'(q) - I_{\text{Inc}}(q)] (q/f_e^2) J_0(q,r) e^{-\alpha^2 q^2} dq \quad (3)$$

Here ρ_0 is the average areal density, f_e is the q -dependent scattering factor per electron, and α is a damping factor that minimizes cut-off errors associated with the finite range, q_m , of the integral of Eq. (3). The pair correlation function that results from the application of Eq. (3) to the data of Fig. 1 is shown in Fig. 2. As expected, $2\pi r(\rho(r) - \rho_0) \rightarrow 0$ at large values

of q . Moreover, the cut-off error alluded to above is <15 electrons as deduced from $\int_0^{1.5\text{\AA}} 2\pi r \rho(r) dr$.

From the known sizes of the K^+ ion and the NH_3 molecule we can deduce the origin of some of the peaks in the pair correlation function. The peak at $r = 3.5\text{\AA}$ or equivalently the broad peak in $I'(q)$ centered at $q = 2.10\text{\AA}^{-1}$ is associated with the $K-NH_3$ and NH_3-NH_3 correlations of a liquid that is dominated by clusters composed of K ions to which four NH_3 molecules are bound.⁶ This four-fold coordination is the natural 2-D analog of the 6-fold octahedral coordination of the 3-D $K-NH_3$ solutions and is compatible with the composition of our specimen if there are 0.33 "spacer" NH_3 molecules per $K(NH_3)_4$ cluster as indicated by preliminary NMR studies.⁷ The peak in $2\pi r \rho(r)$ at $r = 7.5\text{\AA}$ (or equivalently the peak at $q = 0.85\text{\AA}^{-1}$ in $I'(q)$) corresponds to $K-K$ correlations and its position and width indicate that there is no tendency for the K^+ ions to occupy carbon hexagon center sites. Thus, the $K-NH_3$ intercalant does indeed acquire a liquid structure between the carbon layers.

ACKNOWLEDGEMENTS

We acknowledge useful discussions with S.D. Mahanti, X.W. Qian, and D. Stump. Thanks are due to A.W. Moore for providing HOPG. This research was supported by the NSF under grant DMR82-11554.

REFERENCES

1. S.K. Hark, B.R. York, S.D. Mahanti, and S.A. Solin, *Solid State Comm.* **50**, 595 (1984).
2. P. Vora, B.R. York, and S.A. Solin, *Syn. Met.* **7**, 355 (1983).
3. J.C. Thompson, *Rev. Mod. Phys.* **40**, 704 (1968).
4. A. Hèrold, *Bull. Soc. Chim. Fr.* 999 (1955).
5. See e.g. H.P. Klug and L.E. Alexander, *X-Ray Diffraction Procedures*, 2nd Ed. (Wiley, New York, 1974), p. 849.
6. X.W. Qian, D. Stump, and S.A. Solin, to be published.
7. H. Resing, B.R. York, S.A. Solin, to be published.

OPTICAL REFLECTANCE STUDIES OF $C_{24}K$ and $C_{24}K(NH_3)_{4.3}$

D.M. HOFFMAN*, A.M. RAO*, G.L. DOLL*, P.C. EKLUND*, B.R. YORK**, and S.A. SOLIN**, *University of Kentucky, Lexington, KY 40506; **Michigan State University, East Lansing, MI 48824.

INTRODUCTION

Rudorff and Schulze [1] in 1954 reported the synthesis of the potassium-ammonia GIC's. These ternary compounds are now being studied extensively because of recent observations of staging transitions [2] and tuneable intercalate layer thickness [3] associated with variable concentrations of NH_3 in the intercalate layer. The stage n ternary GIC's $C_{24n}K(NH_3)_x$ ($n=1,2,3$) can be prepared by the reaction of the stage $n+1$ binary GIC's $C_{24n}K$ with the vapors of NH_3 [2]. In this paper we report the results of optical reflectivity studies on the NH_3 -saturated stage 1 ternary and $C_{24}K$ in the photon energy range 0.4-6 eV. The data were analyzed via Kramers-Kronig analyses to separate intra- and inter-band contributions to the dielectric function. By comparison of the optical results obtained for the binary and ternary GIC's we were able to determine the change in charge transfer between the intercalate and carbon layers induced by the NH_3 -intercalation. Since the carbon layers in $C_{24}K(NH_3)_{4.3}$ are separated by 6.63 Å we anticipate only weak C-C interlayer coupling. The data are therefore also discussed in terms of the quasi-2D model of Blinowski et al [4] applied previously to acceptor GIC's [4-6].

EXPERIMENTAL DETAILS

The ammonia-saturated ternary GIC's were prepared from highly-oriented-pyrolytic-graphite by NH_3 -intercalation of stage 2 $C_{24}K$ [2]. The $C_{24}K$ samples were transferred to cylindrical quartz tubes suitable for optical measurements and evacuated. An excess amount of anhydrous NH_3 was then distilled into the tube and kept frozen until the tube was sealed off. The stage of the samples were characterized using Raman spectroscopy [7]. The penetration depth for the Raman scattering probe is the same as that for reflectance measurements. Near-normal incidence reflectance measurements were made using single-beam reflectometers described elsewhere [6].

RESULTS AND DISCUSSION

The spectra of $C_{24}K$ and $C_{24}K(NH_3)_{4.3}$ are shown in Fig. 1. The insets to the figure are the respective Raman spectra of the samples. In all the figures we adopt the convention of labeling the $C_{24}K$ data as (a) and the $C_{24}K(NH_3)_{4.3}$ data as (b). The Raman data are in good agreement with that published previously [8]. The dashed lines in Fig. 1 represent the data extensions used to perform the Kramers-Kronig analyses. The data deviate from the dashed lines due to either absorption in the NH_3 vapors or the ampoule walls. Both spectra exhibit metallic character with prominent Drude edges near -1.8 eV associated with intraband absorption; higher energy features are identified with interband transitions [4-6]. Our $C_{24}K$ spectrum is in good agreement with a previously published spectrum [9] in the range 0.6 to 2.2 eV, however this spectrum was not analyzed to determine a plasma frequency. Kramers-Kronig transforms of our data were carried out to determine the real and imaginary parts of the dielectric function. Results for the imaginary part and the energy loss function are shown in Fig. 2 and Fig. 3, respectively. The dashed lines in Fig. 2 indicate the interband contributions. The separation of inter- and intra-band contributions are accomplished by fitting the low energy data to the Drude form for intraband absorption [6] and the results are shown in Fig. 4 where the theory is indicated by the solid lines. The Drude parameters obtained from this analysis are: (a) $C_{24}K$ -- $\hbar\omega_p=3.9$ eV, $\omega_p\tau=27$ and

(b) $C_{24}K(NH_3)_{4.3}$ $\hbar\omega_p=2.7$ eV, $\omega_p\tau=22$. The plasma frequency ω_p is related to the carrier concentration N and the effective mass m via

$$\omega_p=[4\pi Ne^2/m]^{1/2} \quad (1)$$

and τ is the carrier lifetime. Accordingly, the ratio of the square of the plasma frequencies for $C_{24}K$ and $C_{24}K(NH_3)_{4.3}$ is given by

$$[\omega_{pa}/\omega_{po}]^2 = (f_a n_a m_o)/(f_o n_o m_a), \quad (2)$$

where the additional subscripts o and a refer to the $C_{24}K$ and $C_{24}K(NH_3)_{4.3}$ parameters, respectively. We have also incorporated into (2) the relation $N=fn$, where n is the K concentration and f is the fractional mobile charge donated per K atom. In both compounds we assume the K 4s band is above the Fermi level (E_F). Thus $f_o=1$ and, to a good approximation, $m_o=m_a$. Using (2) we therefore arrive at a value $f_a=0.73$, or 0.73 electrons donated to the graphitic pi-bands per K atom. The remaining 0.27 electrons must then reside in lower lying NH_3 -derived states. Our value for f_a can be compared to 0.83 determined recently by NMR studies [10].

In the remaining space we briefly discuss our results in terms of the 2D formalism developed by Blinowski et al [4]. Using $f=.73$ and a value for $\gamma_o=2.4$ eV in the expression [4]

$$E_F=2.33 \gamma_o [f/l]^{1/2} \quad (3)$$

we arrive at $E_F=0.97$ eV. Furthermore, in the 2D limit [4],

$$\hbar\omega_p=[8.69 E_F]^{1/2},$$

which yields $\hbar\omega_p=2.9$ eV. This value compares favorably with the observed value of 2.7 eV. This preliminary analysis seems to indicate that the $C_{24}K(NH_3)_{4.3}$ compounds are quasi-2D and reasonably described by the theory of Blinowski et al [4]. Further study and analysis will be necessary to establish the connection.

ACKNOWLEDGEMENTS

This research was funded, in part, by grants from DOE DE-FG05-84ER45151 (U.K.), American Cyanamid (U.K.), and NSF DMR 82-11554 (M.S.U.).

REFERENCES

1. W. Rudorff and E. Schulze, Adv. Inorg. Chem. Radiochem. 1 (1959) 323.
2. S.K. Hark, B.R. York, and S.A. Solin, Synth. Metals 7 (1983) 255.
3. S.K. Hark, B.R. York, S.D. Mehanti and S.A. Solin, Solid St. Commun. 50, (1984) 595.
4. J. Blinowski, N.H. Hau, C. Rigaux, J.P. Vieren, R. LeToullec, G. Furdin, A. Herold, and J. Melin, Journal de Physique 41 (1980) 47.
5. P.C. Eklund, D.S. Smith and V.R.K. Murthy, Syn. Met. 3, 111 (1981).
6. R.E. Heinz, G.L. Doll, P. Charron and P.C. Eklund, Mat. Res. Soc. Symp. Proc. Vol. 20, 87 (1983), M.S. Dresselhaus, G. Dresselhaus, J.E. Fischer and M.J. Moran, eds. Elsevier, New York.
7. M.S. Dresselhaus and G. Dresselhaus, in Topics in Appl. Phys. 51; Light Scattering in Solids, M. Cardona and G. Guntherodt, eds., Springer-Verlag, Berlin (1982).
8. P. Vora, B.R. York and S.A. Solin, Synth. Met. 7 (1983) 355.
9. M. Zanini and J.E. Fischer, Mat. Sci. Eng. 31 (1977) 169.
10. H.A. Resing, B.R. York and S.A. Solin, to be published.

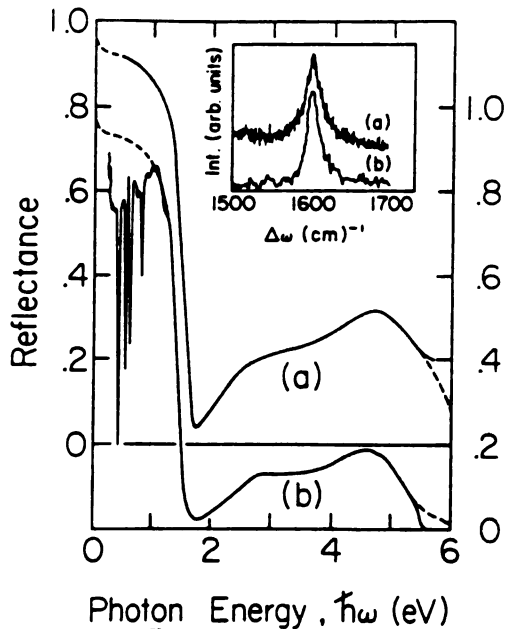


Fig. 1. Reflectance of (a) $C_{24}K$, and (b) $C_{24}K(NH_3)_{4.3}$. The dashed lines indicate extensions used in the analysis.

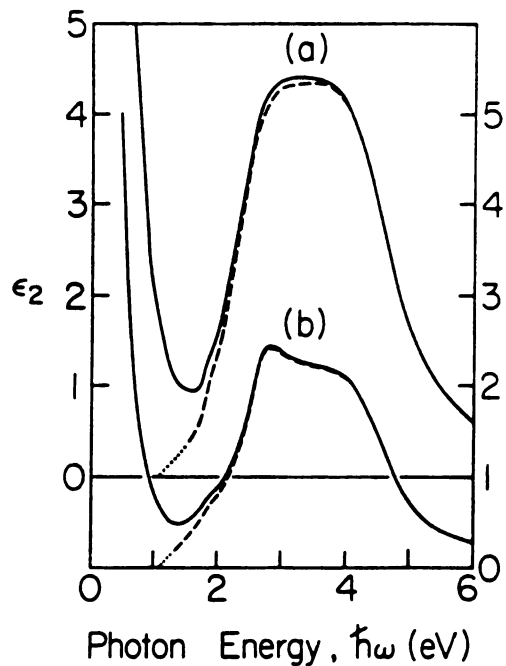


Fig. 2. Imaginary dielectric function of (a) $C_{24}K$ and (b) $C_{24}K(NH_3)_{4.3}$. The dashed lines indicate the inter-band contribution.

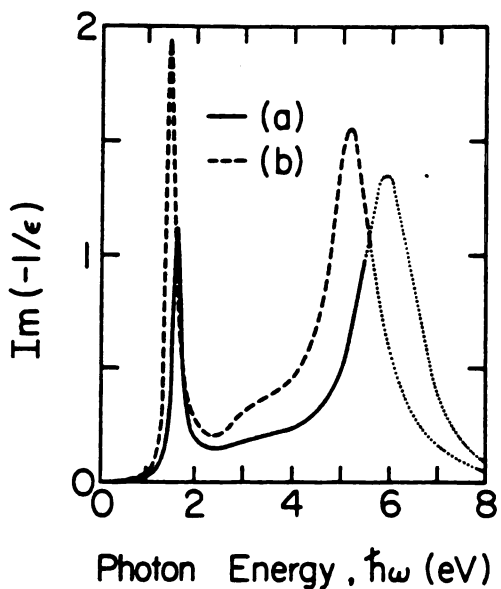


Fig. 3. The electron energy loss function for (a) $C_{24}K$ and (b) $C_{24}K(NH_3)_{4.3}$. Dots were used in the energy ranges where extensions to the data were used.

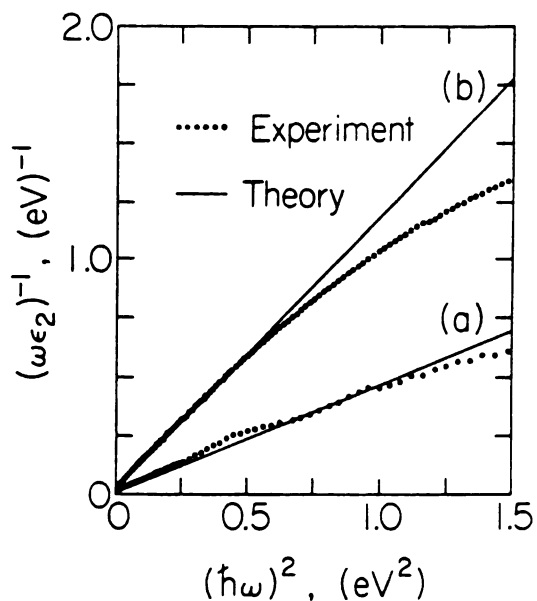


Fig. 4. The solid lines were calculated using the Drude expression for the dielectric function with parameters found in the text for (a) $C_{24}K$ and (b) $C_{24}K(NH_3)_{4.3}$.